PROBING TEMPORAL CHANGES IN MITOCHONDRIAL MEMBRANE POTENTIAL WITH IMPEDANCE SPECTROSCOPY

A Dissertation Presented to

the Faculty of the Department of Physics

University of Houston

In Partial Fulfillment

of the Requirements for the Degree

Doctor of Philosophy

By

Rooplekha Chakraborty Mitra

August 2015

PROBING TEMPORAL CHANGES IN MITOCHONDRIAL MEMBRANE POTENTIAL WITH IMPEDANCE SPECTROSCOPY

Rooplekha Chakraborty Mitra

APPROVED:

Committee Chairman
John H. Miller, Jr., Professor

Donna Stokes, Associate Professor

Jarek Wosik, Research Professor

Lowell T. Wood, Professor

Wanda Zagozdzon-Wosik, Associate Professor

Wei-Kan Chu, Professor

Dean, College of Natural Sciences and Mathematics

I dedicate this thesis to the memory of my father

who

taught me to believe in myself and always guided me

to

seek, reason, believe and know

Acknowledgements

For the last many years, I have been driven by a single dream. I always wanted to achieve the dream for my father, whom I lost in a tragic road accident when I was finishing my Master's in Physics, back home in India. My father aspired for me to be a doctorate in Physics one day. As I am close to my goal today, wherever he is now, I envision tears of joy in his eyes for his little one.

The route for my Ph.D. work at University of Houston has been one of the most fascinating journeys of my life. This period of fabulous learning environment spent here by me at University of Houston symbolizes spectacular intellectual growth and freedom.

First and foremost, I would like to take this opportunity to express my sincere gratitude to my advisor, Prof. John.H Miller, Jr., an expert in the field, for his continuous support in my Ph.D. study and research. Prof. Miller had given me all the freedom for an intellectual stroll to look at the bigger picture of my research and at the same time guided me to keep me grounded. During innumerable episodes of my frustration and befuddled state in context of my research, a simple discussion with Prof. Miller was more than enough to show me light and bring a new lease of vigor in my work. I am truly indebted to him for providing me with motivation, guidance, and thoughts throughout this Ph.D. endeavour of mine. I would also like to thank him for his patience, enthusiasm, profound knowledge, and help in almost everything which I can dream of. I do not think I would have been able to accomplish my Ph.D. in experimental biophysics without his brilliant ideas, enthusiasm, and persistent efforts to make me dream, contemplate and motivate to achieve bigger goals.

Next I sincerely appreciate Dr. Jarek Wosik for all his help, ideas, and stimulating discussions related to my work. Whatever I know today about handling instruments, I owe it to him. I would also like to thank Prof. Wanda Zagozdzon-Wosik due to her constant encouragement with regards to my work. My understanding and knowledge about nanosystems has only been possible because of her lessons.

I would also like to profusely thank Prof. Wei-Kan Chu who has taken so much interest in my work, and has always been kind to help me. His curiosity and fundamental questions about my research topic has made me think harder and harder, which has eventually helped me get a better grasp of the subject.

I am also immensely happy to get this opportunity to thank Prof. Lowell T. Wood. Whatever I can speak about him, will not be enough. I have been touched by his grace in every sphere which I can imagine, whether it's my research, teaching, or even my family and health.

My heartfelt thanks to Prof. Donna Stokes who was generous enough to be on my committee. Her concern about me, my work, and my well being has helped in so many ways, which words cannot express.

I also would like to extend my heartfelt thanks to all my Professors in the Physics Department and TcSUH, University of Houston for providing me with an outstanding academic and research environment.

I am also extremely delighted to extend my recognition to Dr. Martha Suárez Villagrán, whose determination, help and constant encouragement in my research work

along with my thesis writing has been invaluable. I really cherish my friendship with her.

I would also like to thank my wonderful lab members, with whom I shared office space some time or the other, Sladjana Maric, Dr. Asanga Iroshan Wijesinghe, Dr. Kimal Rajapakshe, Dr. Dhivya Ketharnath, Kuang Qin, and Kalyan Sasmal.

This is also a moment to acknowledge the help, friendship, and cooperation of my colleagues and non-academic staff in the department who had always been there for me in any trouble which I had. They are too many to name, but each of them has helped me in some way or the other which I will remain indebted to.

I also thank my friends, relatives, and family members who stood beside me through every phase of my life and have given me the fortitude to live, learn, and grow.

My deepest love and source of strength to pull this off despite of any difficulties I may have faced, goes to my mother who is now fighting in a paralytic state after a cerebral attack, whom I am yearning to see after I finish my Ph.D..

Last but not the least, I have finally got an opportunity to thank my aunt Mima, who has been with me thick and thin. Even at the present critical moment of my life she is the one who is beside my mother and taking care of her diligently, so that I can work peacefully and finish my studies soon here. Whoever knows me well will recognize that whatever I am able to accomplish today is because of my Mima.

PROBING TEMPORAL CHANGES IN MITOCHONDRIAL MEMBRANE POTENTIAL WITH IMPEDANCE SPECTROSCOPY

An Abstract of a Dissertation

Presented to

the Faculty of the Department of Physics

University of Houston

In Partial Fulfillment

of the Requirements for the Degree

Doctor of Philosophy

By

Rooplekha Chakraborty Mitra

August 2015

Abstract

The electrical properties of mitochondria provide fundamental insights into metabolic processes in health and disease. This research studies electrical impedance spectroscopy as a non-invasive, sensitive, and relatively low cost technique to monitor biological processes, such as those involving changes in mitochondrial membrane potential. Our experimental strategy first involves treating suspensions of live mitochondria with the substrate succinate to stimulate activity of succinate dehydrogenase, or more simply Complex II. This triggers electron flux through Complex II and the remaining complexes of the electron transport chain, enabling them to pump protons across the inner membrane and build up a membrane potential. Subsequent variability is introduced by adding various concentrations of the uncoupler trifluorocarbonylcyanide phenylhydrazone (FCCP) and the neurotransmitter dopamine (DA) to mitochondrial suspensions, and measuring changes in impedance. Our results show that adding succinate decreases impedance, consistent with an increase in dielectric response and membrane potential. Overall, our investigation establishes real-time impedance spectroscopy as a non-destructive, potentially powerful method for membrane potential studies of mitochondria.

Contents

List of Figures

List of Tables

Chapter 1

Introduction

1.1 Motivation

All aerobic organisms depend on oxygen for their survival, and must therefore adapt to changes in oxygen concentration, sometimes by altering gene expression, in order to maintain energy metabolism[6, 35, 63]. A tight coupling exists between oxygen consumption and energy demand[77]. Cellular functions directly correlate with cellular energy supplies. A decrease in ATP-utilizing pathways translates into a decrease in cellular respiration rates and demand for oxygen. Since mitochondria synthesize ATP in mammals and other eukaryotes, it is quite natural that all major kinase signaling pathways in mammals target the mitochondrion and influence its function[29, 113, 155]. Thus, mitochondria play key role, not only in providing energy, but also in modulating the cell's central pathways and processes.

Mitochondria are often described as "cellular powerhouses", since they

provide chemical energy, in the form of ATP, largely via oxidative phosphorylation of adenosine diphosphate (ADP)[38]. These organelles play additional roles, such as signaling, synthesis, and apoptosis, which can be cell specific. Most ATP is produced by a series of protein complexes (I-V), known as the electron transport chain (ETC) or respiratory chain[62, 163], in the mitochondrial inner membrane. Complexes I-IV use energy from donated electrons to pump protons across the inner membrane, from the matrix to the intra-mitochondrial membrane space, to build up a proton gradient and membrane potential. Oxygen (about 90% of what we breathe) is consumed by complex IV, also known as cytochrome c oxidase, so the rates of electron transport and proton pumping both correlate with the rate of oxygen consumption, unless dysfunction prevents one or more complexes from pumping protons. The resulting proton gradient and electric potential across the mitochondrial inner membrane drive the rotary motor ATP synthase (complex V) to synthesize ATP from ADP and inorganic phosphates Pi. Since the proton gradient is equivalent to a pH difference, ATP synthesis depends both on the electric potential and difference in pH across the membrane. Biological processes, such as those involving mitochondria, can be probed using a miniaturized 'lab-on-a-chip' device incorporating sensors and microfluidic channels, a biological micro-electromechanical system[18] for example. The impedance sensing approach discussed in this dissertation could readily be adapted to such miniaturized systems for in vitro studies of mitochondrial function or

dysfunction.

Dysfunction of the mitochondrial respiratory chain is implicated in several major diseases, including type 2 diabetes, heart disease, and cancer [82, 149, 158]. The uniqueness of such disorders often lies in their clinical heterogeneity and multiple pathophysiology, making it more difficult to identify the most appropriate personalized treatment. Considerable research has focused on developing sensors or biomarkers that can characterize the biological states of an organism at the cellular and molecular levels[9, 103]. There is a pressing need, both in the clinic and the lab (*e.g.*, for biomedical research and drug discovery), for label-free biosensors that provide higher throughput, smaller sample size, and lower cost. In this regard, sensors relying on biomarkers show both promise and relevance. To provide an example, such biosensors are now widely employed for self-monitoring of glucose and in pregnancy tests. Nevertheless, strategies are needed to detect normal and dysfunctional processes related to metabolism, *i.e.*, in mitochondria. The impedance monitoring approach discussed here, while initially being tested in vitro in the lab, could eventually be developed into instruments for in vivo clinical monitoring of mitochondrial dysfunction since electromagnetic fields, at microwave frequencies and lower, readily pass through the body.

Since the mitochondrial membrane potential ($\Delta\Psi_m$), which drives ATP production, is a key parameter that relates to the state of activity, health, and/or dysfunction of mitochondrial metabolism [91, 93]. A label-free method of

probing temporal changes in $\Delta\Psi_m$, would thus be a powerful tool to help probe metabolic activity in health and disease. Through a couple of recent studies by Prodan *et al.*[130–132], changes in cellular membrane potential have been shown, both theoretically and experimentally, to correlate with changes in impedance of cell suspensions. Our present study is designed to test whether temporal changes in impedance, in certain frequency ranges, correlate with changes in mitochondrial membrane potential. Electrical impedance is a complex quantity that includes both the resistance and reactance (capacitive or inductive) of the material at different frequencies. In case of biological samples, electrical impedance depends on the type of tissue or cell and active processes taking place, including intra- and extra-cellular processes involving biological membranes, as discussed in the next section.

1.2 Electrical Impedance Spectroscopy

Understanding about properties of materials has been greatly enhanced from our insights and knowledge regarding interaction of electromagnetic radiation with matter. As an example, dispersion of dielectric permittivity and energy band absorption for materials has been demonstrated in the frequency range of 10^{-6} Hz - 10^{11} Hz due to the underlying electrical polarization and conduction processes. The details of the mechanisms and precise frequency locations are determined by the physical factors under which the material is subjected to and

the nature of the material. The method which is utilized to study the electrical/dielectric properties of the materials can be generically described by electric impedance spectroscopy (EIS). In general, electrical impedance signifies the "complex" resistance which resist the flow of electrons through the material. The impedance behavior carries the unique fingerprint for a variety of fundamental microscopic processes[11, 96, 115]. As an illustration for a cell, Figure 1.1 shows how impedance signal characterizes various properties of the cell in terms of frequency. The way EIS works is by investigating the system

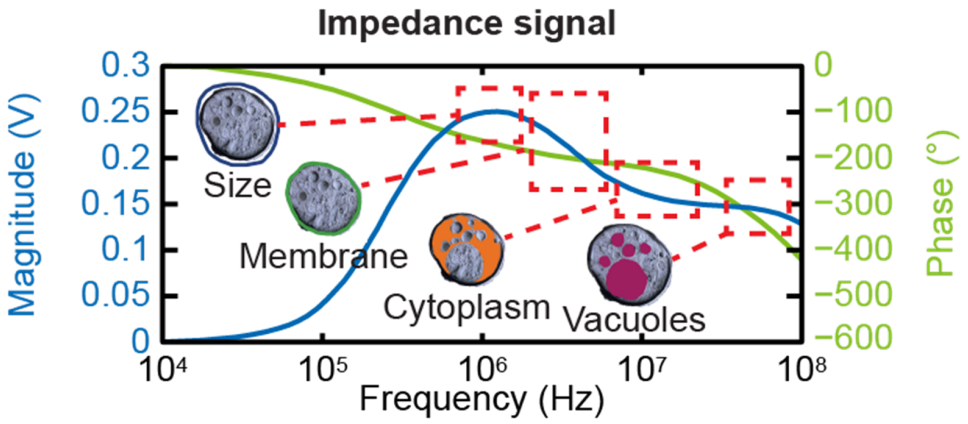

FIGURE 1.1: Cell impedance as a function of frequency[154].

response of an applied signal to a system at various frequencies. The alternating electric field generates a dipole moment on the charges which arises due to the relative motion of the particles in different layers. Measurable quantities are the impedance values, phase angle, and relaxation frequency, which are the macroscopic representatives of the dipole moment. Quantification of the measured variables gives us information about size, shape, and surface of particle

dispersion, nature of dispersed medium, and concentration of particles. The illustration for the cell impedance study reveals how different facets of a biological cell like a) size, b) membrane capacitance, and c) cytoplasm and subcellular component can be understood at different frequencies[130, 132].

The investigation of impedance spectroscopy has been phenomenal in gaining information about structure, reaction, and interference of a system, including the study of bulk transport material properties. The method relies on electrical measurement of resistance, capacitance, and inductance. The impedance spectra produced is dependent on equivalent circuits which has different elements consisting of resistors and capacitances[130, 132].

In Figure 1.2 we have shown a representation of circuits with different configurations. In this case the symbols p, s, and ∞ refer to "parallel", "series", and "open" circuit configurations respectively. The frequency dependent impedance is given by the formula and the associated conductances and capacitance is given by the formula

$$Z(\omega) = R_m(\omega) + \mathrm{i}X_m(\omega), \tag{1.1}$$

where ω is the angular frequency, and R_m and X_m are measured resistance and reactance of the impedance data. In terms of Z-components, the conductance (G)

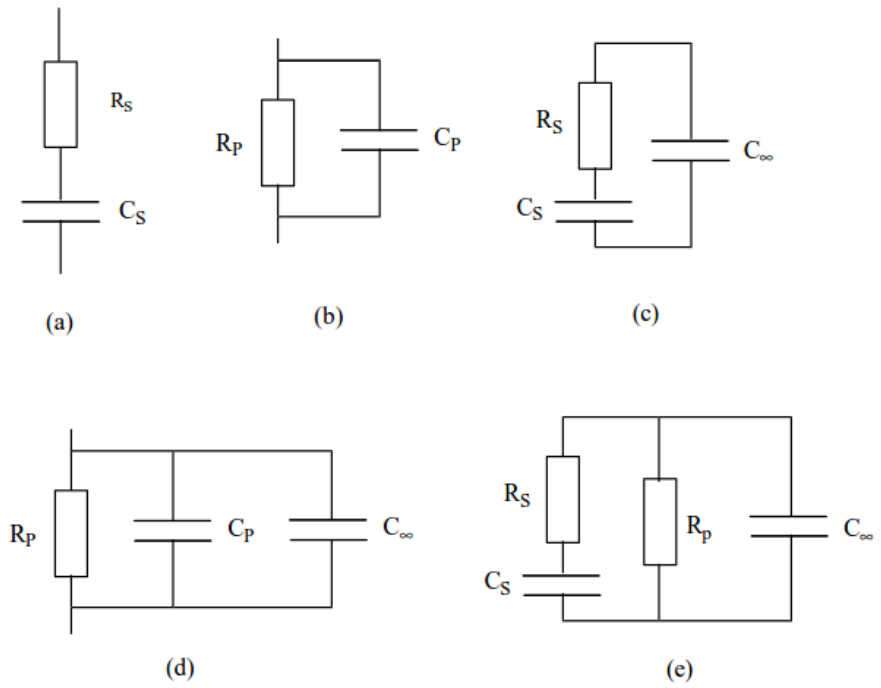

FIGURE 1.2: Model equivalent electrical circuits for different relaxation and conduction phenomena[160].

and capacitance (C) can be given as

$$G_p(\omega) = \frac{R_m}{R_m^2 + X_m^2} \quad and \tag{1.2}$$

$$C_s(\omega) = \frac{R_m}{\omega(R_m^2 + X_m^2)}. \tag{1.3}$$

The conductivity (σ) and the relative permittivity ($\epsilon*$) can be computed through the following formulas

$$\sigma = \frac{d}{a}G \quad and \tag{1.4}$$

$$\epsilon^* = \epsilon' - \mathrm{i}\epsilon'', \tag{1.5}$$

where d is the average separation between the electrodes, A the surface area of the electrode, ϵ' is the relative permittivity of the material, and ϵ'' is the out-of-plane loss factor. The ratio $\frac{d}{a}$ is the cell constant factor. Both the conductivity and relative permittivity depend on the nature of the sample and have a interrelationship among them given by

$$\epsilon' = \frac{d}{a}\frac{C}{\epsilon_0} \quad and \tag{1.6}$$

$$\epsilon'' = \sigma/\epsilon_0\omega. \tag{1.7}$$

The wideband electrical impedance data measurement for each sample is fitted to extrapolate the parameters from data spectra in accordance with Cole-Cole expression[70, 78, 159]

$$Z(\omega)^* = R_\infty + \frac{(R_0 - R_\infty)}{1 + (\mathrm{i}\omega\tau)^\alpha}, \tag{1.8}$$

where R_∞ is the high frequency resistance, R_0 is the low frequency resistance, τ is the time relaxation constant, and α is the parameter which allows for the broadening of the dispersion. We would look into these in more details in Chapter 3.

1.2.1 Instrumentation

Impedance measurement utilizes a frequency response analyzer through which a periodic signal is enforced to a sample compartment through a load. Analysis of

the voltage and current feedback through frequency response estimates the resistive, capacitive, and inductive behavior. The underlying mechanisms in the medium, which includes transport processes and reactions, exhibit physical phenomena at different frequencies indicative of different time-constants. Impedance spectroscopy for a range of frequencies provides a non-intrusive high signal-to-noise ratio procedure to quantify impedance linked with different processes.

1.3 Bioimpedance

There are variety of approaches for understanding dielectric features of cells and tissues due to the development in electrophysiology, microelectronics, and microfluidics. A low-cost, non-invasive alternative is obtained through bioelectrical impedance analysis (BIA)[130, 132]. Biological cells and tissues are characterized by frequency-dependent dielectric properties with high dielectric constant at lower frequency, which decays through different steps as the frequency increases. Thus, as we have discussed in the previous section, the relaxation phenomena at different frequencies enables classification of a multitude of underlying processes. Dielectric studies of biomaterial hold a tremendous potential. Analysis of biological samples through the measurement of electrical impedance is investigated via electrical bio-impedance studies[61, 102, 121]. Generically bio-impedance indicates how living organisms

respond to an applied electric filed/current. Label-free techniques have shown encouraging results for biological analysis. With the advent of new and emerging digital technologies, the efficacy of impedance measurements as non-invasive methodology have drastically improved and are projected as promising alternatives[13].

As shown in Figure 1.3, measurement of impedance for biological cells proceeds by infusing a high-frequency periodic current into the tissue via the drive electrodes, which subsequently creates a voltage difference between the receiver electrodes. The developed potential difference is correlated to the properties of the tissue which is quantified by the impedance measurements. From a biological point of view EIS deciphers data for cell size for lower

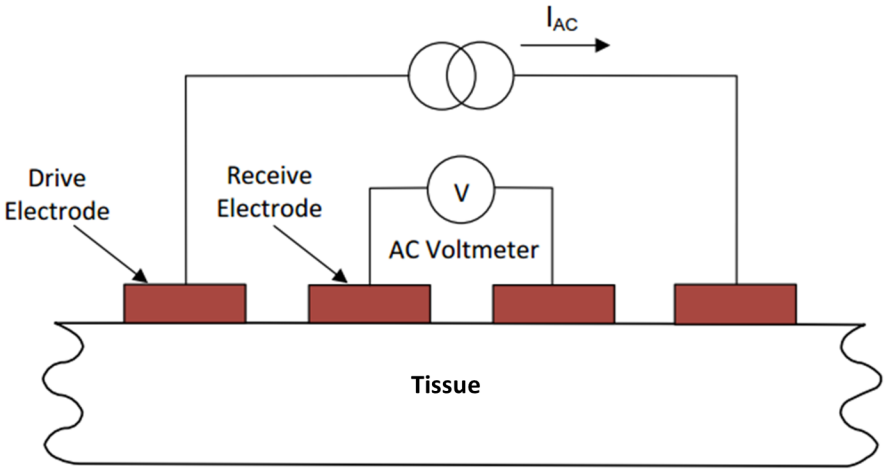

FIGURE 1.3: Generic measurement strategy for bio-impedance[137].

frequencies ranging from ∼100 kHz - 1 MHz, cell membrane capacitance at frequencies around ∼2 - 5 MHz, and dielectric characteristics at much higher frequencies. Thus, from a practical standpoint, owing to the large variation in

material properties and structures, EIS is emerging as an extremely capable tool[13, 132].

The human body is a many faceted biological structure composed of many tissues. All these biological cells contain intracellular fluids and cell envelopes, and are suspended in extracellular fluids. Thus, in general, biological tissues possess complex frequency dependent electrical impedance which can act as vital biomarkers to distinguish between normal and cancerous tissue. BIA is a technique which can be implemented for the whole body as seen in Figure 1.4.

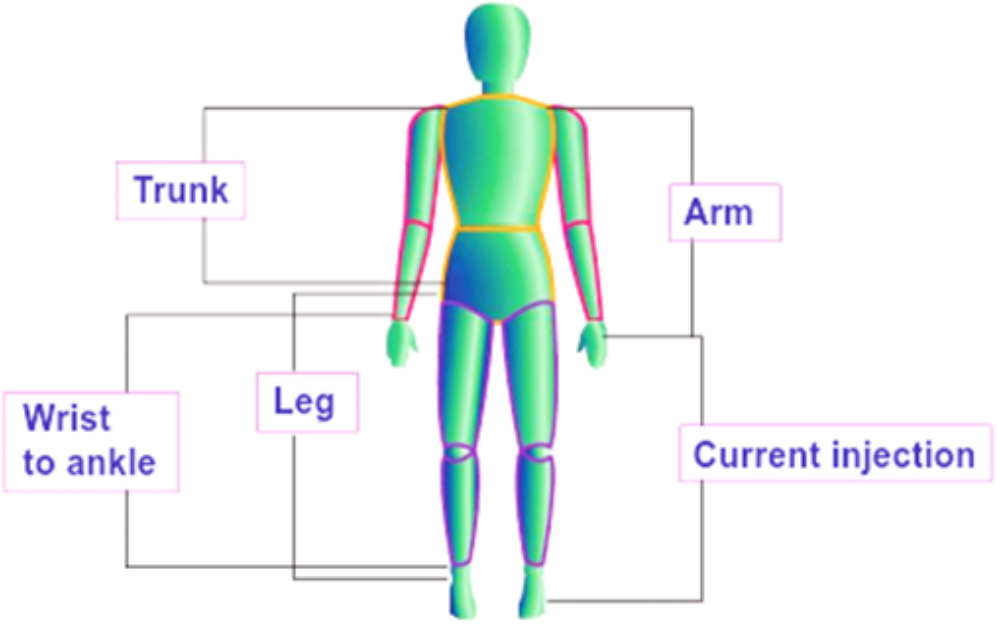

FIGURE 1.4: Body parts screened by bioelectrical impedance analysis[108].

The technology can be readily implemented for clinical applications and research, as the frequency response relies on the anatomical and pathophysiological condition of tissues. Currently, it has been applied to a wide

variety of areas including impedance-cardiography, impedance-plethysmography, and measurement of fluid in pleural cavities associated with the detection of deep vein thrombosis, multiple bioimpedance measurements for monitoring the lung function, monitoring of body composition, and detection of several kinds of cancers[1, 64].

1.3.1 Bioimpedance Methodology

For biological samples, determination of impedance is designed through polarization of dielectric particles under the influence of an electric field[132]. For the range of frequencies used in physiological solutions, bound and free charges give rise to real and imaginary part of impedance values respectively. In the case for suspension, effective permittivity for the particle and medium is given by the mixing equation as

$$\epsilon_{mix} = \epsilon_m \frac{1 + 2\phi f_{CM}(\omega)}{1 + 2\phi f_{CM}(\omega)}, \tag{1.9}$$

where ϵ_{mix} is the complex permittivity of the mixture, ϵ_m is the complex permittivity of the medium, ϕ is the ratio of particle to detection volume, and f_{CM} is the Clausius-Mossotti factor given as

$$f_{cm} = \frac{\epsilon_p - \epsilon_m}{\epsilon_p + 2\epsilon_m}, \tag{1.10}$$

with ϵ_p as the complex permittivity of the particle. The impedance is related to the permittivity as given by

$$Z \propto \frac{1}{\mathrm{i}\omega\epsilon_m}(1 - 3\phi f_{cm}). \tag{1.11}$$

A generic circuit description of biological samples in suspension consists of a resistance of the extracellular fluid in parallel to a series combination of the membrane capacitance and resistance of the intracellular fluid. An equivalent circuit model including cell membrane conductance and cytoplasm capacitance is a general model as shown in Figure 1.5. The electrical components are given by a

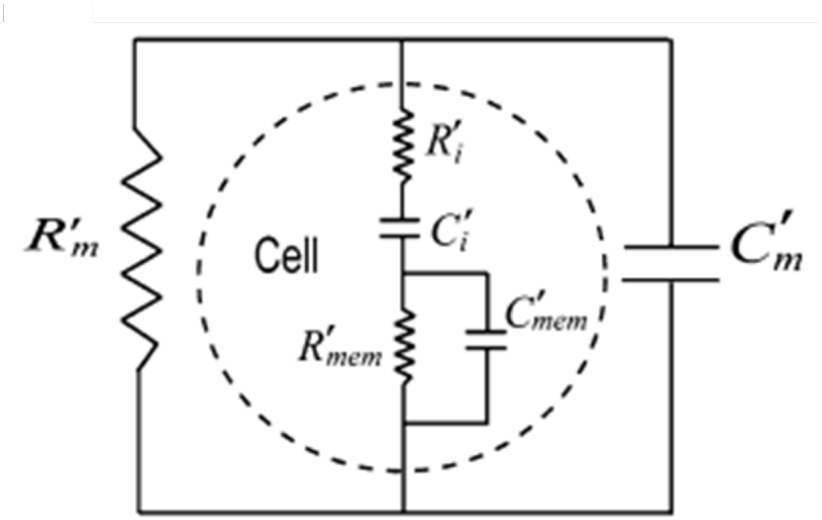

FIGURE 1.5: Circuit model for a single shelled particle in suspension[154].

combination of relaxation processes from polarization of cell membrane suspending medium interface and the other due to the polarization between suspending medium and cytoplasm. In Figure 1.5, R'_m and C'_m denote the effective resistance and capacitance of suspending medium respectively, R'_{mem}

and C'_{mem} the resistance and capacitance of the cell membrane respectively, and R'_i and C'_i the resistance and capacitance of the cytoplasm respectively. Thus, in general, the behavior of biological samples are complex in accordance with Cole-Cole relaxations (which we explain in detail in Chapter 3) as shown in Figure 1.6, where the current passes through the extracellular fluid at low frequencies. In such a scenario the cell behaves as an insulator with a resistance R_0. For higher frequencies, capacitance is close to being ideal and the resistance contribution is from both the extracellular and intra cellular components. The

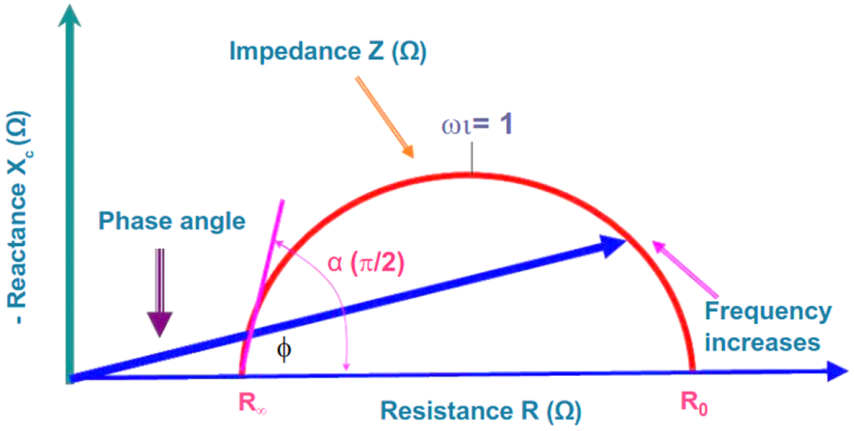

FIGURE 1.6: Cole plot in the impedance plane[108].

complex impedance in this case is described by Cole equation

$$Z = R_\infty + \frac{R_0 - R_\infty}{1 + (\mathrm{i}\omega\tau)^\alpha}, \tag{1.12}$$

with $Z(\omega)$ being the complex impedance, τ the mean relaxation time, and α denoting an empirically determined constant.

In recent years the investigation of BIA has emerged as an extremely popular analytical technique for various biological applications that include characterization of batteries, fuel cells, ceramics, coatings, semi-conductors, sensors, and corrosion[34, 50, 90]. Impedance analysis at multiple frequencies has been introduced to classify the biological mechanisms with better control using dispersions[50, 95, 105]. Nevertheless, one of the disadvantages of BIA is that the surface electrodes have high voltage and current (800 μA)[46, 156]. Thus, novel techniques needs to be implemented to decrease the instabilities related to injection current.

1.4 Objectives and Goals

Bigger Picture

Mitochondrial diseases form a clinically heterogeneous group of disorders. They can be present at birth or develop later in life. About 1 in 2000 children in the U.S.A. develop mitochondrial diseases by the age of ten years. 400-1000 children per year in the U.S.A. are born with a type of mitochondrial diseases. These are invisible diseases and diagnosis is difficult. Muscle biopsy and brain imaging are two procedures which are expensive and anaesthetic risk factors are involved. One single test is not effective, and thereby repeated trial measurements and an integrated approach are necessary.

Goals

Electrical Impedance is a promising tool to probe the changes in the electrical properties of mitochondrial membrane[130, 132]. It can be used in conjunction with any other existing method, such as the patch clamp and the fluorescent dye method, for such studies.

The goals of this project are to: 1) test the extent to which impedance vs. frequency and time of suspended live mitochondria, can be used to monitor changes that correlate with expected changes in mitochondrial membrane potential, induced by various known substrates (succinate, ADP, FCCP, etc.), and 2) use impedance response as a tool to explore whether excess concentrations of novel substrates, in particular the neurotransmitter dopamine, can adversely affect mitochondrial membrane potential in a fashion similar to that of the known uncoupler FCCP.

1.5 Dissertation Overview

The remainder of this dissertation is organized as follows. Chapters 2-4 provide background material on impedance of biological systems and on mitochondria, with particular focus on the mitochondrial electron transport chain. Chapters 5-7 discuss the experimental methods and results for this project, while Chapter 8 provides interpretation and concluding remarks.

Chapter 2

Mitochondria and Membrane Potential

2.1 Introduction

One of the key distinctions between prokaryotic and eukaryotic entities is encapsulated in the existence of genomes containing a membranous nuclear envelope with pores with mitochondria[5, 101]. It is now widely believed that mitochondria were generated 1.5 billion years ago from ancient prokaryote. Mitochondria beget pathways for aerobic respiration, eukaryotic cell generation, and complex multicellular organisms. As we have emphasized in the introduction, mitochondrion is central to the life and death mechanism of a cell. Mitochondria are double membrane cellular organelles which control a variety of processes in eukaryotic cells. The central job of a mitochondrial entity is involved

in energy production. Thus, mitochondrion is the cell organelle which makes oxygen usable for the cells to function. Under aerobic conditions, most of the ATP which the eukaryotic cells utilize is produced via mitochondrial oxidative phosphorylation (OXPHOS)[46]. ATP synthesis proceeds by coupling the phosphorylation mechanism to the mitochondrial respiratory chain for oxygen reduction. From a genetic standpoint, particularly in humans, the mitochondrial genome consists of a circular collection of DNA molecules consisting of around tens of thousand base pairs[20]. The proteins encoded by mitochondrial DNA (mtDNA) are essential ingredients for OXPHOS complex as shown in Figure 2.1. However, mtDNA is capable of generating a small set of proteins which plays a key role for the respiratory chain. Nuclear genes are the ones which encode most of the mitochondrial proteins, whose mutations are the ones responsible for the development of mitochondrial disorders. The symptomatic diagnosis of the diseases are quite varied depending on the specific alteration of the mitochondrial function.

Mitochondria play a key role in governing signalling components in different metabolic pathways. The pathways affect the action of proteins inside the cell which alters gene expression, eventually modifying the mitochondrial chamber. Investigation of the functionality of mitochondria has progressed rapidly in the last couple of years due to the advances in high-resolution microscopy and protein X-ray crystallography.

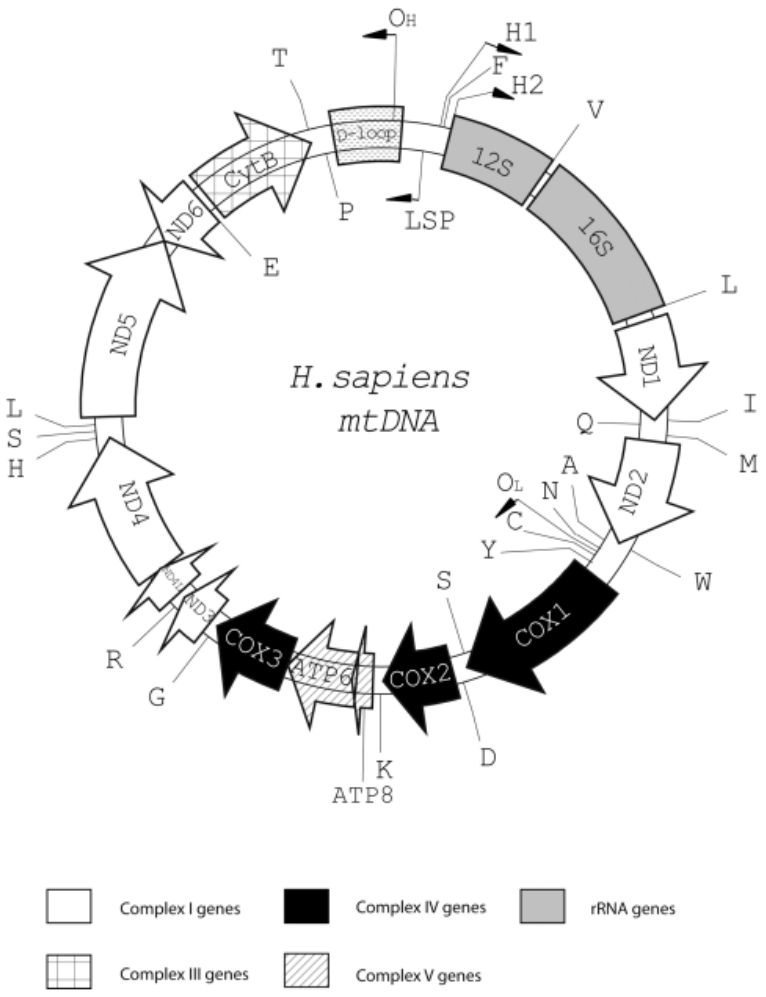

FIGURE 2.1: Human mitochondrial genome[39].

2.2 Mitochondrial Structure and Function

Electron microscopy has revealed that mitochondria exhibit a morphology consisting of a matrix enclosed by an inner membrane, and an inter-membrane space which separates the inner from outer membrane. Structurally mitochondria span length scales to around 0.5-1 μm. The outer membrane contains many copies of a transport protein porin, which forms aqueous channels allowing molecules with an upper bound in molecular weight which penetrates

the membrane. The folding or "cristae" of the inner membrane increases the surface area of the membrane which generate a "baffle-like" model[55, 118], as shown in Figure 2.2. The surface area on the inner membrane, which is

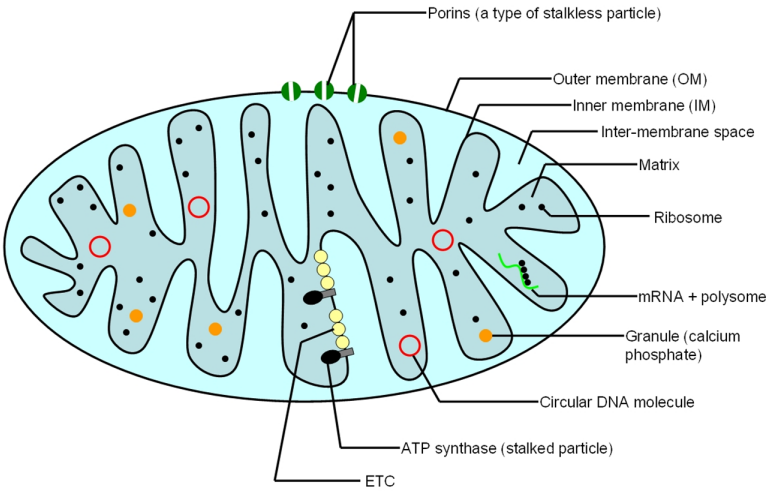

FIGURE 2.2: Structure of mitochondria[3].

topologically continuous on the one hand, spreads into an inner boundary membrane in close proximity to the outer membrane, whereas the other part forms cristae-like lamellar structures and connects with the inner boundary with tubular structures cristae junctions. For an isolated mitochondria, the matrix stays in a condensed form driven by osmosis. So, for most of the circumstances the inner boundary membrane is detached from the outer membrane apart from some contact sites. From a dynamic viewpoint, the structural morphology of mitochondria arises from interactions of proteins on the outer surface of cytoskeleton with various components consisting of intermediate and actin filaments along with microtubule.

Mitochondria play the dominant role in converting food products, such as glucose and fatty acids, into ATP. Mitochondria are also crucial for intracellular signalling, thermogenesis, calcium and iron homeostasis, and apoptosis apart from metabolic pathways via oxidative mechanisms. Oxidative metabolism is sustained through pyruvate, which is generated through the fatty acids from triglycerides and the carbohydrates, which are responsible for glycolysis. Pyruvate is selectively imported into the mitochondrial matrix, which is subsequently broken down into acetyl CoA. The functional acetyl units are the main ingredients for the tricarboxylic acid cycle (TCA cycle), which are generated from pyruvate and release CO_2 or breakdown of fatty and amino acids in the mitochondrion. Eventually citrate is released and helps to have a feedback loop whereby it is converted back to acetyl CoA by ATP citrate lyase. The pathway cycle happens to be α-ketoglutarate and oxaloacetate, which play an important role in the generation of the amino acids. Eventually the succinyl-CoA from this cycle produces porphyrin, which facilitates heme biosynthesis.

Thus, the above functionalities of mitochondria demonstrate their importance, without which the cells will not be able to function properly. Thus, a functional mitochondrion is a key promoter of the metabolic pathways which feeds ATP to drive mitochondrial membrane potential. This justifies mitochondria's role as the predominant machinery for oxidative phosphorylation.

2.3 Theory of Mitochondrial Bioenergetics

Energy flow in mitochondria proceeds through a sequence of steps through which the energy released from carboxylic acids by the oxidation of NADH to NAD+ is utilized to generate an electrochemical gradient by pumping out the protons from the matrix. The gradient creates a difference in pH, and the chemical difference modulates a molecular motor F_0F_1 ATPase crucial for the synthesis of ATP. The functional acetyl unit aids in citric acid cycle producing NADH and FADH for OXPHOS. NADH produces electrons which makes a passage through a series of molecules via the electron transport chain (ETC), giving water and ATP as byproducts. Thus, this mechanism leads to synthesis of ATP via proton transport across mitochondrial matrix down the electrochemical gradient through the respiratory complex. Broadly the scheme works as shown in Figure 2.3.

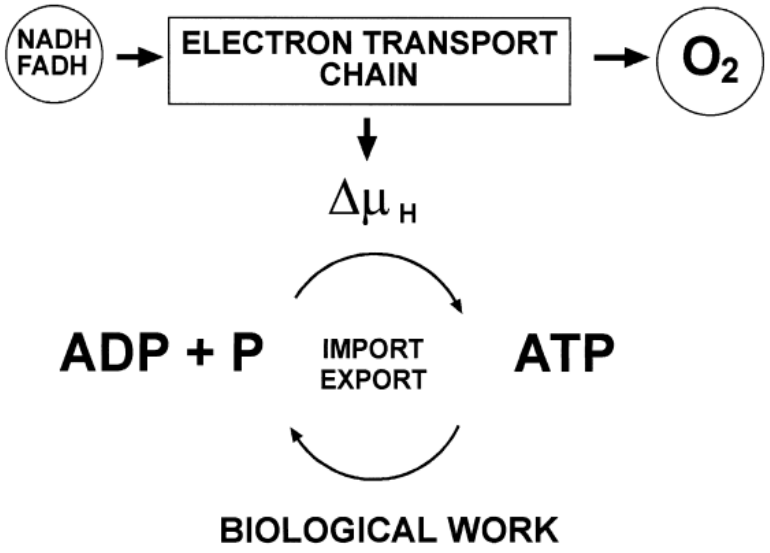

FIGURE 2.3: Electron transport and OXPHOS[138].

OXPHOS relies on the breakdown of glucose to water and carbon dioxide promoted by the combination of NADH and $FADH_2$. These mechanisms are important for donating electrons to mediate the oxygen current via a series of molecular machines through the inner membrane of mitochondria. The feedback loop coalesces the ATP synthase in the inner membrane and the protons into the inner membrane matrix. Thus, the process of ATP generation proceeds via the proton gradient through the electron transport chain whereby ADP to ATP conversion takes place, as shown in Figure 2.4

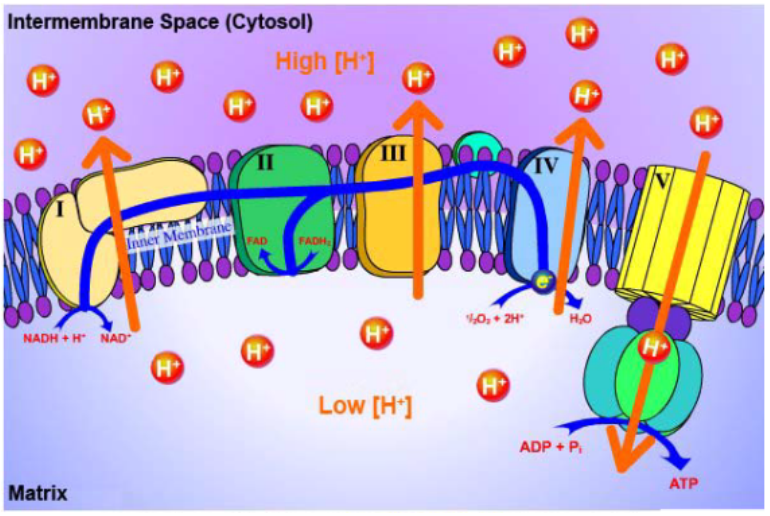

FIGURE 2.4: Proton pumping via the respiratory chain[138].

In terms of the specific players, the molecular motors we mentioned earlier for the mitochondrial pathway, are composed of Complexes I-V, which eventually have the task of proton pumping by oxidizing the electron donors and oxidative phosphorylation. Mitochondrial respiratory chain consists of a group of enzymes consisting of five complexes (Complex I-V) and two electron carriers

(ubiquinone/coenzyme Q and cytochrome c). Energy of the electrons flows through the different complexes of the mitochondrial chain in the form of oxygen, generating a gradient and eventual release of ATP, as shown in detail in Figure 2.5. Proton dynamics through the inner mitochondrial membrane leads to

- the difference of pH (ΔpH)in the matrix compared to the cytosol, and
- a net flow of protons outward resulting in a voltage gradient (ΔV).

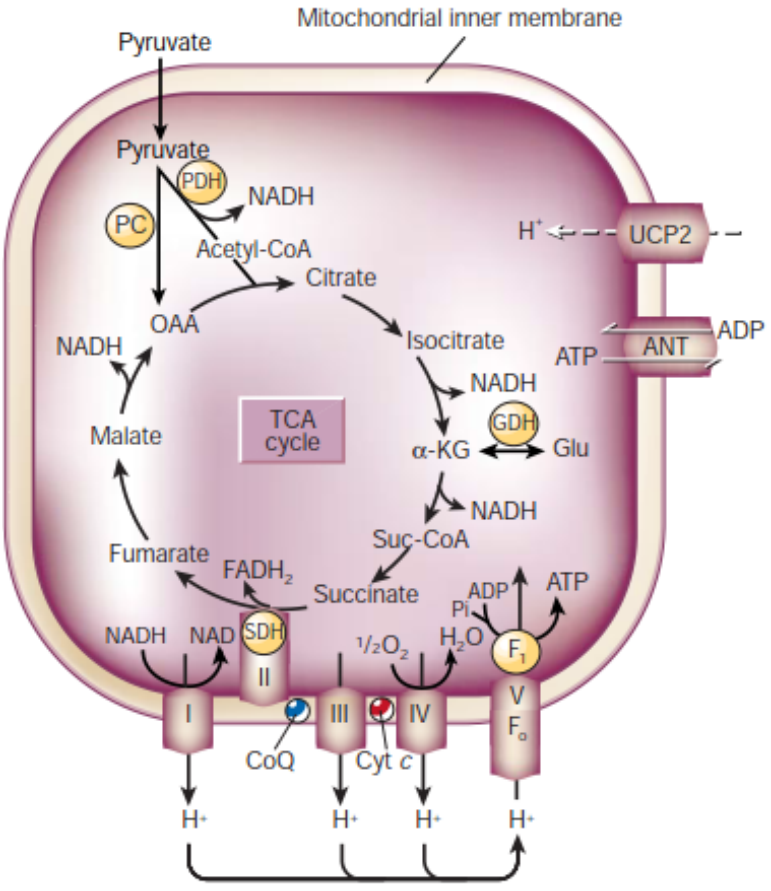

FIGURE 2.5: Mitochondrial respiratory chain[97].

2.4 Mitochondrial Membrane Potential

The rise of the membrane potential is facilitated through an electrical charge difference between the two sides of the membrane. For mitochondrial processes, either proton pumping or passive ion diffusion generates the charge difference. Ionic gradients across the membranes are maintained through molecular ion pumps by which the cells expend energy. The ion channel pumps are pore specific, which help in diffusion of the rate-dependent predominant ion types (Na^+, K^+, Ca^2+, and Cl^-)[26, 95].

As we have seen earlier, it is now well known that two different natures of gradients, one the chemical gradient of protons (ΔpH_m) and the other the mitochondrial membrane potential ($\Delta\Psi_m$), collectively determine the proton-motive force. The negative charge of the matrix side of the inner mitochondrial membrane enables accumulation of acidic contents in the mitochondria, which induces the ATP synthase to benefit from the electrochemical gradient and synthesize ATP. The electrochemical potential is given by

$$\Delta\mu = -F\Delta\Psi_m + 2.3RT\Delta pH_m, \tag{2.1}$$

where F is Faraday's constant, R is universal gas constant, and T is absolute temperature. Non-vanishing electrochemical potential indicate ion transport across the membrane. At equilibrium we have $\Delta\mu = 0$ as in Equation (2.1),

which readily gives Nerst equation as

$$\Delta\Psi_m = \frac{2.3RT}{F}\Delta pH_m. \tag{2.2}$$

Equation (2.2) gives us an estimate of the ionic potential difference across the membrane. The membrane potential, as measured from the concentration of permeable ions outside and inside of the membrane, is given by[128]

$$\Delta pH_m = \frac{RT}{F} ln \frac{P_K[K^+]_o + P_{Na}[Na^+]_o + P_{Cl}[Cl^-]_i}{P_K[K^+]_i + P_{Na}[Na^+]_i + P_{Cl}[Cl^-]_o}, \tag{2.3}$$

where P_K, P_{Na}, and P_{Cl} indicate permeability for potassium, sodium, and chloride respectively. The subscripts o and i denote the concentration outside and inside the membrane respectively.

2.5 Connecting Membrane Potential with Mitochondrial Disorder

Distinction between normal cell functioning, mitochondrial activity, and mitochondrial diseases can be marked via the mitochondrial membrane potential. The membrane potential is an indicator of the energetics of normal cells and the state of mitochondrial permeability[25, 51, 135, 164]. There exist some studies which have established that mitochondria of malignant phenotypes have lower

rates of ATP synthesis and lower capacity of hydrolysis[33, 123]. Thus, mitochondrial potential studies have the promise to develop tools with biomarker capabilities[103, 130, 132].

A variety of measurement techniques have been developed to investigate membrane potential $\Delta\Psi_m$, which include fluorescent probes and electrophysiological methods. The component of electrophysiological techniques relies on voltage/patch-clamping methods[94, 106, 153]. Membrane potential is quantified by the potential difference between the electrodes. Without penetrating the membrane, in patch-clamping technique, a patch electrode contacts the surface of the membrane[106]. The patch electrode is coupled to the cellular cytoplasm, and in the absence of current, the membrane potential is listed with respect to a reference electron in the solution. Despite the advantages, the method is less efficient with a low throughput[66, 153].

Fluorescent methods for membrane potential quantification are optical methods based on the use of voltage sensitive dyes[66, 153]. The success of this easy method is based on rapid data procurement and relatively higher read out. However, there also exists issues related to dye calibration which may lead to difficulty for absolute determination of the membrane potential.

It is now widely believed that mitochondrial membrane permeability plays a conclusive role in cell fate related to survival and apoptosis, irrespective of cell morphology and functionality. The regulation of mitochondrial membrane potential, which controls the permeability of the outer mitochondrial membrane,

is the main contributor for normal cell functioning and death. $\Delta\Psi_m$ is related to the enhanced generation of reactive oxygen species which percolates the antioxidant machinery to induce mitochondrial damage. Increased membrane potential also enables cues for reactive ion species accumulation via generation of ATP synthase inhibitors like oligomycin, which leads to the production of stress response genes leading to bioenergetic crisis. Mitochondria have a high transmembrane potential $\Delta\Psi_m$ under physiological conditions where the proteins are localized in the intermembrane space and outer membrane permeabilization is inhibited. Thus, we clearly illustrate a scheme of a diagnostic marker for cellular pathophysiology in terms of mitochondrial membrane potential[116, 132].

Chapter 3

Dielectric Phenomena

3.1 Matter in a Static Electric Field

Electrical properties of materials are determined by the responses of the materials to an applied electric field. On the application of electric field to a material, two very distinct phenomena can occur: a) the energy in the field is lost by dissipation from the motion of the constituent charge carriers, or b) the energy is stored at the cost of polarization of the material. Polarization arises in a material through the atoms when there is a distortion of the negative electron cloud around the positive atomic nuclei in a direction opposite to the field. This creates a separation of charge, which in turn induces a dipole in the material. Apart from the contribution of dipoles, polarization can be interfacial due to charge accumulation at the surfaces between materials[125]. Apart from the role of dipoles in polarization, there exists another possibility, where the migration of

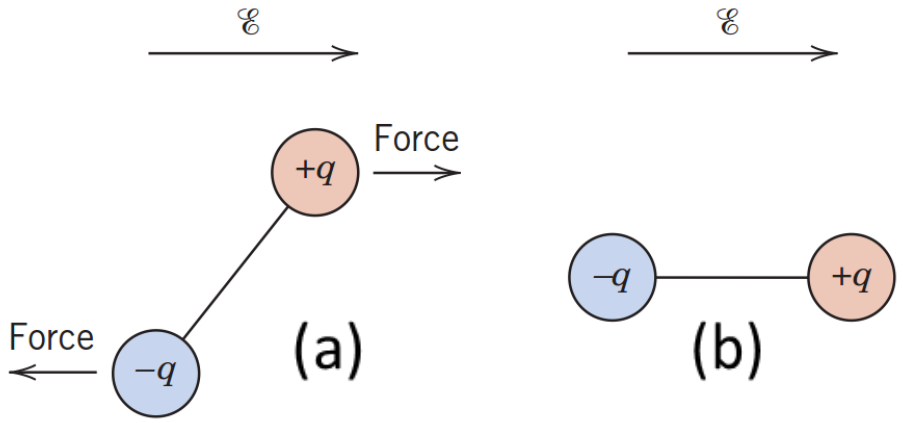

FIGURE 3.1: (a) Forces acting on the dipole and (b) polarization induced in material from the alignment of dipole with the applied electric field.

charge carriers will influence the dielectric/conductive response of the material. In these systems hopping electrons are the free-charge carriers, in contrast to the bound charges for the dipole case which gives rise to polarizability.

A material's response to an applied electric field is modulated by two key parameters, the conductivity σ and permittivity ϵ. Conductivity is determined by the mobility of the charges, whereas permittivity is a measure of the polarizability of the material. As our work focusses on biological materials, we in the following subsections discuss about the behavior of dielectrics.

3.1.1 Dielectric Polarization

Dielectrics are portrayed as materials mostly having bound charges. With the application of an electric field the material acquires a non-vanishing macroscopic dipole moment and bound charges become polarized, giving rise to a polarization P

of the material under consideration. In the linear approximation, the polarization of the dielectric material is directly correlated with the strength of electric field E. For an isotropic and uniform dielectric, the relationship is given by $P = \epsilon_0 \chi E$. Maxwell's theory of electromagnetism has clearly shown that for this classes of materials the field from the bound charges are included in the electric displacement vector D. The interrelationship among these quantities is succinctly given by

$$D = \epsilon_0 E + P. \tag{3.1}$$

In the case for a uniform isotropic dielectric, where the polarization is linearly proportional to the applied electric field, Equation (3.1) simplifies as $D = \epsilon_0 \epsilon_r E$, where $\epsilon_r = 1 + \chi$, is the relative dielectric permittivity or the dielectric constant of the material and χ is the dielectric susceptibility of the material. The polarization in the linear approximation is, in general, independent of the electric field. However, as we will discuss later for time varying electric field, it is dependent on the frequency of the applied electric field, in addition to other factors like temperature, density, or chemical composition[19, 120, 131, 132].

3.1.2 Polarization Mechanisms from Dipoles through Static Charge Distribution

Ordering of charge distribution with a statics process, mostly in the form of dipoles or charge separation in dielectric sample, can proceed via different

mechanisms. Broadly speaking there are four distinct mechanisms of polarization. In Figure 3.2 we have pictorially depicted the three different types of polarization.

Electronic polarization: It is related to the displacement of the nuclei and electron cloud under the effect of the applied field. The field induces a rapid response of the electrons which is usually realizable at optical frequencies. Forces against the displacement of the charges is relatively thermally unresponsive due to the presence of intramolecular forces, making the electronic polarization virtually independent of temperature.

Atomic/Ionic polarization: For materials which are ionic, the applied

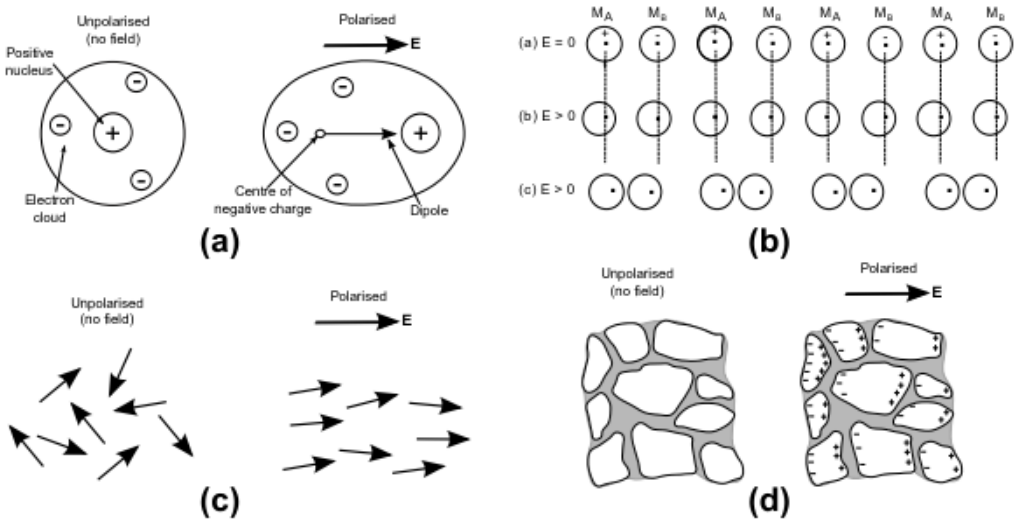

FIGURE 3.2: Different mechanisms of polarization (a) electronic, (b) ionic, (c) orientational and (d) interfacial[32, 84, 161].

electric field creates a dipole moment in the materials by displacing the positive and negative ions in two different directions (positive and negative ions in the

direction and opposite of the applied field respectively). The polarization is dependent on the nature of the interface which gives rise to ion accumulation and operates at the infrared frequency range.

Orientational polarization: This scenario arises from the presence of polar groups (molecules having permanent dipole moments). In this case dipole alignment is induced by an effective torque on the polar molecules. Orientation polarization operates at lower frequencies. Since rotation of the molecules from the torque developed is also effected by thermal turbulence, orientational polarization is strongly temperature dependent.

Space charge/interfacial polarization: This type of frequency-dependent polarization is relevant for our study involving biological samples. Unlike displacement of bound charges for the polarization mechanisms discussed above, in this case macroscopic distortions in the field are induced by trapped positive and negative space charges at interior interfaces or in the bulk of material.

3.1.3 Polarization Mechanisms from Dipoles via Hopping Charges

Polarization through hopping mechanisms provide a distinct alternative process, even though biologically not much relevant. Thus, we will not elaborate much on this, however for the sake of completeness, we discuss them very briefly in the dissertation whenever it is pertinent to discuss in comparison to the dipole

polarization schemes[160].

Hopping polarization arises when localized charges move between adjacent sites. Usually the transport traps the charges in localized sites for most of the time, with small times spent by jumping over a potential barrier to neighbouring sites. The width and height of the potential barrier determines the probability of transition between the states. In Figure 3.3 we have shown a double-well potential

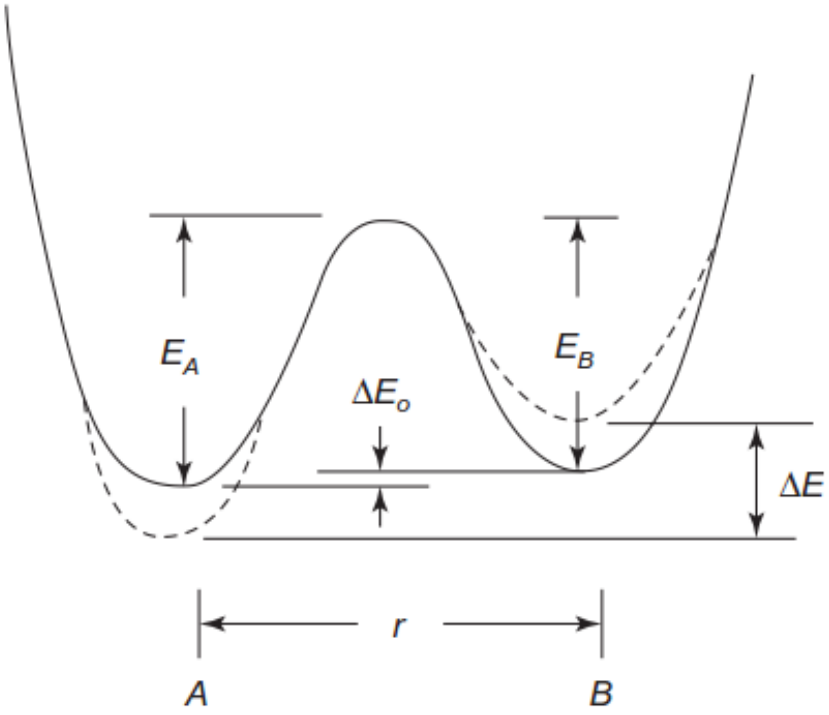

FIGURE 3.3: Illustration of hopping polarization arising due to hopping of charges between two different states A and B via a double potential well[84].

where the hopping transition is determined at thermal equilibrium from time-averaged probability $P_{A\to B}$ and $P_{B\to A}$ of a particle to hop in between two adjacent

sites A and B to form a dipole. The hopping probabilities are given by

$$\begin{aligned} P_{A\to B} &\propto exp(-E_A/kT) \quad and \\ P_{B\to A} &\propto exp(\frac{-E_A - \Delta E_0}{kT}), \end{aligned}$$

where E_A is the activation energy for the transition and ΔE_0 is the energy difference $E_A - E_B$. The hopping probability is given by

$$\alpha_{hop} \propto \langle P_{A\to B} P_{B\to A} \rangle, \tag{3.2}$$

where the angular brackets denote ensemble average.

3.2 Dielectrics in Time-dependent Fields

Dipoles tend to make realignment with the field in situations where the electric field varies or changes its direction with time. Usually depending on the type of polarization, there exists some minimal finite amount of time over which the reorientation takes place. Thus, different polarization mechanisms we have discussed above give rise to a dielectric relaxation process with a characteristic time constant/frequency response[19, 81, 125]. In Figure 3.4 we depict the time-dependent polarization of a material in a time-varying electric field with the asymptotic polarization limits given by P_∞ and P_0. In general, a dipole will not be able to change orientation, and thereby will not contribute to the dielectric

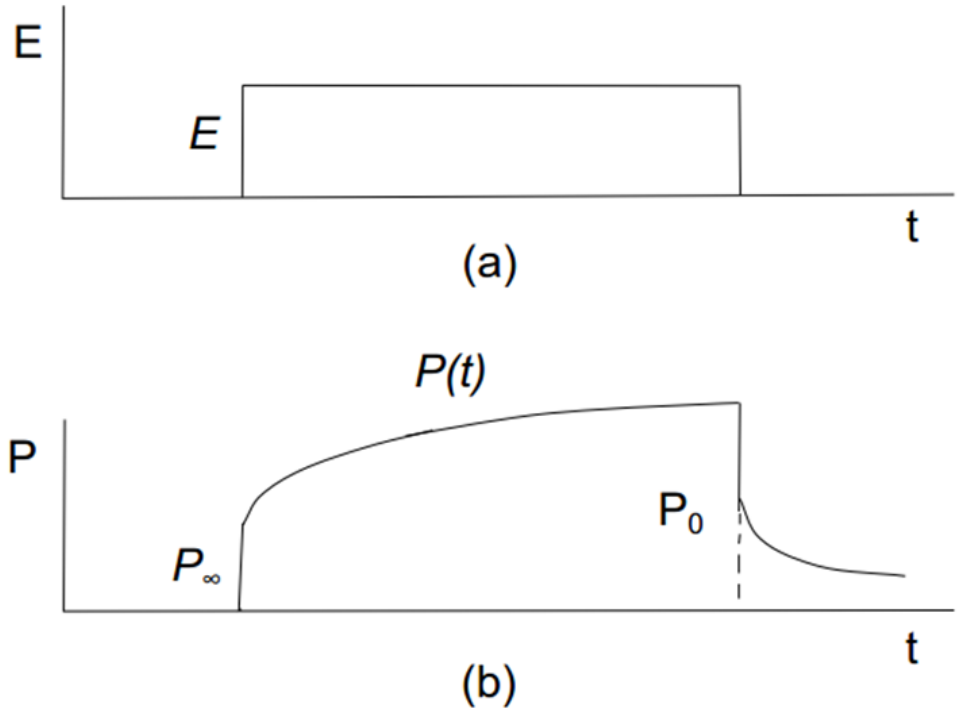

FIGURE 3.4: Effect of time dependence of electric field on polarization as shown above with (a) applied electric field and (b) corresponding polarization[84].

constant if the frequency of the applied electric field is greater than the relaxation frequency.

Quantitatively, polarization of a material on the application of an external field is not instantaneous. After the field becomes operational, a time delay exists for the material to get polarized. Similarly, if the field is withdrawn, polarization decay taking place via thermal cues obey a relaxation process in terms of a dielectric polarization function $\Phi(t)$, which is given by

$$\phi(t) = \frac{P(t)}{P(0)}, \tag{3.3}$$

where $P(t)$ is the time-dependent polarization vector. In this case, Equation (3.1) takes an equivalent form $D(t) = \epsilon_0 E(t) + P(t)$, which is explicitly given by

$$D(t) = \epsilon_0 \left[\epsilon_\infty E(t) + \int_{-\infty}^{t} C E(t - t') dt' \right], \tag{3.4}$$

where $\Phi(t)$ is the dielectric response function given by $\Phi(t) = (\epsilon_s - \epsilon_\infty)[1 - \phi(t)]$ with ϵ_s and ϵ_∞ are the two asymptotic limits of the dielectric permittivity in the low and high frequency limit respectively.

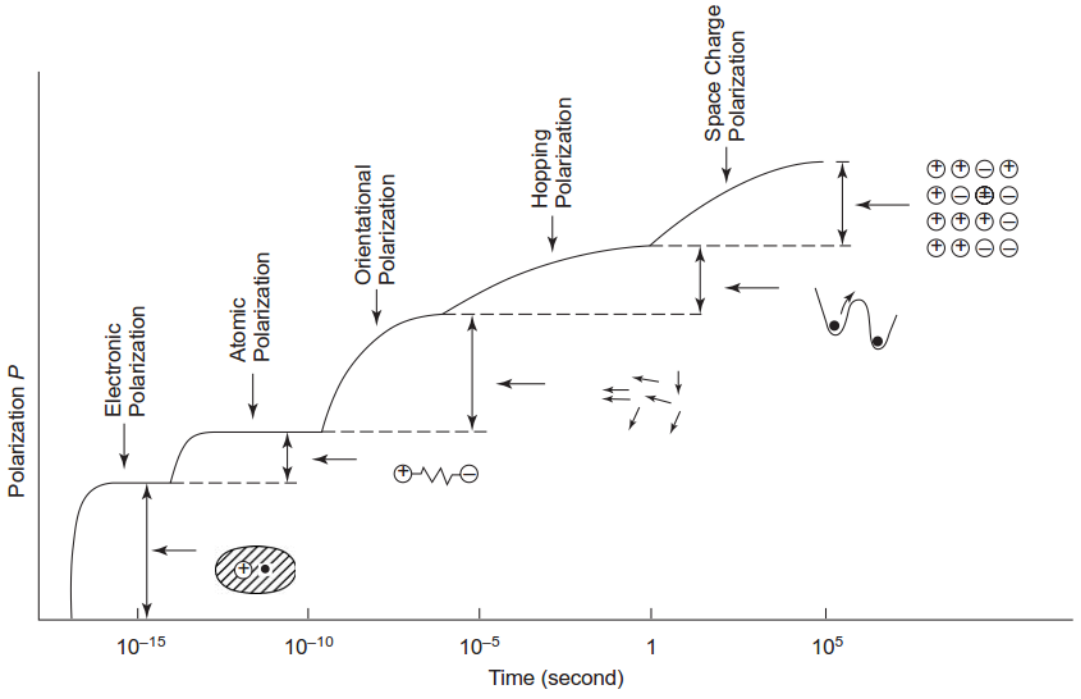

FIGURE 3.5: Polarization as a function of varying electric field for different types of polarization mechanisms[84].

For time-dependent phenomena, the dynamic response of materials subject to the field is usually determined from two distinct approaches: (a) time-domain (TD) analysis or (b) frequency-domain (FD) analysis. From a theoretical perspective,

both the analysis yield equivalent results; however, from a practical point of view each has its own advantages. Experimentally TD is a simpler; however, when it comes to data analysis and interpretation of results, FD analysis is comparatively easier to perform[47, 84].

The possibility of the electric field being either stored or lost in the dielectric material has given rise to an interdependence between conductivity and permittivity, which is expressed as $\epsilon^* = \epsilon'(\omega) - \mathrm{i}\epsilon''(\omega)$. $\epsilon'(\omega)$ is the real part of the dielectric function and $\epsilon''(\omega)$ is related to the conductivity, σ of the material. Permittivity and conductivity are inter-related, as $\epsilon'' = \frac{\sigma}{\epsilon_0 \omega}$. σ can be identified as the dielectric loss function which indicates energy dissipation. A parametrization of the dielectric loss function is also described in terms of the loss angle δ, where $\tan\delta = \epsilon''/\epsilon'$. Figure 3.5 shows the time dependence of the polarization for different regimes of polarization mechanism.

3.2.1 Dielectric Loss and Dispersion

Investigation of the dielectric spectrum leads to the dispersion phenomena ($\epsilon'(\omega)$) and loss ($\epsilon''(\omega)$) as shown in Figure 3.6. Frequency determines the underlying relaxation and resonance processes[37, 89]. Dielectric loss from relaxation processes is captured in $\epsilon''(\omega)$. The function attains its maximum at a characteristic frequency $\omega = 1/\tau$ (τ is the characteristic relaxation time of the material)[73, 145].

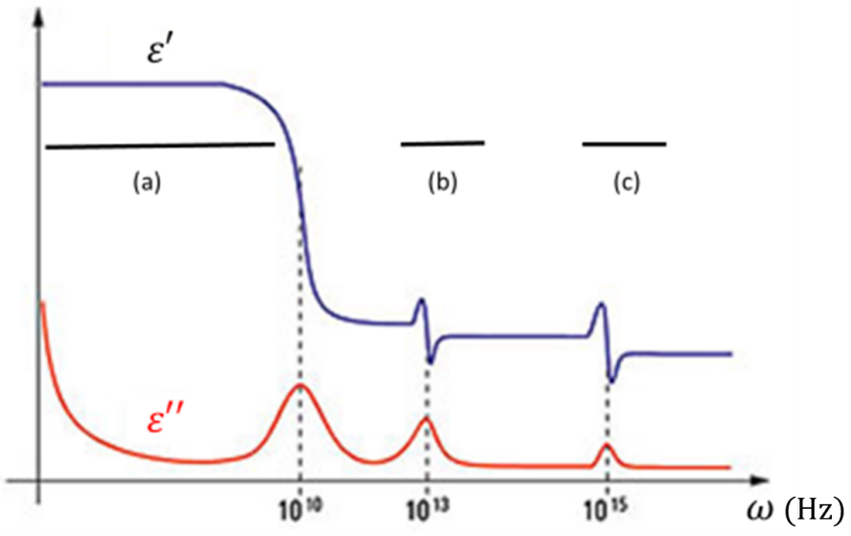

FIGURE 3.6: Dielectric response as a function of frequency, with the regions (a) showing relaxation processes and (b) & (c) showing resonance mechanisms.

3.2.2 Debye Relaxation

As we have explicitly observed in Figure 3.6, dipole relaxation phenomena are typically characterized by dispersion and absorption curves. More rigorously, the real and imaginary parts of permittivity are connected through Kramers-Kronig relations given below:

$$\epsilon'(\omega) - \epsilon'_\infty = \frac{2}{\pi} P \int_0^\infty \frac{\omega' \epsilon''(\omega')}{(\omega')^2 - \omega^2} d\omega' \quad and \tag{3.5}$$

$$\epsilon''(\omega) = \frac{2}{\pi} P \int_0^\infty \frac{[\epsilon''(\omega') - \epsilon'_\infty]\omega}{(\omega')^2 - \omega^2} d\omega', \tag{3.6}$$

where P denotes contribution of of the principal part to Cauchy's integral, and ω' is an integration variable. The rest of the quantities have been discussed previously in this chapter. Kramers-Kronig relations in this case correlate the dissipative and

reactive response of a system under the influence of an applied field.

One of the simpler models to understand the relaxation process is based on a model developed by Debye[43]. The model assumes an exponential decay of the polarization with the switching off of the applied field, as $P(t) = e^{-t/\tau}P_0$. In Figure 3.7 we have explicitly shown the permittivity frequency spectrum for a single relaxation dielectric system for an interfacial polarization response. The time

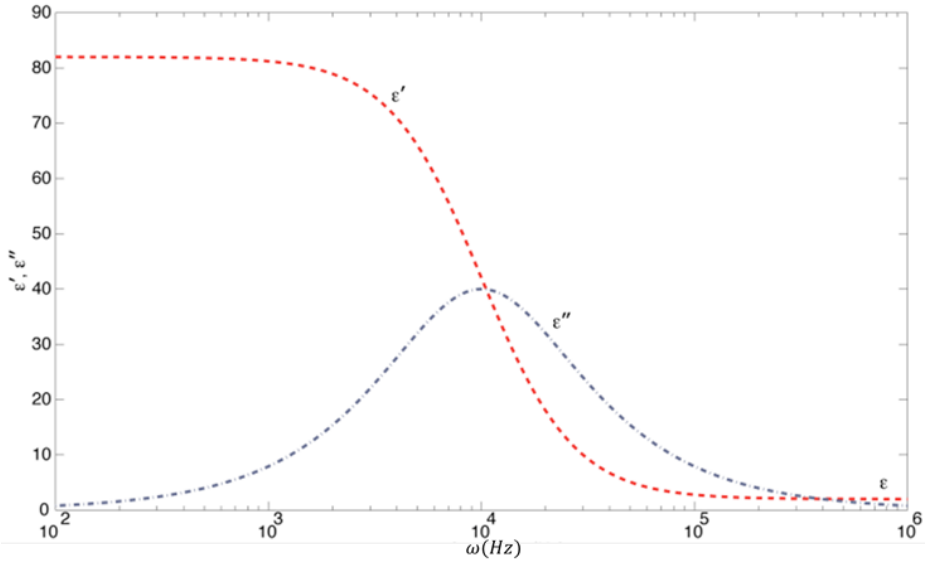

FIGURE 3.7: Dielectric permittivity spectrum for interfacial polarization[58].

scale is denoted by the relaxation time $\tau \sim \frac{4\pi\eta}{kT}$, which depends on the viscosity of the material and thermal motion in the medium. The real and imaginary parts of the permittivity which satisfies Kramers-Kronig relations in this case are given by

$$\epsilon' = \epsilon_\infty + \frac{\epsilon_s - \epsilon_\infty}{1 + \omega^2\tau^2} \quad and \tag{3.7}$$

$$\epsilon'' = \omega\tau\frac{\epsilon_s - \epsilon_\infty}{1 + \omega^2\tau^2}. \tag{3.8}$$

As Equation (3.8) shows, in the Debyean case, both ϵ' and ϵ'' are symmetric on the frequency ω.

At the molecular level the dispersion $\Delta\varepsilon = \epsilon_s - \epsilon_\infty$ is related through the Clausius-Mosotti formula given by

$$\frac{\epsilon_s - 1}{\epsilon_\infty + 2} = \frac{N}{3\epsilon_0}(\alpha + \frac{p^2}{3kT}), \tag{3.9}$$

where α is the polarizability and the polarization is approximated through Langevin function by $P = \frac{Np^2\vec{E}}{3kT}$.

3.2.3 Non-Debye Relaxation

Debye's model is characterized by a single relaxation process and thereby is not able to describe experimental results for many class of systems. It has been shown that the experimental results are more amenable to non-exponential relaxation processes. In general, a system with a distribution of shape and size is characterized by a spread of relaxation times[24, 52].

Generically, non-Debye relaxation schemes can be described in terms of a normalized function $G(\tau)$ which encodes a distribution of relaxation times. In such a scenario, the dielectric permittivity is expressed as

$$\frac{\epsilon^*(\omega) - \epsilon_\infty}{\epsilon_s - \epsilon_\infty} = \chi(\mathrm{i}\omega) = \int_0^\infty \frac{G(\tau)}{1 + \mathrm{i}\omega\tau} d\tau. \tag{3.10}$$

The decay function depends on the generalized function $G(\tau)$ denoted by

$$\phi(t) = \int_0^\infty G(\tau) e^{-t/\tau} d\tau. \tag{3.11}$$

The functional behavior of $G(\tau)$ is based on the assumption of a continuous distribution of relaxation times. However, the key aspect is the choice of an appropriate distribution function which depict the system under investigation.

Specifically, the non-Debye behavior can be encoded by using Havriliak–Negami (HN) formula [73] given by

$$\frac{\epsilon^*(\omega) - \epsilon_\infty}{\epsilon_s - \epsilon_\infty} = \frac{1}{[1 + (\mathsf{i}\omega\tau)^\alpha]^\beta}, \quad 0 \leq \alpha, \beta \leq 1. \tag{3.12}$$

In Equation (3.12), α and β denote constants determined empirically. HN equations are general relaxation framework which gives a wide spectrum of the distribution laws as enumerated below:

1. Debye Relaxation: $\alpha = 1$, $\beta = 1$,

$$\frac{\epsilon^*(\omega) - \epsilon_\infty}{\epsilon_s - \epsilon_\infty} = \frac{1}{1 + \mathsf{i}\omega\tau}. \tag{3.13}$$

2. Cole-Cole (CC) Relaxation[37]: $\beta = 1$, $0 \leq \alpha \leq 1$

$$\frac{\epsilon^*(\omega) - \epsilon_\infty}{\epsilon_s - \epsilon_\infty} = \frac{1}{1 + (\mathsf{i}\omega\tau)^\alpha}. \tag{3.14}$$

3. Cole-Davidson (CD) Relaxation[42]: $\alpha = 1$, $0 \leq \beta \leq 1$

$$\frac{\epsilon^*(\omega) - \epsilon_\infty}{\epsilon_s - \epsilon_\infty} = \frac{1}{[1 + \mathrm{i}\omega\tau]^\beta}. \tag{3.15}$$

The parameters α and β needs to be chosen properly depending on the nature of the physical system to get a better fit. As we have mentioned earlier, the non-Debye response is due to the presence of several underlying relaxation processes.

Chapter 4

Dielectric Behavior of Biological Materials

4.1 Introduction

Measuring the electrical properties of biological materials imparts valuable insights into a wide variety of biophysical processes. Biological systems interact with the electromagnetic energy through the dielectric properties of the biological material. In general a biological specimen can be construed as a conductor which is made up of tissues having different electrical properties. Thus, biological samples exhibit a large extent of heterogeneity on length scales ranging up to several microns. This property has made the investigation of biological specimens through electrical characterization techniques very promising both from a fundamental and diagnostic probe point of view.

Measurement of dielectric properties of the tissues can shed light on the tissue structure and composition, and can also detect differences between a normal and tumor cell. In this context impedance techniques have been utilized to look into the dielectric properties of cells and tissues[122, 126]. For biological samples, the electromagnetic field interacts with the segments in the sample which have a net non-vanishing component of electric multipole moment, which in turn arises mainly from polar molecules in the macromolecules consisting of proteins and lipids in the cells.

High membrane potential results in an enhanced net negative charge inside the cell or mitochondrion, which induces a higher electric dipole moment per cell (or mitochondrion). For a low-frequency applied electric field E, a higher average bulk dielectric constant of the entire suspension is obtained. Consequently, polarization becomes very close to the displacement field as, $P = D - \epsilon_0 E = \epsilon_r \epsilon_0 E - \epsilon_0 E \sim \epsilon_0 \epsilon_r E = D$, for $\epsilon_r \gg 1$. Since P is the average dipole moment per unit volume, increasing the dipole moments of numerous cells or mitochondria in suspension will increase P, and therefore ϵ_r of the entire suspension[130, 132].

As a general prescription emphasizing our earlier discussion, the response to the applied electric field is described by: (a) conductivity (σ), which is a measure of the ability of the cells to conduct, and (b) permittivity (ϵ), which depicts the electric energy storage capacity of the cell. The dielectric behavior in the biological samples is due to the mobility of the ions and bound charges within the tissues. The motion of the ions in the aqueous environment produces a

conduction current I_c within the cells, described in terms of temperature-dependent σ, as the motion of the ions are affected by thermal fluctuations. The polarized bound charges from the double layers at membrane surfaces give rise to complex dielectric behavior through the displacement current I_d, which generates a time-varying electrical phenomena. For the majority of cases, biological specimens are characterized by a large dielectric constant at low frequencies and step-like decay at high frequencies. From the molecular perspective, the varying electric field forces the cell membrane to structurally organize by undergoing a variety of intramolecular transitions and intermolecular processes. Thus, the frequency dependency of dielectric properties of cells has helped to investigate biological processes arising from different underlying mechanisms. The presence of the membrane potential has a specific effect on the dielectric behavior of cell suspensions[132].

4.2 Electrical Properties of Biological Samples

In biological materials, charge distributions arise from electrical double layers[50, 98]. The charges are characterized by permanent dipole moments which are localized around membrane surfaces or solvated macromolecules like proteins, as shown in Figure 4.1. The modulation of the electric double layer is maintained through an ionic concentration gradient and the potential ϕ across the charged surface. The equilibrium concentration of the charges is dictated by

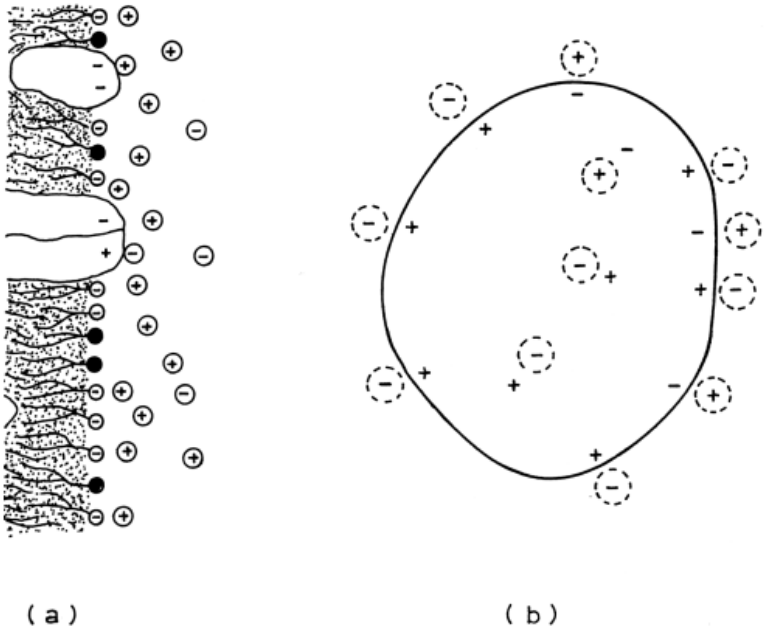

FIGURE 4.1: Charge distribution from double layers at (a) membrane surfaces and (b) macromolecule[4].

the Boltzmann distribution, which for most practical purposes can be described by an exponential decay law, as shown in Figure 4.2, where the Debye screening length is given by

$$\lambda_D = \sqrt{\frac{\epsilon_0 \epsilon_s kT}{2z^2 q^2 n_0}}, \tag{4.1}$$

where z is valency, q the fundamental electron charge, and n_0 the ion concentration of electrolyte. For most biological materials λ_D is pretty small, which imparts large capacitance to the samples. As an illustration for the protein solutions, the decay function for electrical polarization is given by

$$G(t) = \Delta\epsilon \cdot \Gamma(t), \tag{4.2}$$

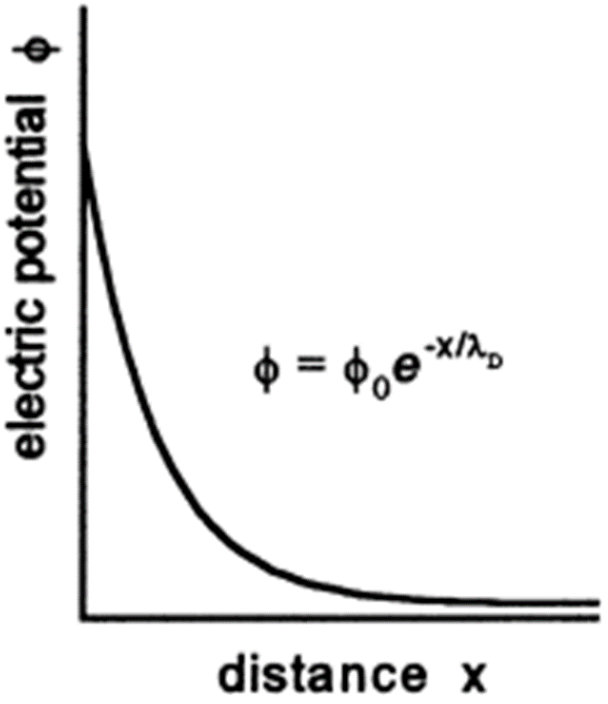

FIGURE 4.2: Distribution of electric potential across a double layer.

where $\epsilon \propto \mu C/2kT\epsilon_0 M$ is the dielectric dispersion and $\Gamma(t)$ is the dipole correlation function. μ is the dipole moment of the protein molecule, C denotes protein concentration, M is the molecular weight of protein, and T is the absolute temperature. The dipole correlation function of the protein arises from combination of motion for the Brownian, intramolecular, and slow motion modes. Electrical properties are dependent on pH and conformation of the molecules.

From a rigorous point of view, the cell is inherently an electrochemical system generated from fluctuations in ionic concentrations arising from the cellular components and partly from redox reactions. Thus, fundamentally electrical properties of a cell depends on the electrical behavior of the intracellular cytoplasm and cell membrane. To describe the physics of this

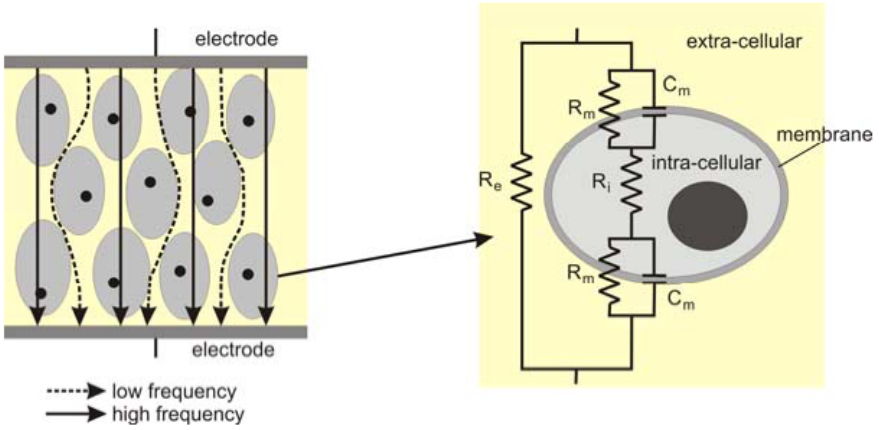

FIGURE 4.3: Circuit model of the cell, R_e: resistance of extracellular medium R_i: resistance of intracellular medium, C_m: capacitance of cell membrane[87].

system, a basic model is depicted as resistor with different resistances using an extracellular and intracellular ionic solution consisting of charged ions and proteins. The cellular membrane acts as a capacitor which plays a role in charge storage. The ion channels can be depicted by the conductance of the membrane. For the simple scheme, the model is drawn in Figure 4.3. The circuit model in Figure 4.3 can be mathematically described by a simple non-Debye like the Cole-Cole relaxation process we saw in Equation (3.14), whose corresponding circuit equivalent becomes

$$\frac{Z - R_\infty}{R_e - R_\infty} = \frac{1}{1 + (\mathrm{i}\omega\tau)^\alpha}, \quad 0 \leq \alpha \leq 1, \tag{4.3}$$

where $R_\infty = \frac{R_i R_e}{R_i + R_e}$ and the characteristic relaxation time is given by $(R_i + R_e)C$. Understanding the electrical properties of biological cells and tissues has extreme importance, both from a fundamental, as well as from a diagnostic perspective.

This has led to a large collection of studies, for the practical implementation of the techniques using electric double layer models[132].

4.3 Relaxation Processes in Biology

As we have noted in Chapter 3, electric polarization is not instantaneous, and has an associated relaxation time τ. As a consequence of this behavior, the phenomena of dielectric dispersion arises, making the permittivity frequency dependent. The biological cells and tissues under the influence of applied electrical field are characterized by a frequency-dependent impedance fingerprint[130, 132]. The dielectric spectrum of the biological samples as shown

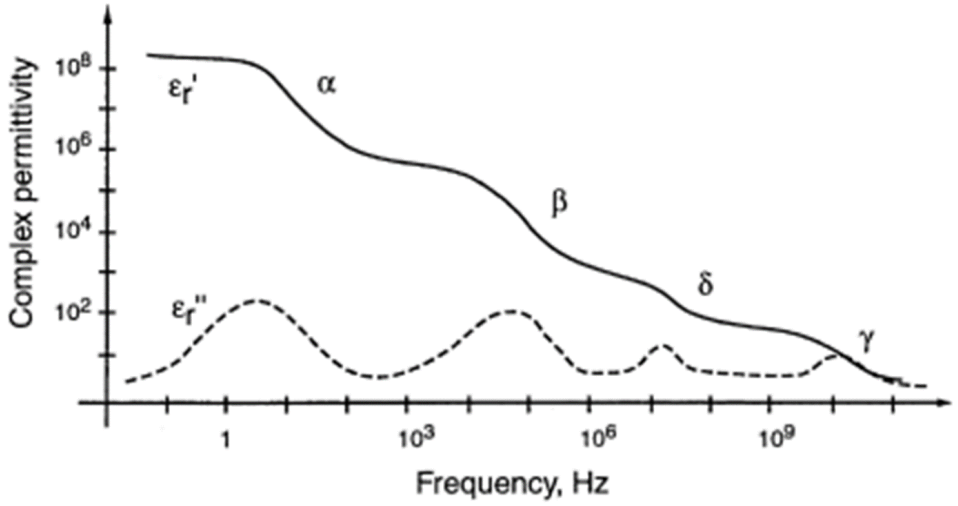

FIGURE 4.4: Dispersions regions of the biological sample[74].

in Figure 4.4 has some distinct characteristics based on frequency ν as listed below[8, 23]:

- $\nu \leq$ **100Hz** : Steep dielectric permittivity is characterized in this zone.

- $\nu \approx \mathbf{1 - 10kHz}$: Processes are dominated by ionic mechanisms with the relaxation phenomena characterized by α dispersions.
- $\nu \approx \mathbf{10 - 100kHz}$: β dispersion is dominant in the radio frequency region which arises from polarization of cellular membranes. They are instrumental as blockages for separating ion flow between extra cellular and intra cellular media.
- $\nu \approx \mathbf{1 - 10MHz}$: Relaxation of bound water molecules in vicinity of the biological macromolecules fives rise to δ dispersions.
- $\nu \approx \mathbf{1 - 100GHz}$: γ dispersions in the microwave frequency range arise due to relaxation of water molecules in suspension.

4.3.1 α Dispersion

The underlying mechanism for this type of dispersion stems from the effect of electrical double layers and ionic surface charges of the membrane neighbourhood. The ions percolate through the membrane via the counterion layer, generating an electric field which is perpendicular to the applied field. In Fig 4.5 we have shown the α dispersion through ionic movement. The direction of the motion of counterions induces a dipole moment aligned in the direction of electric field. The distance moved by the charges is closely related to the diameter of the cell, which gives large induced dipole moments. This model developed by Schwarz[145], assumes that the counterion movement occurs

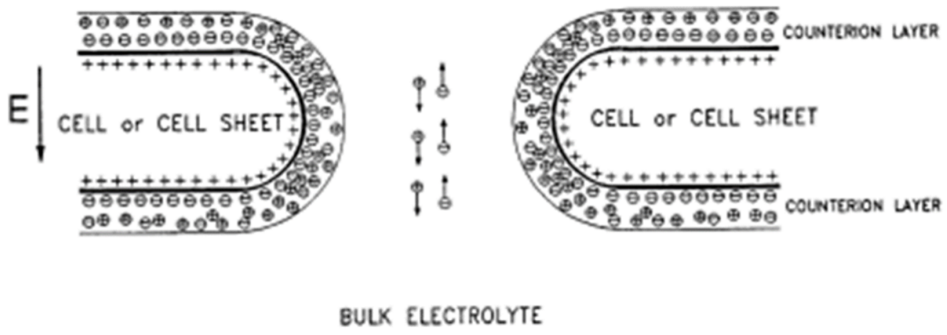

FIGURE 4.5: Ionic movement giving rise to α dispersion[89].

through diffusion and electron migration along the membrane surface. Restriction is also imposed on particle exchange with bulk.

To elucidate the details, the generic description of the dispersion is based on the assumption of spherical colloidal particles. An underlying assumption for the description is that ion diffusion takes place only within the double layer, given by[89] the Cole-Cole relaxation law,

$$\frac{\epsilon - \epsilon_\infty}{\Delta\epsilon} = \frac{1}{1 + (\mathrm{i}\omega\tau)^\alpha}. \tag{4.4}$$

Here $\Delta\epsilon$ is given by

$$\Delta\epsilon = c_0\epsilon_s \frac{9(\frac{R}{\lambda_D})^2}{16} + \frac{2 + \frac{R}{\lambda_D}}{1 + \frac{R}{\lambda_D}}, \tag{4.5}$$

where c_0 is the particle concentration, z the number of valence ions, q, the electron charge, R the radius of particles, ϵ_s is the low frequency limit of permittivity, and λ_D is the Debye screening length as previously explained. The relaxation time is given by $\tau = \frac{zqR^2}{\mu kT}$, where μ is the induced dipole moment from the double layer.

One of the limitations of the α dispersion stems from an ambiguity from a double layer effect. The ambiguity arises due to the electrode polarization in addition to the membrane surface polarization, where ion charge distribution is detected at the surface of the electrode. This cloaks dispersion of the sample which leads to high dispersions at low frequencies[45, 132].

Though α dispersions on colloidal suspensions have been successful models, still for living cell suspension, new observations have been projected relating α dispersion to membrane potential[22, 44, 47, 53, 99, 111, 131, 132].

In this context the Prodan model[132], which we use to validate our results, pertains to the range of frequencies corresponding to α response, and shows a direct correlation between low-frequency α dielectric response and membrane potential. The basic idea is that a higher membrane potential results from a greater negative charge within the cell or organelle, which affects its dipole moment induced by an applied field, as shown in Figure 4.6 below. This model, discussed in greater detail in section 8.1, has been used to correlate changes in impedance with changes in membrane potential.

4.3.2 β Dispersion

As we have mentioned earlier, the β dispersion emerges from interfacial polarization due to the accumulation or barrier of ions on the membrane surface. The weak temperature-dependent dispersion is an important tool for the measurement of membrane capacitance and fluid resistivities in intra- and

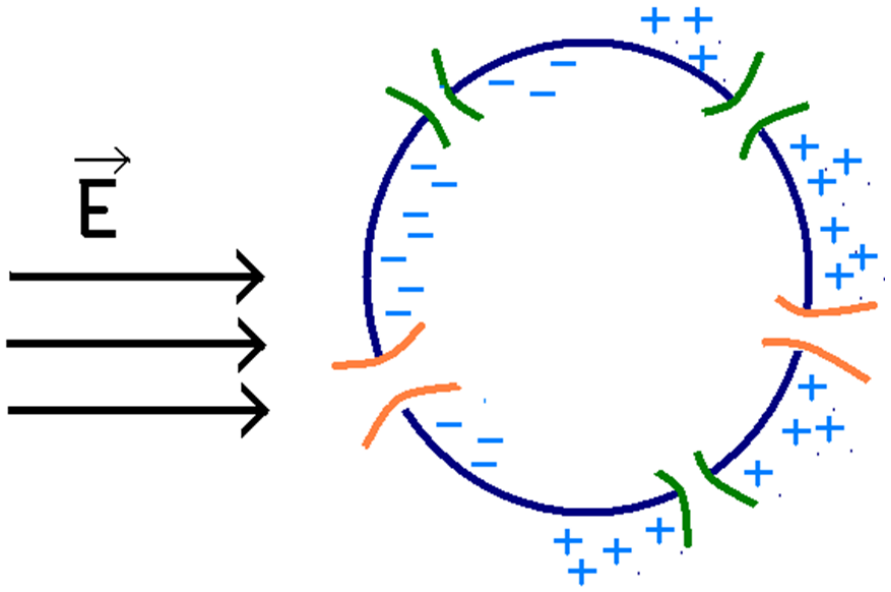

FIGURE 4.6: Polarization in presence of electric field[130, 132].

extra-cellular environment. In Figure 4.7 the frequency dependence of beta dispersion is depicted in detail. At low frequencies, cells act as non-conducting

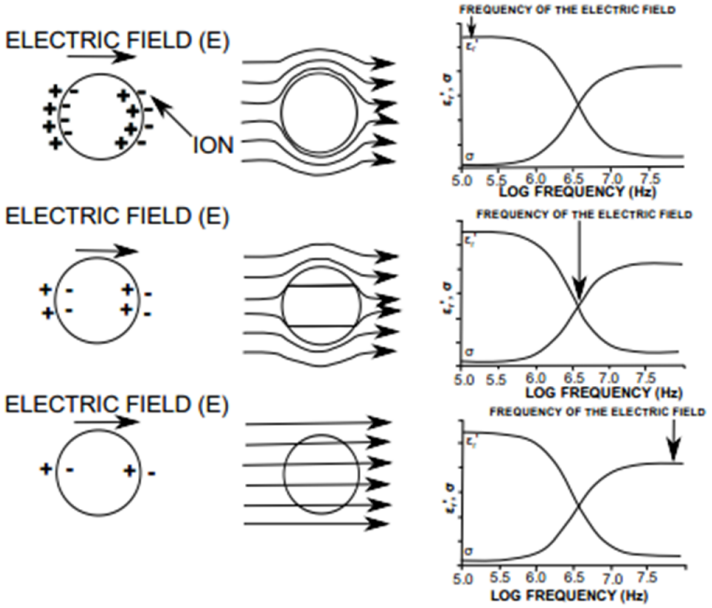

FIGURE 4.7: β dispersion for spherical shell suspensions. Frequency increases from top to bottom[7].

spherical particles, and experience a current through them. This implies an increase in permittivity and drop in conductivity. For higher frequency ranges, Prodan *et al.*'s work[132] clearly establishes that relaxation time is small, which entails no substantial change of current through the cell. This implies a conductivity increase and permittivity loss, which ties together well in explaining our data.

4.3.3 δ Dispersion

Substantially diminished δ dispersion arising from relaxation of bound water enclosed in biological macromolecules has been observed in biological suspensions in regions between much pronounced β and γ dispersions[59, 68, 130]. In general, for a biological system along with all its components, the dielectric dispersion curve depends on a variety of factors. As a matter of fact, precise determination of bound water crucially depends on the relative amplitude of γ and δ dispersion. Eventually the data interpretation is also not straightforward, and requires appropriate mixture theory. We will discuss this briefly in Chapter 5.

A simpler model[31] for the estimation of bound water is obtained by calculating the water of hydration, where a spherical cavity is assumed for a hydrated molecule of low permittivity buried in a medium of high dielectric constant. This is shown in Figure 4.8. The results for the bound water can be

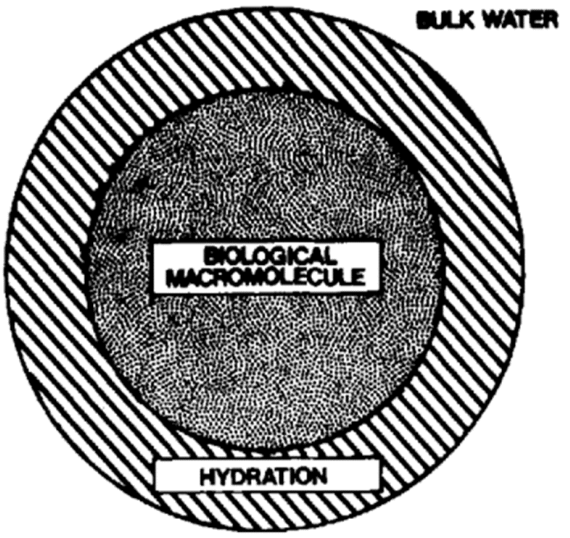

FIGURE 4.8: Hydrated biological macromolecule [31].

found from permittivity data at frequencies close to 1 GHz using the formula

$$v\frac{\epsilon_p - \epsilon_w}{\epsilon_p + 2\epsilon_w} = \frac{\epsilon_1 - \epsilon_w}{\epsilon_1 + 2\epsilon_w}, \tag{4.6}$$

where ϵ_p and ϵ_w are the frequency-dependent relative permittivities of the biological macromolecule and water, respectively. From a physical point of view, some studies have directly observed the role of hydration for the lower values of δ dispersion[117, 124, 132, 140], implying the role of protein side chain rotation.

4.3.4 γ Dispersion

Relaxation of free water molecules has a distribution with a median around 10 GHz, which gives rise to γ dispersion at microwave frequencies. The relaxation frequency for the water in bulk is larger than the water on the protein surface.

In this frequency zone, conductivity σ is enhanced due to the dielectric relaxation of conducting water molecules. A biological environment with a very high water content has a comparable γ dispersion to that of water. In the frequency zone for γ dispersion, the frequency-dependent dispersion is given by

$$\epsilon^*(\omega) - \epsilon_\infty = \frac{\epsilon_s - \epsilon_\infty}{1 + (\mathrm{i}\omega\tau)^\alpha} + \frac{\sigma}{\mathrm{i}\omega\epsilon_0}. \tag{4.7}$$

In Equation (4.7), the dispersion has contributions from Cole-Cole behavior, along with the effect of conductivity which takes into account low frequency polarization effects for the dipolar dispersion of water and electrolyte dispersion. A significant number of studies[54, 60, 126, 144], have illustrated that the correlation between water content in the cells and ϵ_s is direct. In general, the parameter α is non-vanishing for cells immersed in water, with a larger relaxation time, indicative of a restricted rotational motion of the water molecules in the cells[49, 146, 147].

Chapter 5

Materials and Methods

5.1 Materials

There are two important chemicals used in this work: first, trifluorocarbonylcyanide phenylhydrazone(FCCP), molecular formula $C_{10}H_5F_3N_4O$ with a molecular weight of 254.17 g/mol; and, second, dihydroxyphenylethylamine(dopamine), with the molecular formula $(HO)_2C_6H_3CH_2CH_2NH_2$ and a molecular weight of 153.18 g/mol. FCCP is 95% soluble in ethanol and dopamine is water-soluble. For lab uses, dopamine is used in solvent form as dopamine hydrocloride $(HO)_2C_6H_3CH_2CH_2NH_2HCl$. In the next two sections we discuss in detail the chemicals used.

5.1.1 FCCP

FCCP is a protonophore (H+ ionophore) and uncoupler of oxidative phosphorylation in mitochondria. The chemical structure with the aromatic ring is shown in Figure 5.1. It abolishes the obligatory linkage between the respiratory chain and the phosphorylation system which is observed with intact mitochondria. All protonophores are small amphipathic molecules which dissolve

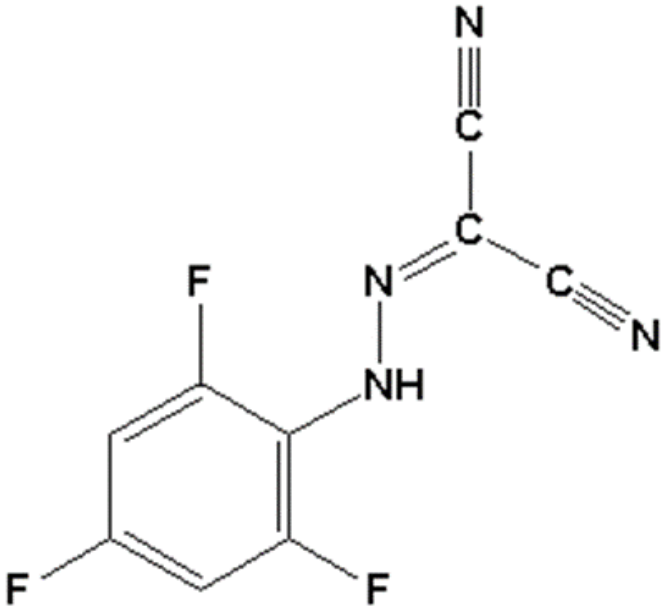

FIGURE 5.1: Chemical structure of FCCP.

in phospholipid bilayers and enormously increase their ionic permeability. FCCP has dissociable protons allowing it to carry protons from the intermembrane space to the matrix which collapses the pH gradient. FCCP shields the electric charge as the ion passes through the membrane, providing a polar environment for the ion and a hydrophobic face to the outside world. It is, therefore, capable of depolarizing plasma and mitochondrial membranes. This influences the

collapse of the chemiosmotic gradient by dissipating protons across the inner mitochondrial membrane. In Figure 5.2, we have depicted the proton-moving aspect of FCCP. The top panel of the figure depicts where protonation/deprotonation of FCCP occurs in the presence of a weak acid. In the bottom panel of the figure, the uncoupler is shown after the protonotaion/deprotonation mechanism.

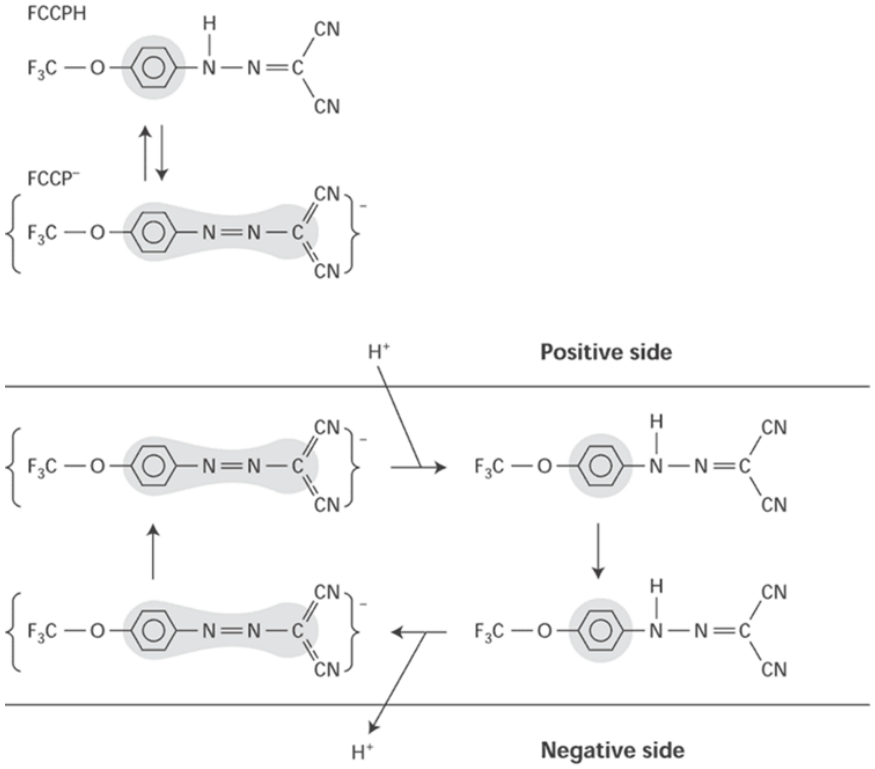

FIGURE 5.2: Protonopheric mechanism of FCCP uncoupler[110].

In the presence of an electrochemical proton gradient across the membrane, FCCP will become protonated, and thus, pick up a proton on the positive side of the membrane, move across the membrane in the neutral form, and lose the proton on the negative side. This is driven by the electrochemical proton gradient. In

the negative form, FCCP will be driven back out across the membrane by the membrane potential. The net result is the movement of one proton from the positive to the negative side of the membrane. This results in the dissipation of the electrochemical proton gradient, and the movement of one electrical charge from the negative to the positive side of the membrane. This, in turn, results in the dissipation of the electrical gradient. Upon addition of FCCP there is a clear indication from Figure 5.3, that there is an immediate and dose-dependent increase in oxygen consumption. FCCP caused significant increase in O_2 consumption at

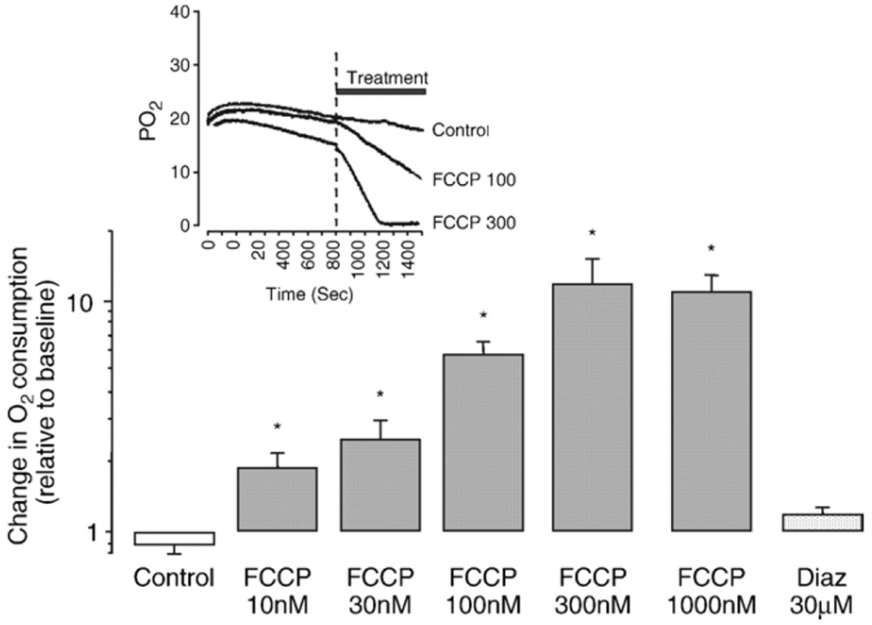

FIGURE 5.3: O_2 consumption during treatment with FCCP[29].

all concentrations, indicating significant mitochondrial uncoupling. In section 7.2, this has been further validated by use of the impedance spectroscopy technique.

5.1.2 Dopamine

Dopamine has been called our "motivation molecule". It is basically a neurotransmitter of the catecholamine and phenethylamine families that plays a number of important roles in the human brain and body. The severe mental illness schizophrenia has been shown to involve excessive amounts of dopamine in the frontal lobes of the brain, whereas too little dopamine in the motor areas is responsible for Parkinson's disease, which involves uncontrollable muscle tremors.

Figure 5.4 presents the structure of dopamine. Study of the neurotransmitter

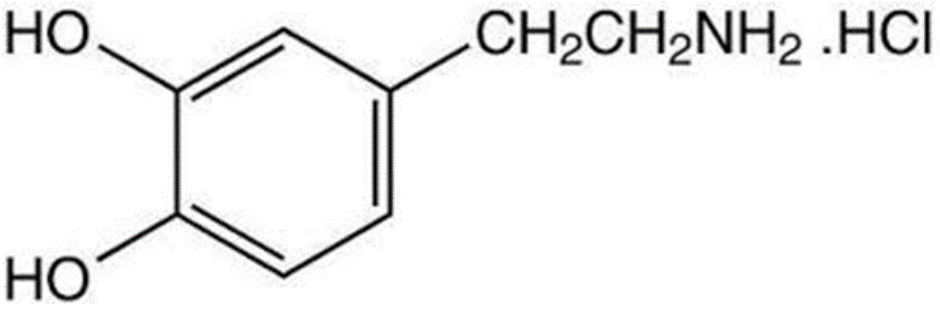

FIGURE 5.4: Chemical structure of dopamine.

dopamine may provide important clues for the treatment of such neurodegenerative diseases and stimulate further research in the various fields of biophysics, physiology, and psychology. A number of observations further suggest a role for mitochondrial dysfunction in the pathophysiology of such diseases.

All chemicals used in this study were bought from Sigma Chemical Co. (St. Louis, MO, USA. Solutions of dopamine in distilled water were made with various concentrations. Knowledge of the redox state of dopamine is critical. The electrochemical behavior of dopamine strongly depends on the pH values of

the solution. This is determined by measuring the pH of dopamine for each concentration[104]. As shown in Table 5.1, the pH range indicate that dopamine seems to coexist in all three forms: cationic, anionic, and zwitterionic. This is an

TABLE 5.1: Temperature and pH of different concentration of dopamine.

Temperature (^{o}C)	Concentration	pH
23.5	500nM	4.93
23.0	1μM	5.09
23.1	0.5mM	4.13
23.3	1M	4.91

important parameter when determining the inhibitory effect on the mitochondrial function and the site at which the interaction occurs. Dopamine, being an oxidisable neurotransmitter, contributes to the conductivity variation. When dopamine is completely oxidized to dopamine-o-quinone, as in Figure 5.5, two electrons from dopamine are transferred to the electrode and two H+ ions stay in the solution, which actually contributes to the conductivity variation. This is further discussed in Chapter 7. In Figure 5.6, we see that both the

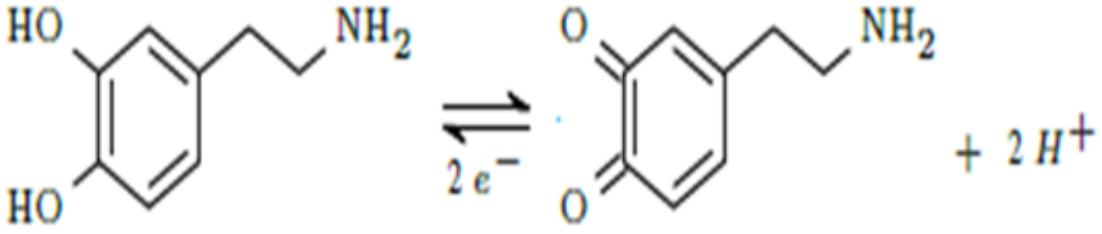

FIGURE 5.5: Increase of capacitance and conductivity of dopamine with concentration.

capacitance and the conductivity of dopamine are directly proportional to the

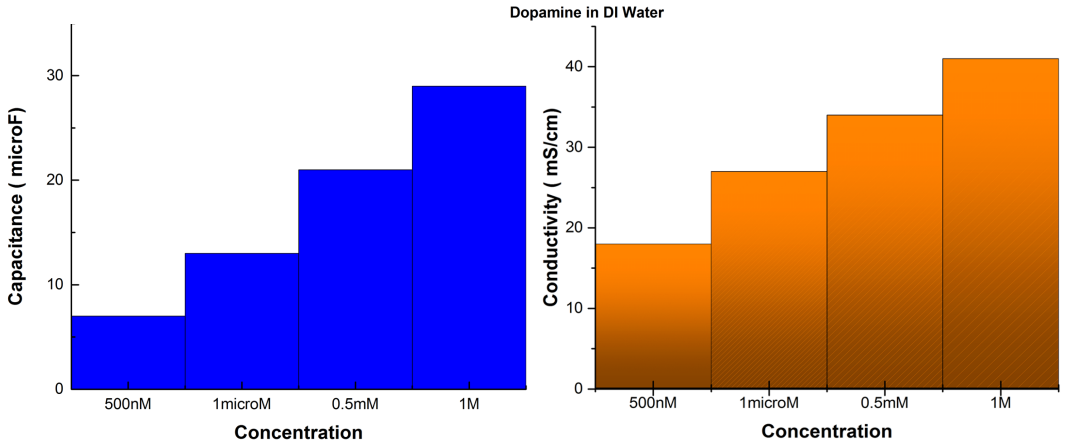

FIGURE 5.6: Dopamine and oxidation reaction[30].

concentration. Hence resistivity of dopamine, is inversely proportional, and the dielectric constant is directly proportional to the concentration, as shown in Figure 5.7.

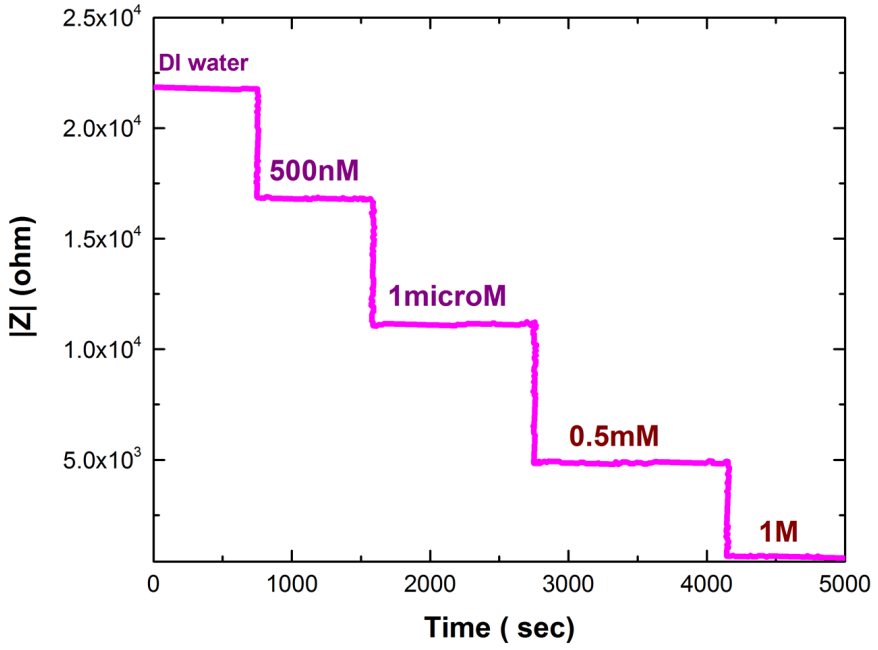

FIGURE 5.7: Temporal variation of $|Z|$ for different concentrations of dopamine in DI water at the operating voltage 10mV and frequency at 2MHz.

A higher concentration of dopamine is related to hallucination, which is a

psychological phenomenon[2]. The change of impedance with dopamine concentration, seen in from Figure 5.7 suggests that the electrochemical behavior of dopamine is important. In Chapter 7 it will be shown how this behavior of dopamine also has a vital effect in physiological functions[162].

5.2 Research Design

5.2.1 Isolation of Mitochondria from Mice Heart

The experimental protocol and program care were reviewed and approved by the University of Houston Institutional Animal Care and Use Committee. (Protocol number 13-016 – John H Miller, Title - "Physical Mechanisms of Mitochondrial Electron and Proton Transport"). Each animal employed for tissue harvest of mammalian mitochondria for the coupled/uncoupled experiments was subjected to high standards of care. For mitochondrial extraction we used isoflurane for anesthetizing mice, followed by immediate euthanization by cervical dislocation, after which the tissue was removed. The mice were decapitated.

The mice used here were available preconditioned from Charles River Laboratory and Jackson Laboratory. Each experiment used a minimum of 5 mice hearts. Experiments took place usually 3-4 times per month. Mitochondria were isolated with minor modifications, using the protocol described in Palmer *et al.*[119]. The measurements were done on freshly pelleted out mice cardiac

mitochondria extracted using the typical extraction protocol mentioned above. The protocol consisted of the steps listed below in detail:

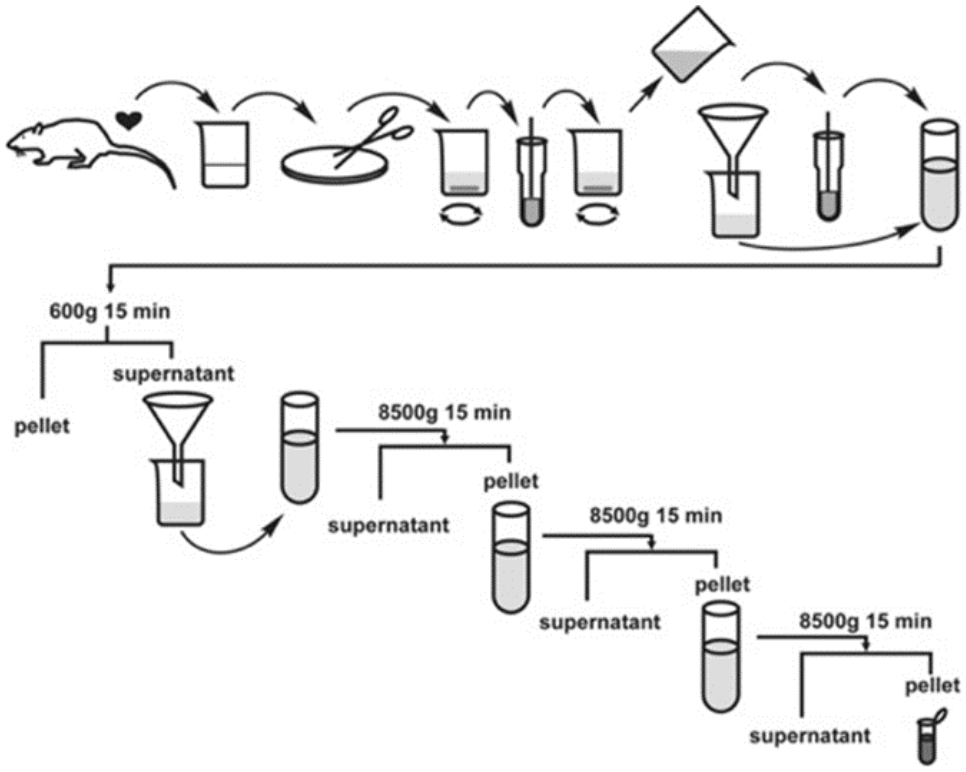

FIGURE 5.8: Scheme demonstrating the step-by-step procedure of isolation of mice heart mitochondria[129].

- The mouse was isofluoraned for 15 seconds;
- Heart was extracted, weighed and placed in a glass test tube on ice;
- The heart was washed four times with Buffer A and then minced on ice;
- The minced heart was put in 6 ml of Buffer B and then into polytron treatment at low for 60 seconds;
- The minced treated heart was then centrifuged for 600 g for 10 min at 4^{o}C and then the supernatant was saved;

- The pellet was resuspended in 4 ml of Buffer A and then centrifuged 600 g for 10 min at 4^oC;
- The supernatant was combined and then centrifuged again at 3000 g for 15 minutes at 4^oC;
- Finally, the pellet was resuspended in Buffer C.

The buffers used were:

1. Buffer A: 40.08 g 220 mM mannitol (MW=182.17) + 23.96 g 70mM sucrose (MW=342.3) + 1.05 g 5 mM Mops (MW=209.3) in 1 liter of water.
2. Buffer B: 0.076 g 2 mM EGTA (MW=380.4) + 4 ml of 5% FAF BSA for 0.2 % BSA in 100 ml of Buffer A.
3. Buffer C: 0.019 g 0.5 mM EGTA in 100 ml Buffer A.

Mice cardiac mitochondria were obtained and the concentration determined to be 4 mg/ml by spectrophotometer, based on the Biuret Method[56, 79].

An important parameter is the time-length of the procedure; the isolation had to be performed as quickly as possible and the obtained preparation had to be used immediately. So, it was important that mitochondrial samples be kept ice-cold during preparation and that functional studies be performed within a relatively short time ($\sim$4 hr) on viable mitochondria.

Once we performed the extraction, we immediately followed with several assays. We began by performing a traditional Biuret assay to determine the concentration of mitochondria. This is a necessary step for all subsequent assays. This also allowed us to determine our yield. We extracted approximately 22 mg

from our mouse isolation. The starting weight was approximately 0.400 gm of mouse heart.

5.2.2 Oxygen Consumption

Mitochondrial respiration is a key element of cell physiology. Respirometry reflects the function of mitochondria as structurally intact organelles. It is the aerobic flux of life. Multiple substrate uncoupler–inhibitor titration protocols for analysis of oxidative phosphorylation improve our understanding of mitochondrial respiratory control and the pathophysiology of mitochondrial diseases.

Oxygen is the terminal acceptor in the mitochondrial respiratory chain by Complex IV, cytochrome oxidase, which produces water in the process and pumps protons from the matrix to the intermembrane space. Determination of mitochondrial oxygen consumption is carried out by means of a Clark-type electrode, as shown in Figure 5.9. The Clark-type electrode is one that measures oxygen on a catalytic platinum surface. The classical Clark-type is basically composed of two electrodes, a cathode and anode.

The electrical signal arises from the current developed on the cathode. The voltage supply unit feeds the system with electrons, and when oxygen diffuses through an oxygen permeable membrane (commonly Teflon-based) to the platinum electrode, the cathode is reduced. The current is proportional to the oxygen tension in the solution in which the mitochondria were placed. The silver ions combine with chloride ions in solution, precipitating silver chloride over the silver

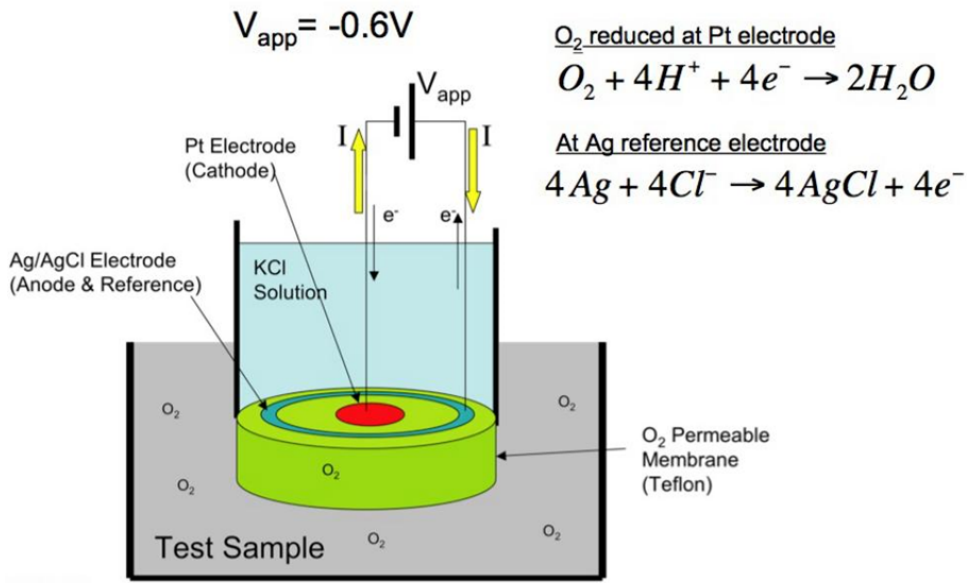

FIGURE 5.9: Clark oxygen electrode[148].

electrode, according to the overall equation

$$4\mathrm{Ag(s)} + 4\mathrm{Cl}^- + \mathrm{O}_2 + 4\mathrm{H}^+ + 4\mathrm{e}^- \longrightarrow 4\mathrm{AgCl}.2\mathrm{H}_2\mathrm{O}.$$

The electric signal can pass through an analog to-digital converter and later be analysed through a signal transducer coupled to a personal computer.

In our experiment, a Mitocell micro-respirometer (Strathkelvin Instruments Limited, Scotland) was the oxygen electrode used, as shown in Figure 5.10. It was comprised of a 782 oxygen meter, 1302 oxygen electrode, MT200 respirometer, and respirometry software. This software included a program for mitochondrial research that calculated State 3 and State 4 respiration rates, P/O ratios, and RCR. The MT 200 respirometer consisted of a glass chamber of volume 100 microliters, a transparent polycarbonate plunger, and an integral

FIGURE 5.10: Mitocell miniature respirometer model MT 200.

magnetic stirrer. The substrates, inhibitors and uncouplers were injected directly into the chamber with corresponding Hamilton syringes.

The respiratory rates of the mitochondrial suspension were determined using the oxygen probe at 25^{o}C, with continuous stirring. The substrate used included 5 mM succinate, which evaluated the integrity of the TCA cycle and electron transport chain. Oxygen consumption rates were expressed in nmoles O_2/min/mg dry weight. The respiratory parameters measured are shown in Figure 5.11.

The different states of oxygen consumption method are listed below

1. **State 1:** Oxygen consumption rate of mitochondria alone prior to addition of exogenous substrate or ADP. Oxygen consumption rate was minimal.
2. **State 2:** Mitochondrial respirations in the presence of substrate but in the absence of any added ADP.
3. **State 3:** Maximal stimulated mitochondrial respirations, which were initiated by adding 1mM ADP (in the presence of substrate).

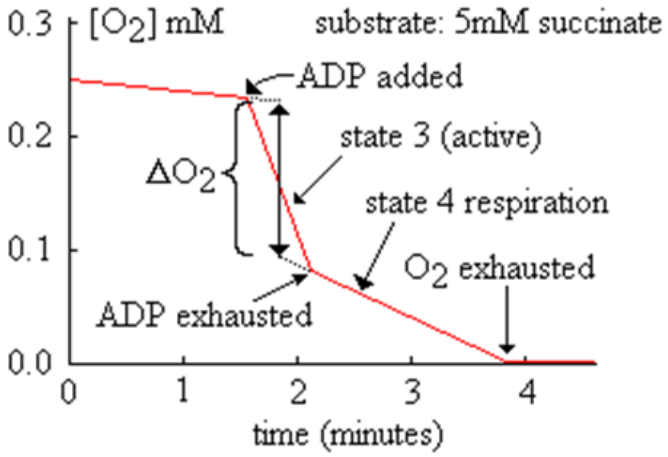

FIGURE 5.11: Oxygraph recordings.

4. **State 4:** Mitochondrial respiration in the absence of ATP synthesis, which was achieved by adding the uncoupler FCCP 2μM. An increase in State 4 respiration would be suggestive of mitochondrial uncoupling.

Respiratory control ratio (RCR) is the ratio of State 3 to State 4 respirations. This ratio was used as a general index of the viability of the mitochondrial preparation. Low RCR ratios raised the possibility of mitochondrial damage. Typical RCR values ranged from 3-10.

The P/O ratio for mitochondrial oxidative phosphorylation is the number of ATP molecules that are synthesized for each two electrons that enter the electron transport pathway. Thus, it is the relationship between ATP synthesis and oxygen consumption by measuring the decrease in oxygen concentration during rapid burst of State 3 respiration after adding a known amount of ADP. In Figure 5.12 (a) we present a snapshot taken at the time of RCR recording. In Figure 5.12 (b) and (c) we show calculated RCR of mitochondria for two different samples. The

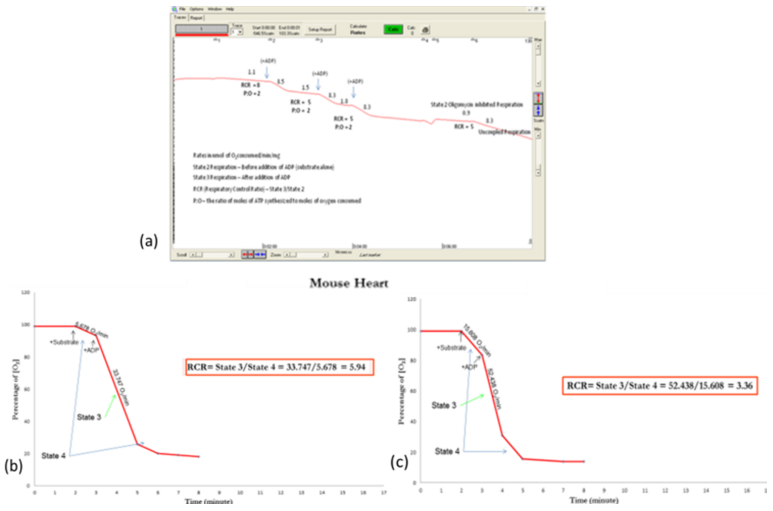

FIGURE 5.12: (a) Snapshot from PC during measurement of RCR, (b) and (c) RCR measurements for different state configurations.

results clearly indicate that RCR $>$ 3.4, which confirms the functional integrity and coupling of mitochondria.

Figure 5.13 depicts the result when substrate succinate was added, triggering the electron activity of Complex II. The uncoupler FCCP was added for this measurement. The decrease in RCR values obtained in this case demonstrate the protonopheric effect of FCCP.

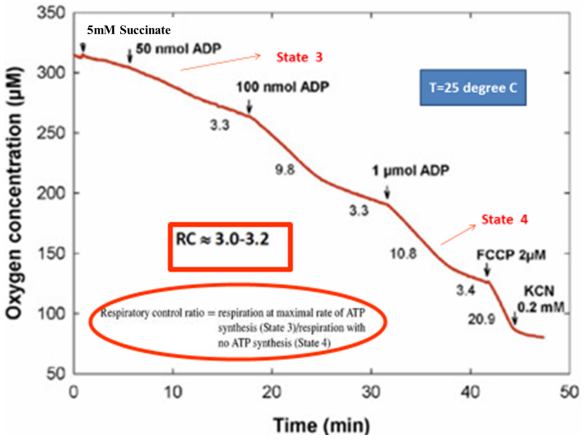

FIGURE 5.13: RCR measurement with uncoupler FCCP.

5.2.3 Experimental Set-up

Figure 5.14 shows the typical set-up we used for measuring electrical properties

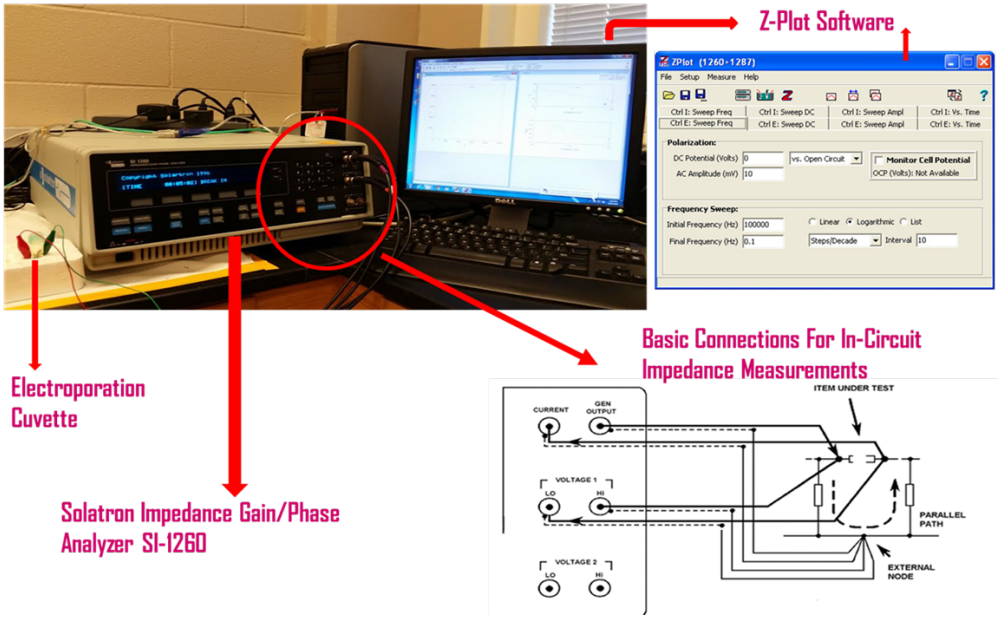

FIGURE 5.14: Electrical measurement set-up.

of mitochondria by impedance analysis. The mitochondrial suspension was kept in the electroporation cuvettes. These cuvettes were purchased from BioRad Laboratory, California. The cuvette gap was 0.4 cm and is used for mammalian cells, including primary and stem cells, and plant protoplasts. The area of each electrode was 2.73×10^{-4} m^2, yielding a sample volume of $\sim$ 4.0 mL. The electrodes were made of aluminium.

Figure 5.15 shows different components and functionalities of the cuvette we used. The electroporation cuvette used in this work operated at 10V had a 4 mm width, which allowed for low field strength. It was ideal for mammalian cells. The cuvette containing the sample was connected to the impedance analyzer by an

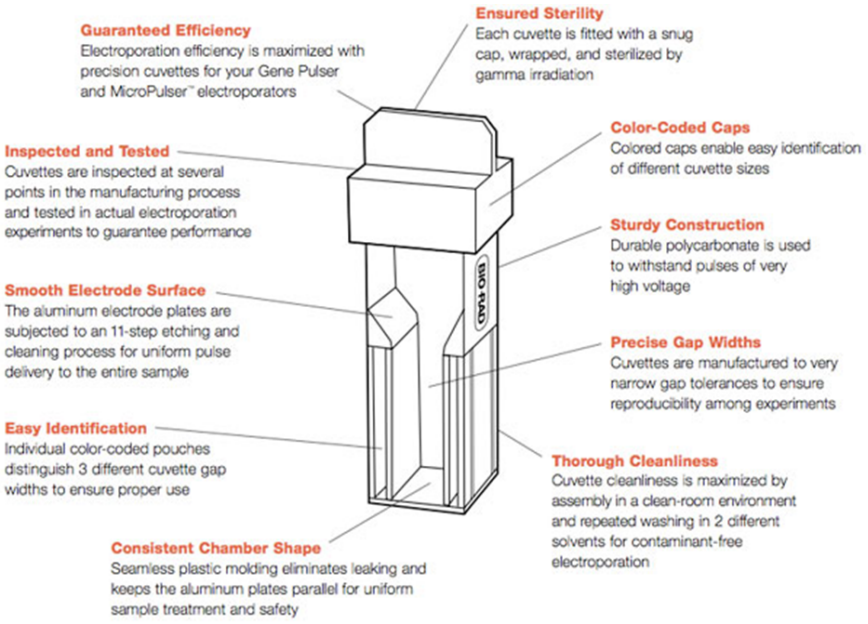

FIGURE 5.15: Schematic of cuvette.

alligator clip test lead, which was then connected to the PC. Shortly before the pulse was triggered, the mitochondrial sample loaded cuvette, was stored in ice, as the temperature of the samples was extremely high, since they were placed on the aluminium electrodes.

Figure 5.16 shows a scheme for the insertion of metal electrodes in the cuvette to make it possible for electroporation.

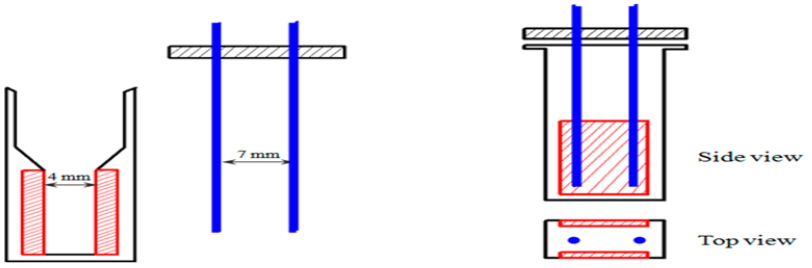

FIGURE 5.16: The bulk electroporation apparatus of in-vitro experiment, with cross-sectional view with and without metal electrodes.

The corresponding flow diagram for the impedance analysis is shown in Figure 5.17. The data collection was accomplished by the Solartron Gain Phase-Analyzer, model 1260, depicted in Figure 5.18. The Solartron Analyzer is capable of communicating with a connected computer with an accuracy of 0.1% for magnitude and 0.1^o for phase measurements. With the Z-Plot software

FIGURE 5.17: Illustration of the system components for impedance analysis.

provided by Solartron it was possible to control the analyzer and view the collected data. When connected to the system, the instrument collected voltage and current data. The software was able to utilize these data and automatically plot the impedance versus the applied frequency.

FIGURE 5.18: Model 1260A impedance Solartron Gain-Phase Analyzer.

The analyzer was equipped with generator output, generator input, and two sets of voltage input terminals. All of the interfacing to the Solartron was done

through a shielded coaxial cable. The length of the cables between the analyzer and the sample was kept as short as possible. Longer cables added capacitance to the measurement, particularly to the generator input and the LO input of the voltage terminals. Once the cables were attached to the analyzer proper, connections to the electrodes were made through alligator clips.

To measure in-circuit impedance, connections were made to the Solartron using the generator output and input and the first set (VI) inputs, as shown in Fig 5.19. Z-plot software for windows was utilized to communicate to the Solartron. This software made it easier to set up the measurement equipment, collect the data and preview the data. The software was installed in the PC and it communicated with the analyzer through the GPIB port and a PCMICA data acquisition card. For impedance investigation as a function of frequency, the AC response of the

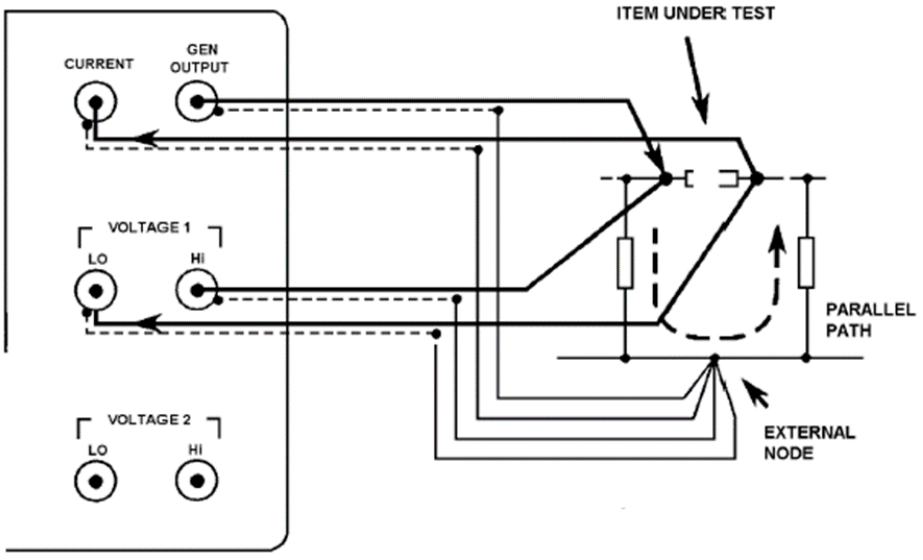

FIGURE 5.19: Solatron basic configuration to measure in-circuit impedance.

system "Control E" and "Control I" procedures were used. "Control E" sweep frequency method yielded better results in comparison to those of "Control I", which were prone to more noise. The "Control E" held a constant applied voltage of 10mV throughout, while varying the applied current. Impedance spectra were recorded by the impedance gain/phase analyzer SI-1260 in the frequency range of 1kHz to 1MHz every 25 min. A pure sinusoidal AC voltage of 10mV amplitude (peak-to-peak) was supplied, and 10 data points per frequency decade chosen to be equidistant on the logarithmic scale were recorded. A resistance of 10kΩ was placed between the analyzer and the cuvette. This limited the current in the system in the μA range, preventing stress on the mitochondria. The data were recorded in real time as impedance modulus $|Z|$ and phase ϕ. Real and imaginary parts were also measured. In this way, conductances and capacitances were calculated during data analysis.

When analyzing data in a real-time environment, two things must be considered. First, a proper time has to be given to the system to react to the changes in the applied frequency, and secondly, the collection scheme should not be so slow that it will miss the data[139].

Before collecting data on the mitochondria, calibration of the equipment was performed using resistors, capacitors, and combinations across the electrodes. This is described in Chapter 6. This calibration confirmed the order of magnitude of the data collected from the impedance meter.

Chapter 6

Impedance Set-up and Characterization

6.1 System Calibration

Calibration of the equipment, *i.e.*, the Solartron, was important to confirm the order of magnitude of the data collected. Before the impedance measurement of different solutions, the system was tested with standard resistors and capacitors. It should be mentioned here that the method of calibration was based on a linear system[12]. Based on our measurement procedures on RC circuits, we validated the stability of the process, thereby eliminating any quasi-dispersion at high frequencies enhancing band-width. Pure resistors have the same impedance at any frequency. AC impedance of a resistor is the same as its DC resistance and is shown in Figure 6.1 and with the formula $|Z|$ = R. Theoretical impedance values

at relatively higher resistive circuits matched quite well with the experimental values. For lower resistance ($< 1k\Omega$), as can be seen in Figure 6.2, fluctuation

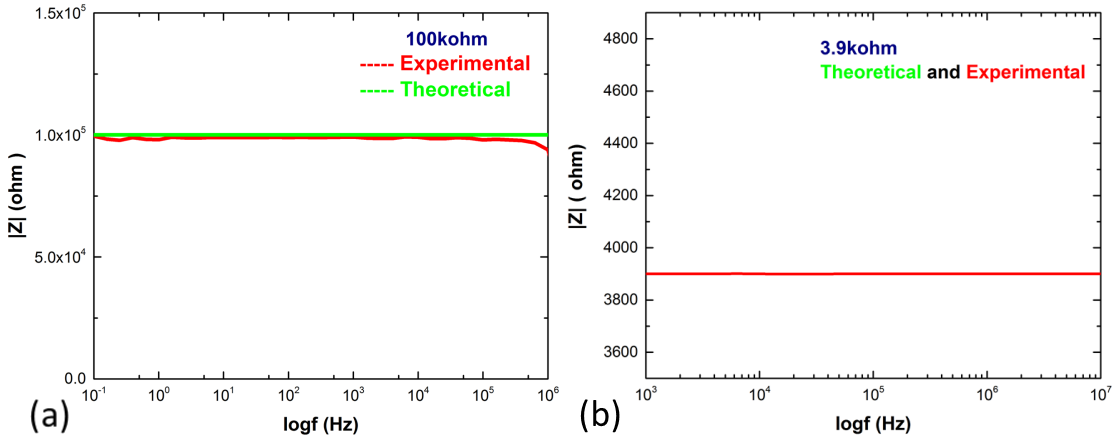

FIGURE 6.1: Impedance result of pure resistor (a) 100 kΩ and (b) 3.9 kΩ.

between theoretical and experimental impedance values were appreciable at higher frequencies. The capacitive reactance $X_C = |Z|$ is given by the equation,

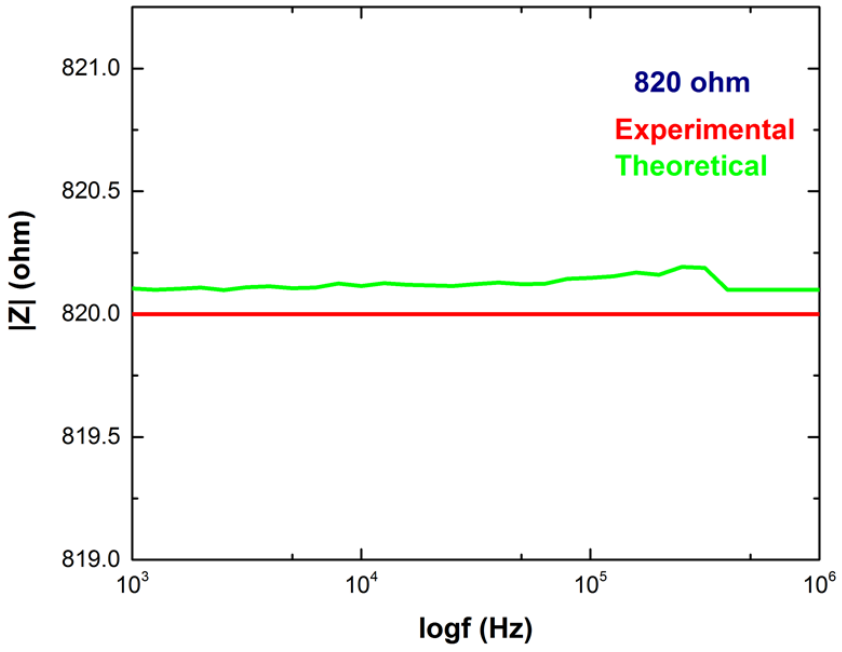

FIGURE 6.2: Impedance as a function of frequency of pure resistor with 820 Ω.

$$X_C = \frac{1}{2\pi f C} = \frac{1}{\omega C}. \tag{6.1}$$

The graphs in Figure 6.3, corroborate the observation from Equation (6.1) that if either the frequency or capacitance is increased, the overall capacitive reactance would decrease. This is similar to a perfect conductor, in which the capacitor reactance would reduce to zero as the frequency approached infinity. For a series

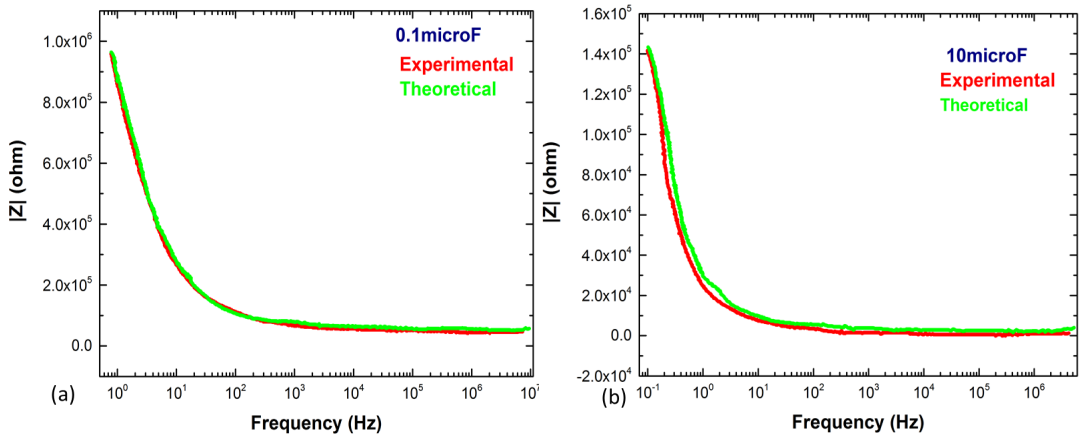

FIGURE 6.3: Impedance result of pure capacitor (a) 0.1 μF and (b) 10 μF.

RC circuit, the impedance is given by

$$Z = [R^2 + 1/(\omega C)^2]^{1/2}]. \tag{6.2}$$

For a series RC circuit, as frequency increases, R remains constant, X_C decreases, and Z decreases as shown in Figure 6.4. Total impedance in parallel RC circuit is given by

$$Z = (R/(\omega C))/[R^2 + 1/(\omega C)^2]^{1/2}]. \tag{6.3}$$

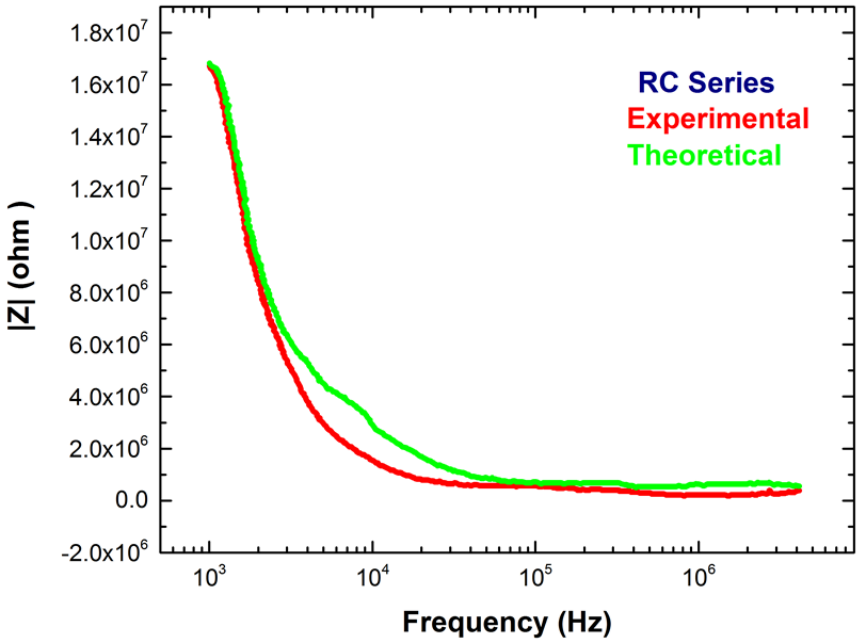

FIGURE 6.4: $|Z|$ vs frequency for a RC series circuit R = 100kΩ and C=0.1μF.

At low frequencies, the impedance approaches that of the resistor, R. At high frequencies it approaches that of the capacitor, $1/i\omega C$. Because the capacitor's

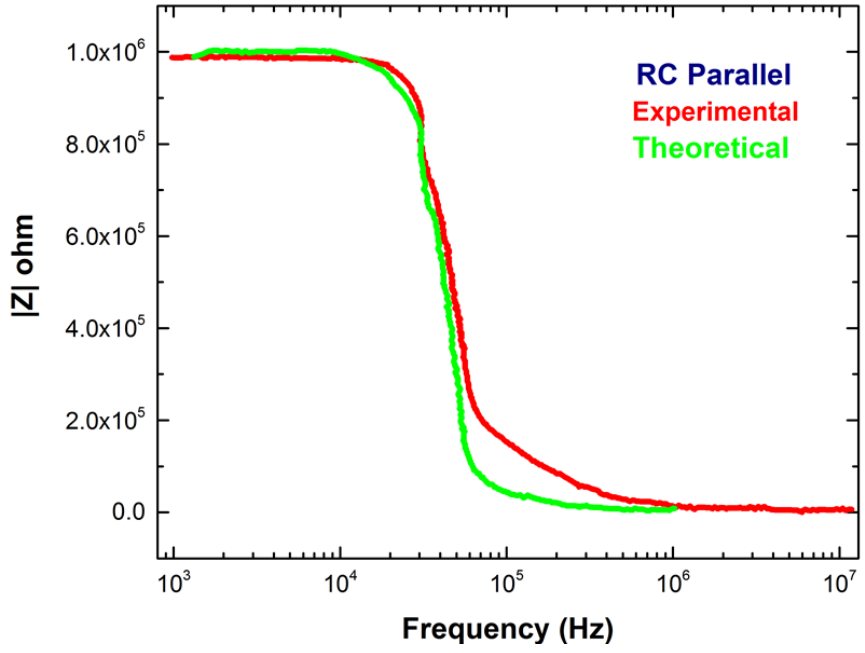

FIGURE 6.5: $|Z|$ vs frequency for a RC parallel circuit R = 100kΩ and C=0.1μF.

impedance is bigger at low frequencies, it is more important than the resistor's impedance. Consequently, the magnitude is inversely proportional to frequency and the phase angle remains at a constant -90^o. At high frequencies, the capacitor almost becomes a short circuit, by leaving just the resistor, which implies that magnitude is independent of frequency and that the phase angle is zero. This conclusion is evident from the data in Figure 6.4 and Figure 6.5.

In order to acquire the electrical measurements of mitochondrial suspension, the impedance analyzer had to be first calibrated using standard solutions. In order to maintain accurate calibration, only the purest, deionized water at 25 ^{o}C was used. The results obtained are depicted in Figure 6.6. DI water has a high

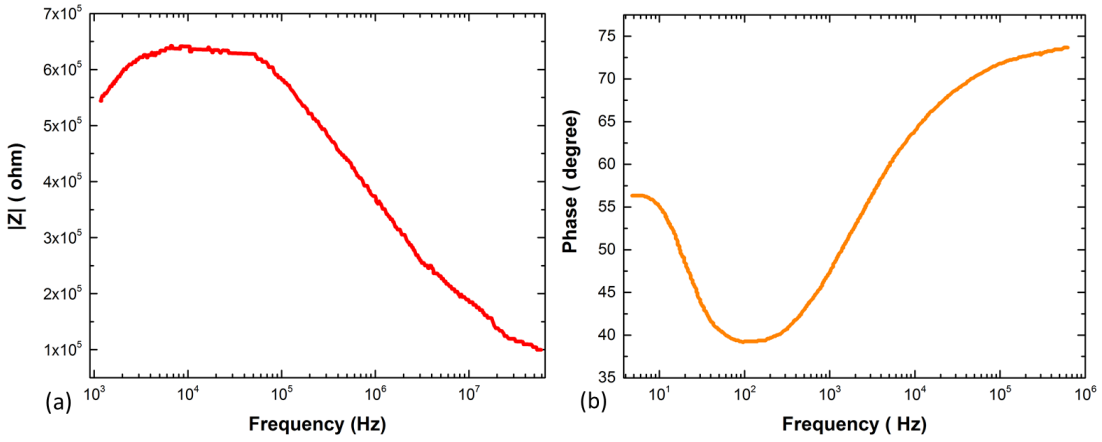

FIGURE 6.6: Bode plot of (a) $|Z|$ and (b) phase variation with frequency of DI water.

resistivity, so it has a high magnitude response. As observed in Figure 6.6 (a) and in 6.6 (b), we see that the phase for DI water starts to decrease when frequency is greater than 100 Hz.

The semi-circular curve known as the Cole-Cole impedance plot obtained in Figure 6.7 indicates that the system had only one relaxation time, when T = RC. At this point, the imaginary part of the complex impedance of water was plotted against the real part, each point representing characteristic one frequency of measurement. Having higher magnitudes, the low frequency data are on the right side of the plot, and the high frequency data are on the left, as impedance falls with increase in frequency. For truly complex impedance, as observed in Figure 6.7, the Cole-Cole impedance plot is a semicircle, due to second order variation from the equation of the circle $r^2 = a^2 + b^2$.

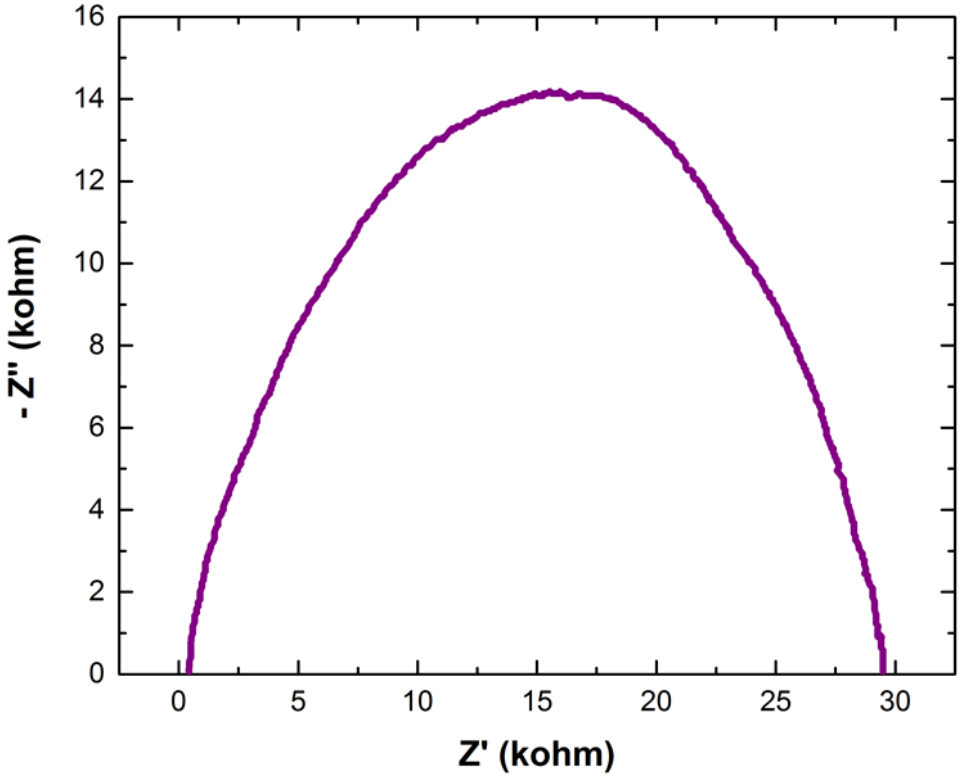

FIGURE 6.7: Nyquist's plot of DI water.

Typical frequency spectra for DI water, shown in Figure 6.8 showed that the

real part of the impedance was associated with resistive pathways, whereas the imaginary part was associated with capacitive pathways. The measured

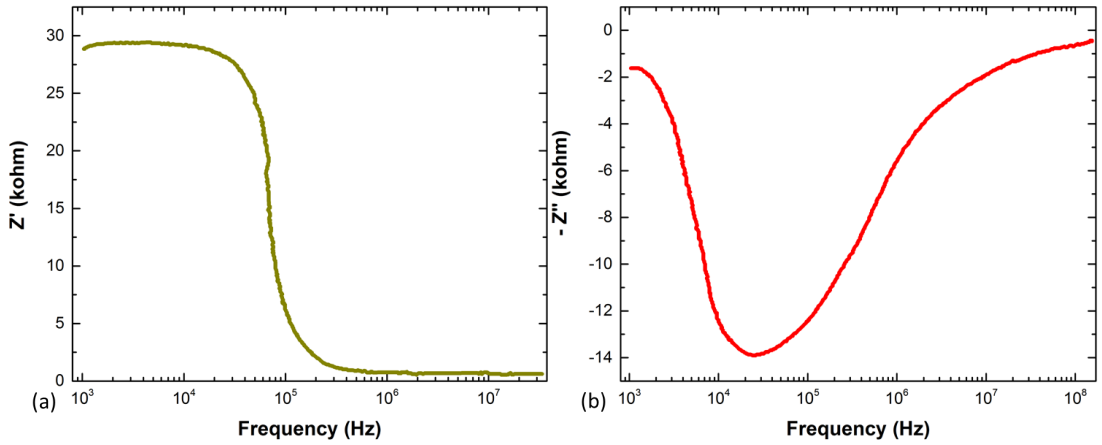

FIGURE 6.8: Resistance variation with frequency of DI water.

capacitance of DI water decreased as the frequency increased. Figure 6.9 shows a non-linear variation of capacitance as a function of frequency. DI water had a

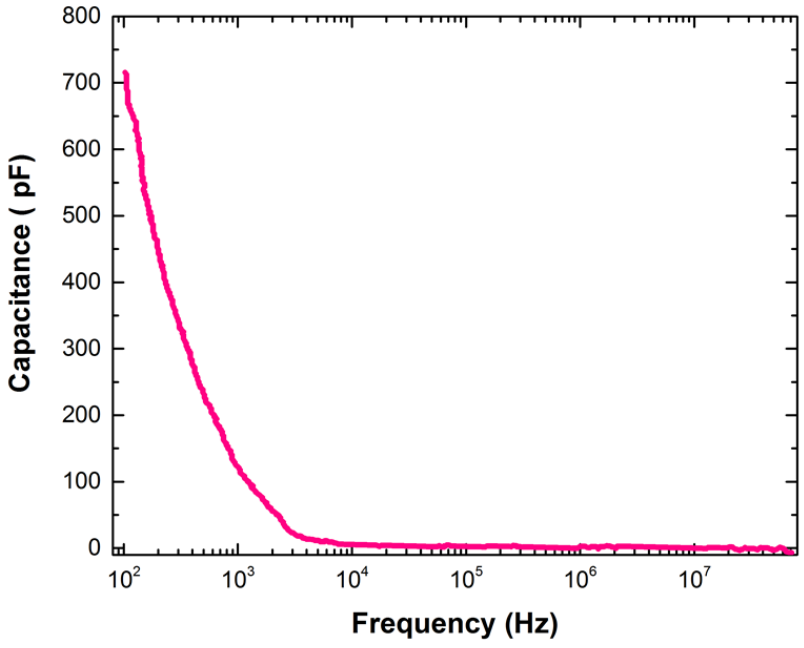

FIGURE 6.9: Capacitance variation with frequency of DI water.

known static dielectric constant of 80.

These data were taken from the value of actual permittivity to calculate the background and stray capacitance of the system over a frequency range of 100 Hz–10 MHz. The results showed that the background and stray capacitance was only constant for frequencies greater than 10 kHz.

For the impedance measurements, three concentrations of sodium chloride solutions of 0.26g/ml, 0.23 g/ml, and 0.18 g/ml were used. Figure 6.10 shows that the differences in impedance of sodium chloride solutions with different concentrations could be distinguished when below 50 MHz. Below 50 MHz, the

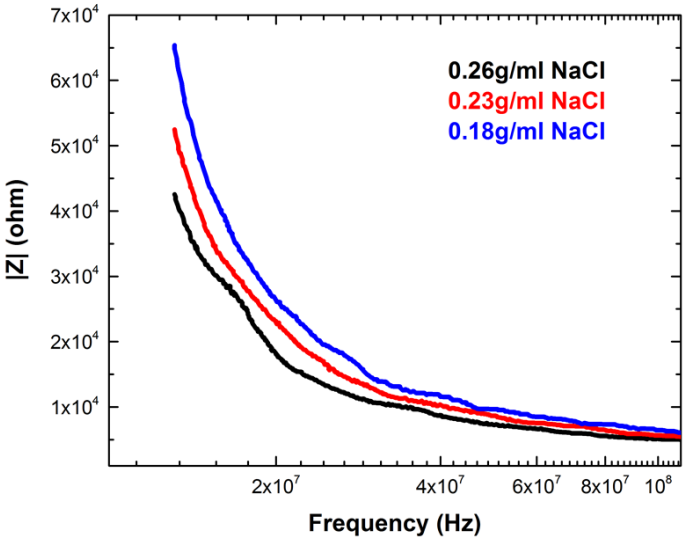

FIGURE 6.10: Impedance result of NaCl at different concentrations.

results showed that the magnitude of impedance increased as the sodium chloride concentration decreased, which coincided with the fact that the conductivity was proportional to the electrolyte concentration. The differences in impedance decreased as the frequency increased as shown in Figure 6.11. Each

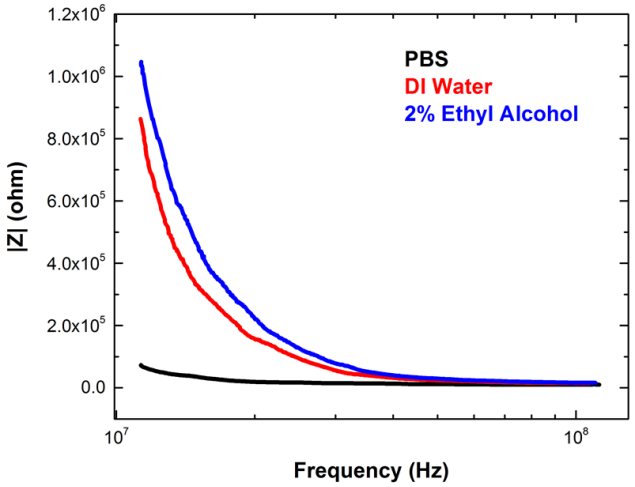

FIGURE 6.11: Bode plot of impedance magnitude variation with frequency of PBS, DI water and 2% ethyl alcohol.

curve had a distinct signature, and phase angles exist in the frequency range from 10^3 to 10^6 Hz. In Figure 6.12, we have plotted the phase as a function of frequency, which shows a logistic-like behavior. With a frequency of over 50

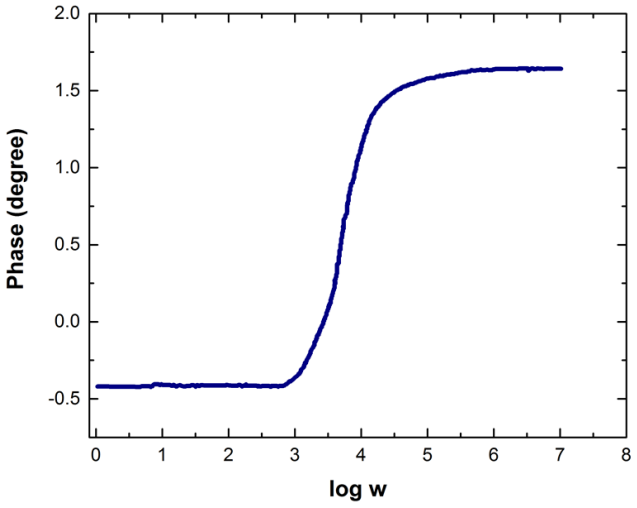

FIGURE 6.12: Phase variation with frequency of 2% ethyl alcohol.

MHz, the differences in impedance of sodium chloride solutions with different

concentrations became small, because the capacitance effect of the solution decreased at high frequencies.

The corresponding spectrum had a nearly perfect semicircular shape, as apparent in Figure 6.13. The center of the semi-circle is below the X axis, the

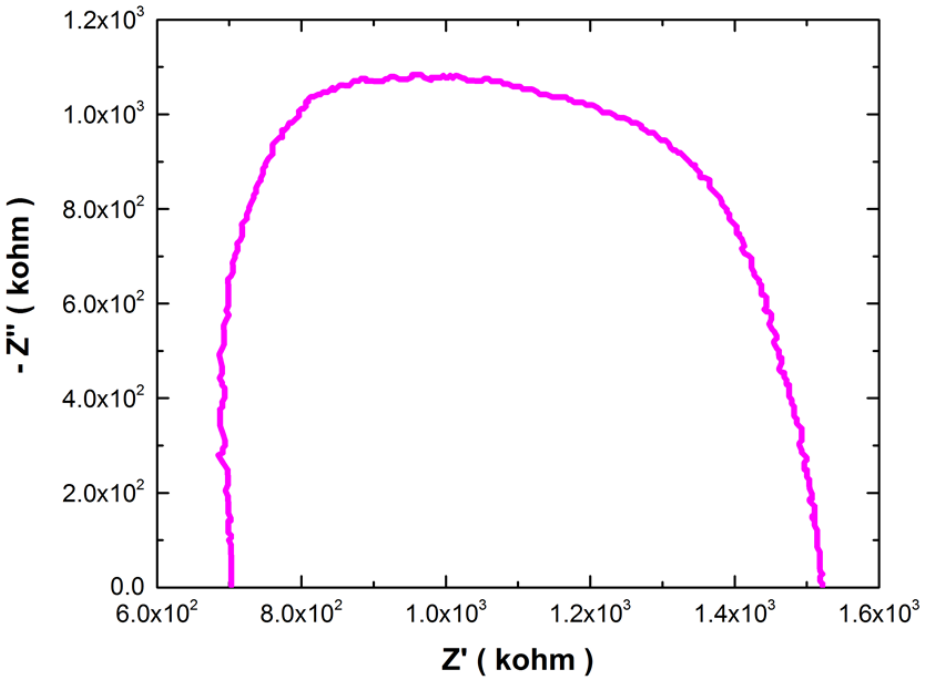

FIGURE 6.13: Nyquist's plot for 2% ethyl alcohol.

reactance in general has negative values. The frequency-dependent relationship between impedance (Z), conductivity (σ), and relative permittivity (ϵ_r) is given by the following expression[114]:

$$Z = Z' + \mathrm{i}\omega Z'' = 1/(\sigma + \mathrm{i}\omega\epsilon_o\epsilon_r), \tag{6.4}$$

where Z is the total and complex impedance, Z' and Z'' are the respective real and imaginary components of Z, ω is the radial frequency, and ϵ_o is the permittivity

of free space. Both Z' and Z'' were measured, and from these measurements the conductivity and relative permittivity could be calculated, as demonstrated in Table 6.1. The variations in the experimental and theoretical data are due to the challenges mentioned in the following section.

TABLE 6.1: Calculated versus experimental dielectric constants.

Liquid	Experimental	Theoretical
DI Water	95	80
NaCl	55	40-65
Ethyl Alcohol	24.3	4.13
PBS	78	136

6.2 Challenges in Impedance Spectroscopy

The sensitivity of label-free systems has so far been inferior to biosensors that use labels. Additionally, the required instrumentation for measuring electrical impedance spectroscopy is complex, as bulky and expensive bench-top systems are currently an integral part of its platforms.

There is one process, where a fully integrated EIS IC-based system was developed, by using semiconductor fabrication processes[100], however, semiconductor compatible bio-functionalization is a limiting challenge even in this case. Apparatus contributions, such as cabling, leads, and sample holder, to experimental impedance spectra can be significant, especially at high frequencies, and can obscure the true sample response. Background and stray capacitance, or

residual impedance due to the measurement fixture itself and the connecting leads must be removed from the measured capacitance before any analysis is performed. Stray capacitance can occur when a sample into which electrodes are placed is able to present alternative paths through which currents can flow, leading to a capacitive effect, which can contribute to the potential measured between the electrodes.

These effects can be removed by the calibration procedures mentioned in Section 6.1. The next important challenge is the polarization impedance, which appears at the interface between electrodes and ionic solutions, and is a major source of errors in dielectric spectroscopy measurements. This challenge is explained in detail in the next section.

6.2.1 Role of Electrode Polarization

When a metal electrode is immersed into a biological medium, a double layer is formed at the contact interface between the electrode and the biological medium, as depicted in Figure 6.14. Figure 6.15 a) shows a schematic of the electric double-layer structure that forms near the surface of an anode. Solvated cations of diameter "a" migrate and adsorb to the electrode surface due to electrostatic forces. The Stern layer is defined as the compact layer of immobile ions strongly adsorbed to the electrode surface. There are no free charges within the Stern layer. Beyond the Stern layer is the so-called diffuse layer, where ions are mobile under the coupled influence of electrostatic forces and diffusion. In Figure 6.15

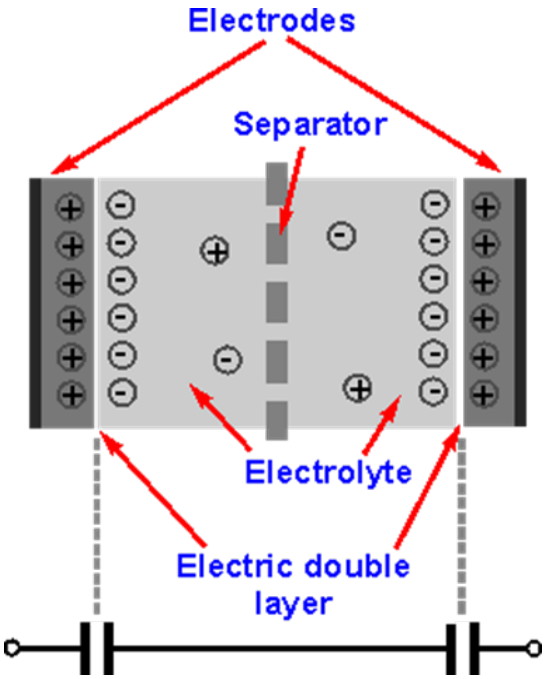

FIGURE 6.14: Basic double layer capacitor cell[80, 88].

b) we see the electrical circuit representation of an electrical double-layer capacitance, the electrode resistance, the Stern layer, and diffuse layer capacitances in series. The electrical double-layer scheme surrounded a

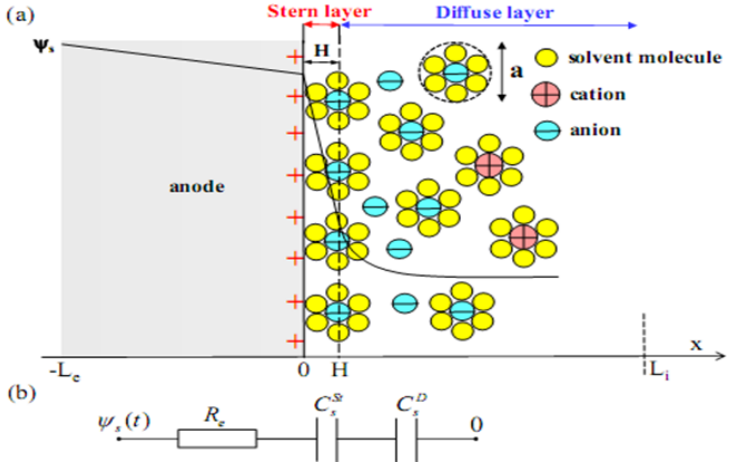

FIGURE 6.15: a) Illustration of interfacial double layer and b) the electrode resistance along with the Stern and diffuse layer capacitances in series[127].

biomolecule surface with potential of magnitude V and was superposed with a layer of negative charges at the biomolecule surface. This is surrounded by a positively charged counterion layer, which consists of a thin Stern layer and a diffuse layer with characteristic length, as depicted in Figure 6.15 b).

In order to study the relationship between the distance of the distance of the sample and the plane of the electrodes, simulations were run using the electromagnetics module COMSOL Multiphysics, a commercially available modelling package. These simulations showed the presence of an electrical double-layer, shown in Figure 6.16.

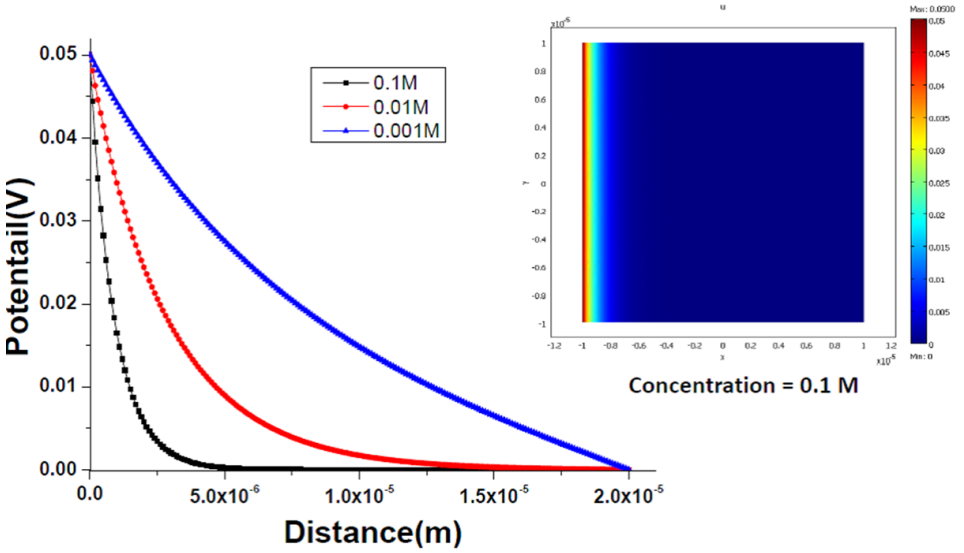

FIGURE 6.16: Numerical analysis of double layer[150].

Counterions adjacent and close to the sample form the Stern layer[127]. Counterions further away from the sample and Stern layer are more diffuse and screen the sample charge in such a way as to attract co-ions. As the distance of the sample from the plane of the electrodes increased, the change in impedance

decreased. The decrease in the impedance change was due to the drop in the electrical field gradient and the distance from the plane of the electrode[150].

The equivalent circuit in Figure 6.17 a) was not suggested by any polarization theory and hence it was arbitrary. Polarization resistance and capacitance are functions of frequency. Electrode polarization was important in biological impedance measurements, carried out at frequencies up to 1kHz, since β dispersions are predominant around these zones. From Figure 6.17 b) it can be seen that at a frequency below 1 MHz, C_{dl}, the double layer capacitance was inactive and was modeled as an open circuit. Two double layer capacitances,

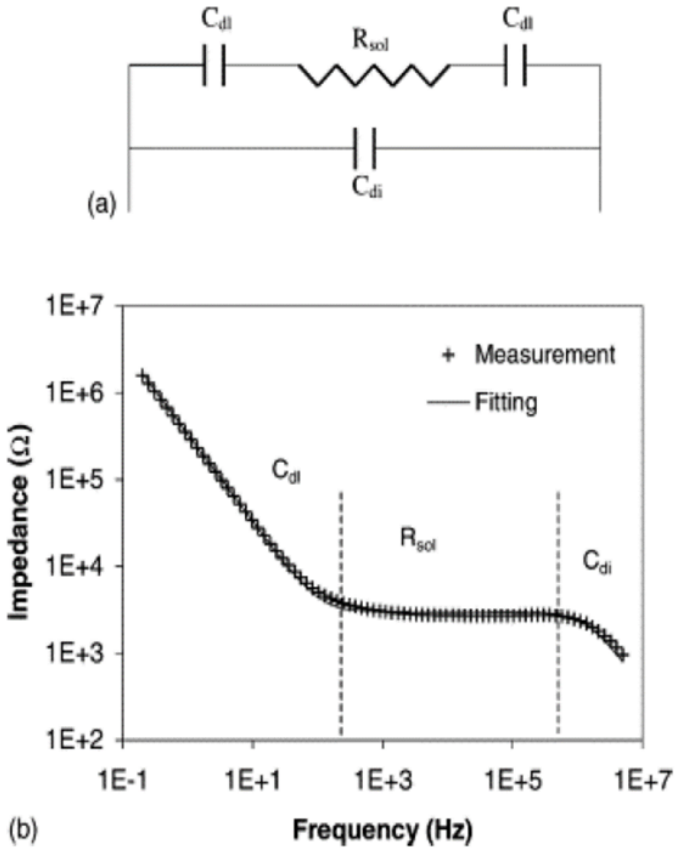

FIGURE 6.17: (a) a) Electrical equivalent circuit of impedance measurement system with interdigitated electrode and (b) typical impedance spectrum[92].

existed at each electrode. C_{dl} was connected to the medium resistance R_{sol}. The dielectric capacitance of the medium (C_{di}), depended on the parallel and series configuration of the circuit elements, C_{dl} and R_{sol}.

Current was unable to pass through the branch of dielectric capacitance, and the total impedance was expressed as Z. Both C_{dl} and R_{sol} were included in this frequency region, and they dominated at different frequencies, as shown in the impedance spectrum in Figure 6.17 b). At a low frequency range, the spectrum showed capacitive characteristics, which were contributed by C_{dl}. The impedance decreased with increasing frequencies, thus, we find that the effect of polarization on the resistive part of the total impedance was, in most cases, a minor one in comparison with that of the capacitive part.

6.2.2 Procedure to Correct Electrode Polarization

In order to correct the effect of electrode polarization, first we measured the biological sample. Next, we replaced the biological sample with the physiological solution in which it was stored and again measured the total impedance. The scheme and the circuit representation is shown in Figure 6.18. We determined the impedance and capacitance of the double-layer from the solution reading, represented by (depicted with the subscript "p" in Figure 6.18), the following

equations:

$$\begin{aligned} R &= R_{sol} + R_{dl} + (R\omega C)^2 \cdot R_{sol} \quad and \\ C &= C_{sol} + 1/\omega^2 R^2 C_{dl}. \end{aligned} \tag{6.5}$$

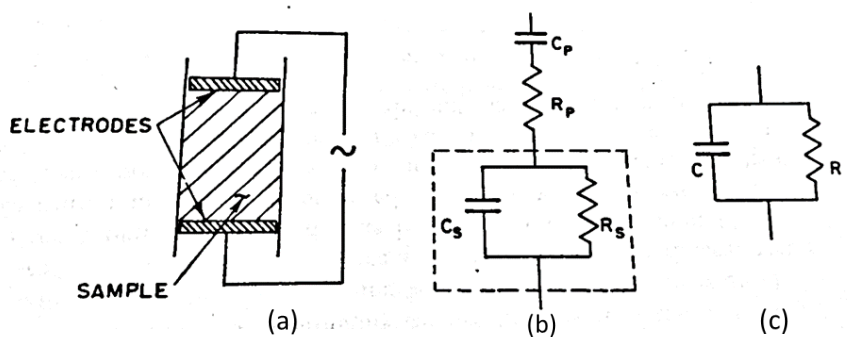

FIGURE 6.18: (a) Polarization between electrodes and test solution, (b) R_{eq} for sample polarization, (c) observed equivalent circuit[143].

Subsequently, using these polarization impedance data, we corrected the measurements of the biological samples for electrode polarization. The validity of this technique was based on the assumption that the polarization impedance involved in the measurements of the biological sample and of the contact fluid are identical[65, 132]. Equation (6.5) was valid in the limit $R\omega C < 1$ and $R_p < R_s$. Some of the principal techniques to correct for electrode polarization are mentioned in the following. The best choice, of course, must be adapted to the particular measurement problem involved, and to the desired accuracy of the final results.

1. Electrode distance variation technique;
2. Substitution technique, which was mentioned above;
3. Frequency variation technique; and
4. Four electrode technique.

Successful elimination or correction for existing polarization difficulties was attained through the implementation of alternating current steady-state techniques.

In the consideration of a simple method to account for the background capacitance and stray capacitance, the assumption was that the capacitance would be constant and independent from frequency, and a first-order correction term was calculated[13]. To determine the background capacitance from the probe and the cables, a capacitor with a known capacitance was attached, in order to short-out each of the inner electrodes to one of the outer electrodes, effectively closing the circuit. These capacitances needed to remain constant for the frequency range of interest. The capacitances also needed to be independent of the conductance. If these conditions were met, then the existence of background and the stray capacitance would be possible by presenting the probe with an open circuit. Measurements of the capacitance and conductance of a 4 pF capacitor showed that these conditions were satisfied over the frequency range of interest, *i.e.*, 10^3-10^7 Hz.

The results shown in Table 6.1 indicated that the system was still susceptible to electrode polarisation effects. Some electrode polarisation at very low

frequencies could be expected to increase capacitive effects however, results should still be considered preliminary, and further research needs to be conducted with the measurement system to confirm our findings.

Chapter 7

Impedance Measurements to Probe Physiological Changes in Mitochondria

As discussed in the preceding chapters, oscillatory electric fields can induce motion of charges in biological systems, and these responses can be used to probe physiological processes. Dielectric response measurements, in particular, can provide valuable information about the structures, functions, and metabolic mechanisms of biological specimens[27, 132]. Some of this information includes changes in cellular or mitochondrial membrane potential. A key hypothesis for the results presented here was that various chemicals, known as substrates in the biochemistry terminology, that cause changes in mitochondrial membrane potential lead to corresponding changes in the impedance of a mitochondrial

suspension over certain frequency ranges. This hypothesis was motivated by the predictions of Prodan *et al.*[132], that low frequency dielectric response and impedance are greatly influenced by the membrane potentials of cells or organelles suspended in water or a saline solution.

In the case of mitochondria, the ATP-producing organelles in our study, the synthesis of ATP is driven by the electrical potential and proton gradient (pH gradient) across the mitochondrial inner-membrane. Knowledge of the electrical properties of this membrane was critical for our understanding of mitochondrial structure and function[86]. As discussed in previous chapters, electrical impedance is a complex, frequency-dependent quantity, containing both resistive components caused by conductance of the medium, and reactive components caused by capacitance of the medium. By measuring electrical impedance against mitochondrial frequency, using impedance spectroscopy, we uncovered physiological processes that, for basic research or for drug discovery applications, constitute a novel approach to reveal the underlying biological phenomena[36, 108].

Key findings from our study, discussed in detail in this Chapter, are summarized here: 1) added substrates, known to either increase or decrease mitochondrial membrane potential, caused significant changes in mitochondrial suspension impedance over certain frequency ranges; 2) the changes in impedance agreed qualitatively with those expected from theoretical predictions[130, 132]; 3) in particular, the mitochondrial uncoupler FCCP, known

to create a proton leak that drastically reduces mitochondrial membrane potential at high concentrations, caused an increase in impedance at certain frequencies, consistent with a predicted drop in capacitance[132] and increase in capacitive reactance; and 4) we observed that the neurotransmitter dopamine, in sufficiently high concentrations, caused changes in impedance similar to those induced by FCCP. This last observation strongly suggests that excess dopamine can also act as a mitochondrial uncoupler. This may have important implications in, the extremes of behavior seen in bipolar disorder or catatonic schizophrenia, where the depressed phase of the former or the catatonic stupor of the latter may result from insufficient ATP production caused by mitochondrial uncoupling, triggered by excess dopamine.

7.1 Impedance of Mitochondrial Suspension

All the experiments performed in this research were conducted on mitochondria extracted from mice hearts as part of an approved IACUC protocol. The procedures were in accordance with institutional guidelines and in compliance with the recommendations of the "Guide for Care and Use of Laboratory Animals"[14]. In the present study, impedance spectroscopy was performed on freshly pelleted-out mouse cardiac mitochondria suspended in a respiration buffer solution, and the mitochondria were extracted using a typical extraction protocol mentioned in Chapter 5. The impedance measurement of the mitochondria

suspension was carried out in an electroporation cuvette with a 4mm gap-width. Impedance spectra were recorded by the impedance gain/phase analyzer SI-1260 (Solartron Instruments Farnborough, UK) in the frequency range from 10kHz to 10MHz. A pure sinusoidal AC voltage of 10mV amplitude (peak-to-peak) was applied, and ten data points were recorded per frequency decade chosen to be equidistant on the logarithm scale. The current in the system was in the microampere range, preventing mitochondrial stress and death.

The data were recorded in real-time, as impedance modulus and phase. Real and imaginary parts were calculated afterwards during data analysis[71]. Based on the Biuret method, the mitochondrial sample concentration was determined to be 4 mg/ml, using a spectrophotometer. Much of the goal of in-vitro or in-situ studies is to replicate, as much as possible, the environment of mitochondria in-vivo. Initially, 4ml of the respiration buffer was added to the cuvette and the impedance-phase angle values were measured[56]. The respiration buffer was composed of 225 mM mannitol, 75 mM sucrose, 10 mM KCl, 10 mM Tris-HCl, and 5 mM KH_2PO_4, with a pH 7.2. The buffer served as a control and a baseline for the impedance measurement system[107].

Isolated mitochondria were generally prepared in media rich in sucrose, which was intended to promote the stabilization of mitochondrial integrity. Subsequently, mitochondria suspended in the 4ml respiration buffer were added to the cuvette for impedance spectroscopy. To study the response of the mitochondrial membrane potential changes, 200 mM of the Complex II-linked

substrate succinate were added. Succinate is widely used as a physiological substrate to initiate mitochondrial oxidative phosphorylation. Complex II refers to coenzyme Flavin Adenine Dinucleotide (FAD). Succinate binds the succinate dehydrogenase complex II directly, which then oxidizes succinate to fumarate and reduces FAD in the process. Therefore, once succinate, which is added in considerable excess, binds to the complex, its electrons are immediately donated to the ETS. Two electrons from the reduced $SDHFADH_2$ complex are then transferred to ubiquinone, a soluble component of the electron transport system Complex II. This is shown in Fig 7.1. It is worth mentioning here that when an

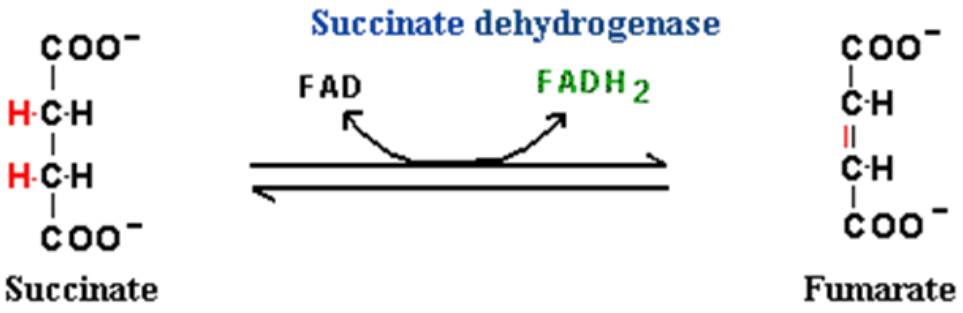

FIGURE 7.1: Succinate dehydrogenase activity of mitochondria[15].

electrical current with a low frequency was applied, the current passed through the outside of the mitochondria. Thus, impedance measurements at low frequencies could not be used to determine the pathological changes taking place inside the mitochondria. Nonetheless, increasing the frequency of the electrical current made the capacitive impedance of the mitochondrial membrane decrease, allowing the electrical current to flow through the organelle. Moreover,

double-layer capacitance made it impossible to express the integrity of the membrane using quantitative analysis.

To overcome the shortcomings of low frequency measurement, high frequency measurement was used to reduce the electrical shielding effect and the double-layer effect. With an increase of the frequency, the capacitive impedance of the mitochondria decreased and the electrical current flowed through the mitochondria, and was used to obtain impedance characteristics in different pathological statuses. The Bode magnitude of a respiration buffer without mitochondria, decreased with frequency, as shown in Fig 7.2. Figure 7.2 also

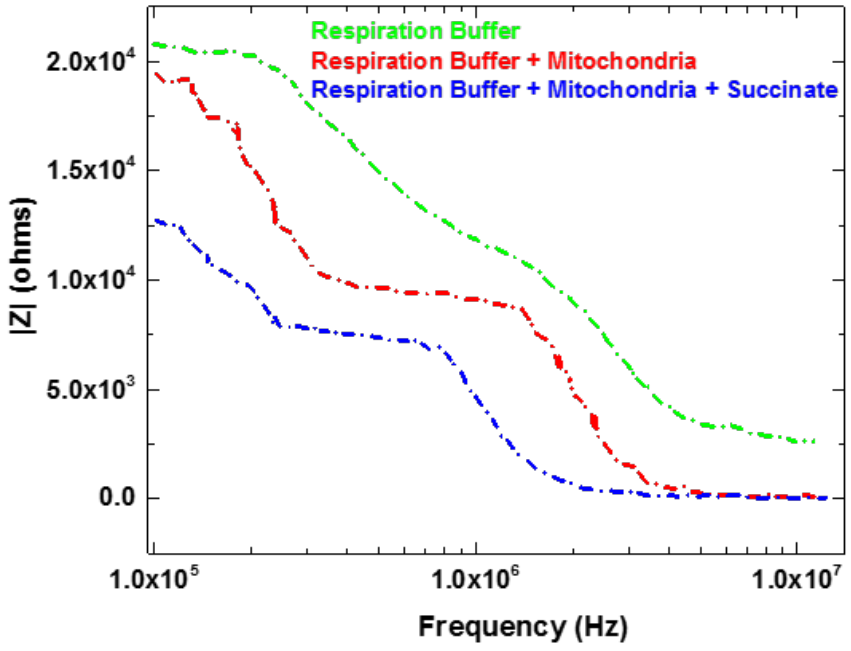

FIGURE 7.2: Bode diagram for $|Z|$ vs frequency for respiration buffer media for different conditions at operating voltage 10mV.

shows the effect of adding mitochondria into the respiration buffer on the impedance data. Since the buffer becomes more conductive, the impedance was

comparatively lowered. As result of the polarization of bound charges on membrane surfaces and proteins, dispersions were expected, and beta dispersions were observed at the frequency around 1 MHz in the experiments.

It is clear that dispersion can be attributed to the mitochondrial membrane only. Therefore, these measurements reflect membrane response[69, 132]. The decrease in impedance was consistent with an increase in capacitive reactivity, which was due to an increase in capacitance caused, in turn, by an increase in mitochondrial membrane potential. The phase angle, as seen in Fig 7.3 decreased at a low frequency for both the respiration buffer media with and without suspended mitochondria and also for those with the substrate succinate. From

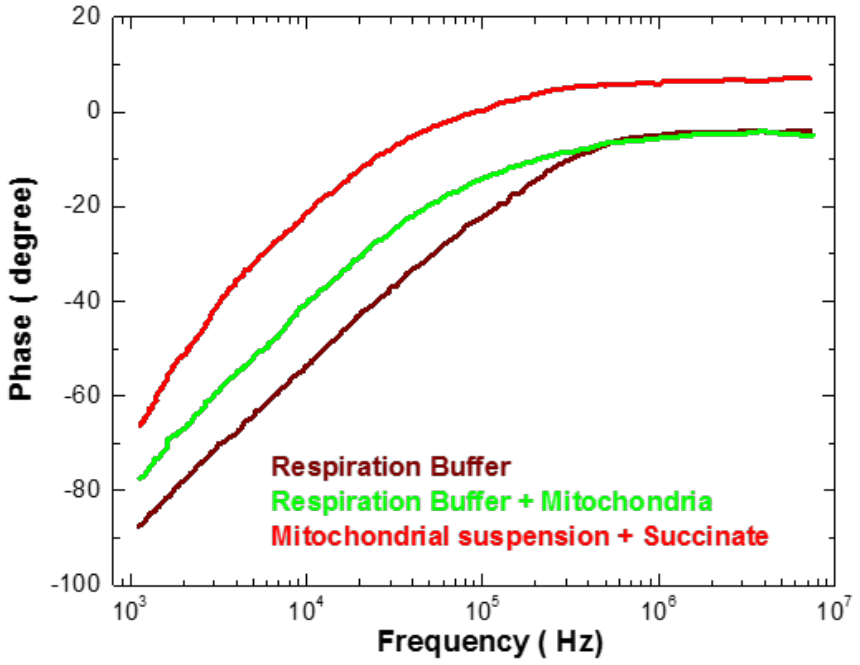

FIGURE 7.3: Bode diagram for phase Φ vs frequency for respiration buffer media for different conditions at operating voltage 10mV.

Figure 7.4 it can be seen that the largest observed change in impedance was at

3×10^3 kHz, and then it gradually decreased with frequency. At low frequencies, the membrane exhibited high capacitive impedance, thereby rendering membranes highly impermeable to electrical fields. As the frequency increased, membrane impedance decreased, and eventually the electrical field penetrated the membrane, leaving the membrane transparent at very high frequencies. The relaxation process, which occurred at around 3×10^3 kHz, came from the mitochondrial membrane, as it too had a capacitive nature that is further

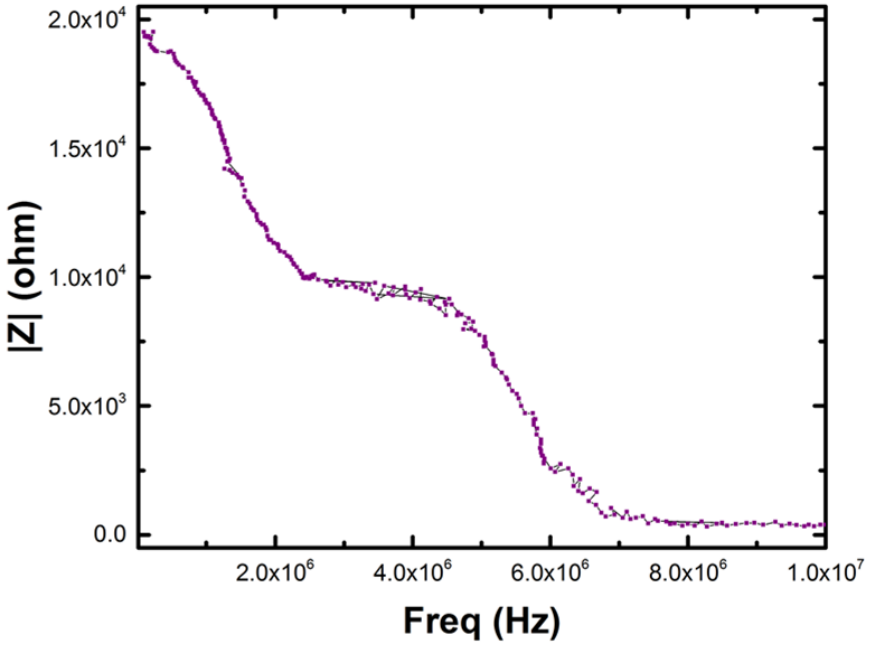

FIGURE 7.4: Frequency response of the mitochondrial membrane matrix. This result matches the beta dispersions reported by Schwan[141].

demonstrated by the phase versus frequency plot (Figure 7.3). The impedance values decreased with increasing frequency as the membrane's charge decreased, and subsequently became transparent from the applied sinusoidal signal. Phase angle is a potentially important clinical tool for the assessment of the trajectory

of general health of the mitochondria. Phase angle can be viewed as an indirect measure of the redox potential. As the phase angle decreases, there was a loss of electrochemical gradient and lowered bioenergetics.

In Fig 7.5 we show that at lower frequencies, the phase angle being less than 90 degrees denoted capacitive reactance of the membrane, and as frequency increased it shifted to 0 degrees, being resistive in nature. The mitochondrial membrane was open-circuit at very low frequencies, while it was short-circuit at high frequencies. The beta dispersion, first analyzed by Fricke and Cole[57], normally occurs over

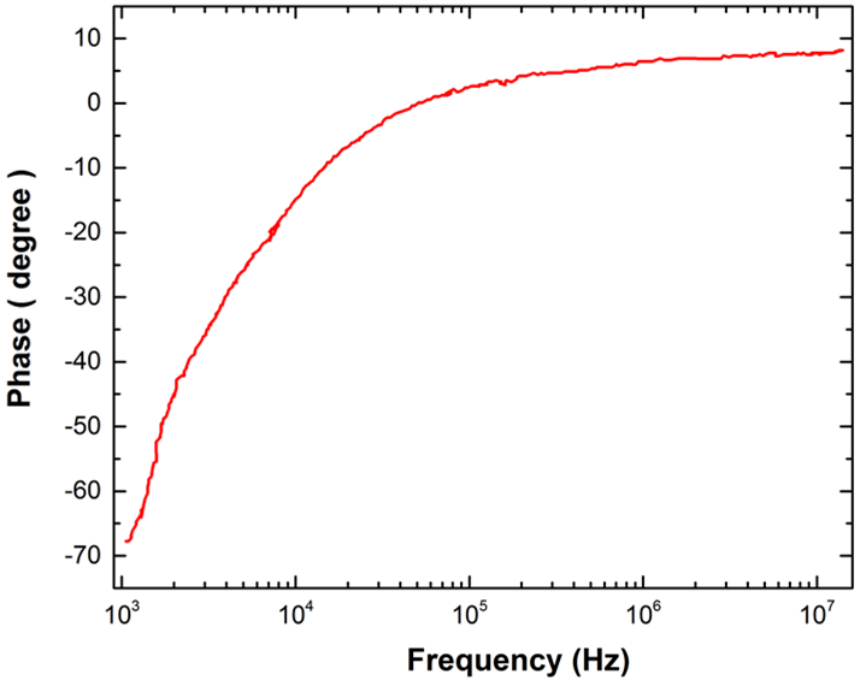

FIGURE 7.5: Bode plot of phase variation with frequency for mitochondria suspension and substrate succinate added to it at operating voltage 10mV.

a frequency range of 104–107 Hz. Electrical dispersion occurred when the applied AC field and the movement and orientation of the dipoles of the membranes did not vary in accordance with the changes in the field. The mitochondria have

poorly conducting membranes that separate the cytoplasm from the mitochondrial matrix, which causes the beta dispersion[48].

The beta dispersion of the frequency spectrum was caused by changes in surface charges and recharging processes occurring in the membrane. The dispersion effects were due to the Maxwell-Wagner mechanism at the interface between the mitochondrial matrix, the cytoplasm, and the inner and outer phospholipid membranes of the mitochondria[72]. Additional insight and understanding was gained by examining the data in terms of other electrical properties, such as capacitance and conductivity, as shown in Figure 7.6 and Figure 7.7. In the β-dispersion range above 10^3 kHz, the membrane capacitance

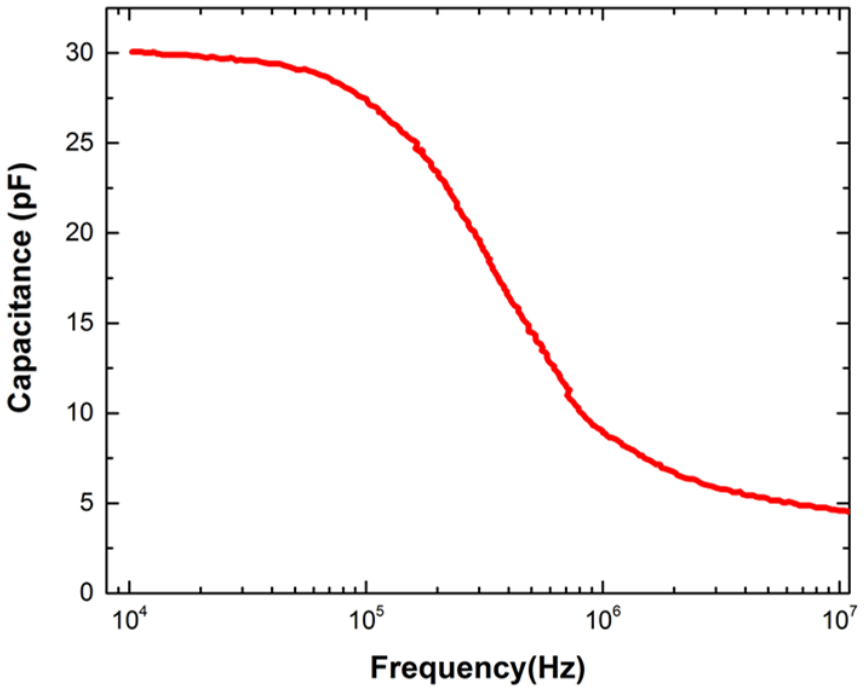

FIGURE 7.6: Capacitance variation of mitochondrial membrane.

became almost constant in the range of few picofarads, which closely matches the

general accepted value of mitochondrial membrane capacitance. Thus, the charge gradient across the membrane was reflected in the inter-membrane capacitance, and is a good parameter to study membrane potential. It was also seen that conductivity increased as frequency increased. The present study also examined

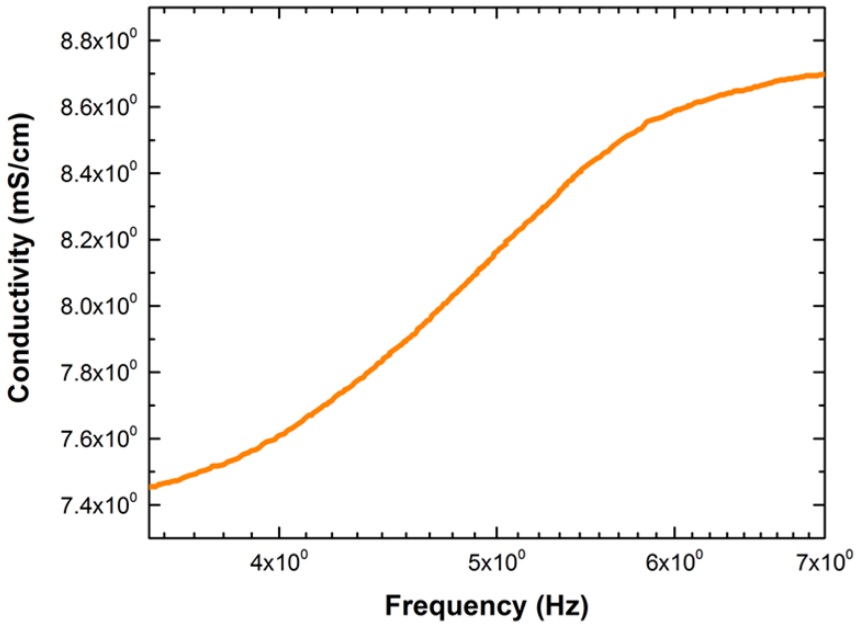

FIGURE 7.7: Conductance variation of mitochondrial membrane.

mitochondrial function over a wide range of succinate concentrations that span the physiological succinate range.

Succinate reacted with succinate dehydrogenase to yield FADH. FADH further donated electrons farther down the ETC to the component known as ubiquinone. When 100 ml of succinate was added, the electron activity of Complex II was triggered. The membrane became more conductive, and there was a decrease in impedance values. When the concentration of succinate was gradually increased, the value of impedance further decreased, but the decrease was low as shown in

Figure 7.8. The membrane potential reached it's maximum value and so, the decrease in impedance reached the point of saturation[136]. The results shown in Figure 7.8, suggested that elevated levels of succinate in correlation with a decrease in levels of impedance, indicated an increase in the polarization of the mitochondrial membrane.

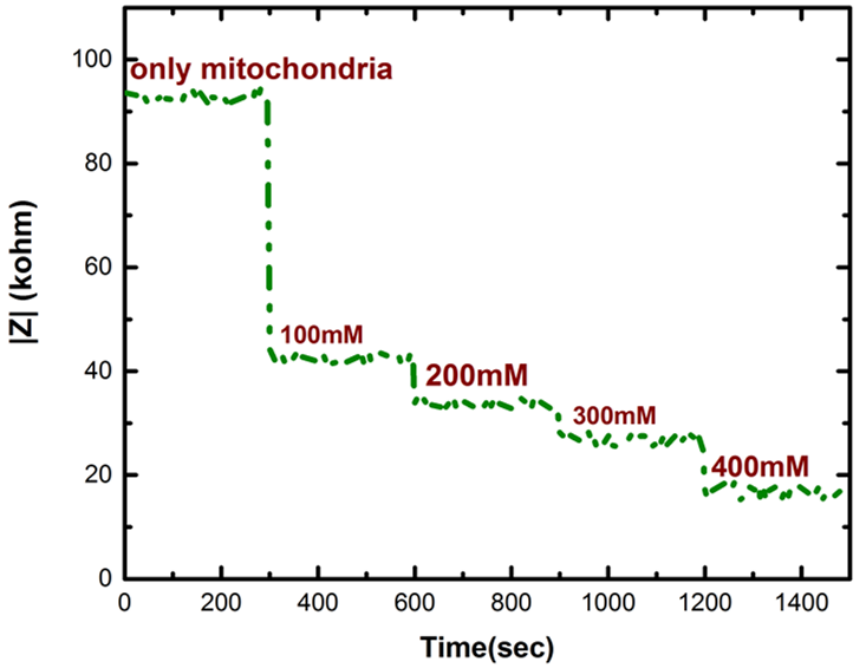

FIGURE 7.8: $|Z|$ variation for mitochondria suspension and substrate succinate at different concentrations at operating voltage 10mV and frequency at 2MHz.

7.2 Effects of FCCP on Mitochondrial Impedance

Uncoupling of the mitochondria, as mentioned in Chapter 6 involved the dissociation of electron transport from ATP synthesis. In this process, uncoupled

respiration continued to generate a proton (H+, or cation) efflux, but immediately dissipated due to high H+ conductance through the membrane, and without a H+ gradient, ATP synthesis through the F1/F0-ATPsynthase was inhibited[75, 157]. The process is shown schematically in Figure 7.9. In this

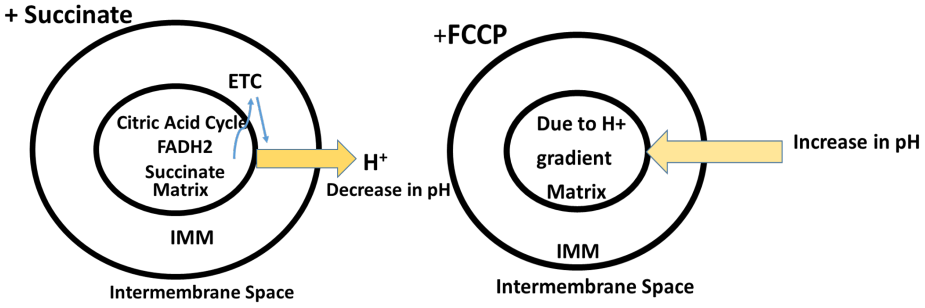

FIGURE 7.9: Schematic description of influence of succinate and FCCP on external pH[117].

process, respiration was initiated by adding 200 mM succinate. At the end of the run, 0.3 μM FCCP (carbonyl cyanide p-trifluoromethoxyphenylhydrazone) was added to fully uncouple the mitochondria. FCCP has been universally described as a potent mitochondrial uncoupler.

It is already established that there was an increase in the oxygen consumption on addition of the protonophore FCCP, which caused the collapse of the mitochondrial internal membrane potential, through the permeabilization of the membrane to protons[29, 75, 120]. It was observed that the impedance of the suspension increased when FCCP was added, as made explicit in Figure 7.10. This impedance increase was attributed to the reduction in outward current flow across the inner membrane as protons rushed inside the matrix when FCCP was added. Thus, FCCP depolarized mitochondria by increasing their permeability

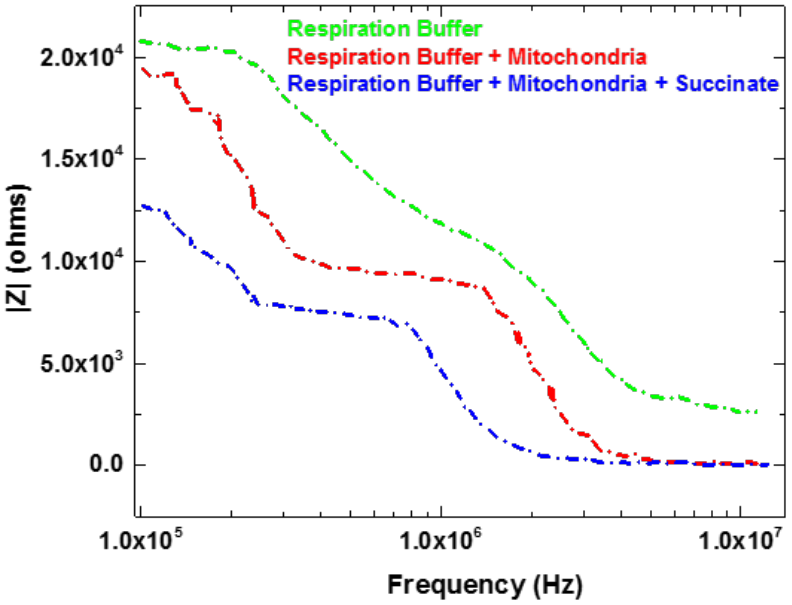

FIGURE 7.10: Impedance variation with frequency for FCCP addition to mitochondrial suspension.

to protons.

The FCCP-induced depolarization was caused by a reduction in membrane conductance resulting from the inhibition of an outward current. The reduced membrane conductance, leads to a dissipation of mitochondrial membrane potential[26, 109].

The experiment with FCCP was repeated at different frequencies, including 100 kHz, 1 MHz, and 10 MHz. From these additional experiments, we observed that the largest change in impedance occurred at 100kHz. No change in impedance was observed at 1 MHz and 10 MHz, respectively. This lack of change happened because the electrical field had not yet penetrated the membranes, which we observe in Figure 7.11. As frequency increased, the membrane became

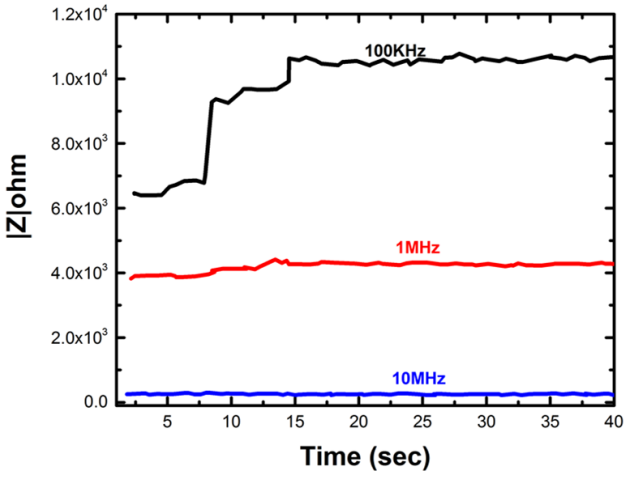

FIGURE 7.11: Influence of FCCP at different frequencies.

transparent from the applied signal, indicating a negligible response. The transparency happened at around 1 MHz, implying a very small change in impedance at higher frequencies. Higher FCCP concentrations dissipated mitochondrial membrane potential and exacerbated injury, indicating significant dose-dependent uncoupling of mitochondrial respiration. This indication was validated in the results presented in Figure 7.12.

Here it can be seen that for concentrations of 500 nM, 1 μM, and 0.5 mM, significant mitochondrial oxidation took place, and thereby mitochondrial membrane depolarization was caused, which is obvious from the elevation in the magnitude of the impedance[29].

Low concentrations of 50nM and 100nM FCCP caused an increase in mitochondrial oxidation with no detectable depolarization, as seen in Figure 7.13. FCCP at 200nM had an increase in impedance, indicating dissipation of mitochondrial membrane potential. Thus, FCCP is effective in uncoupling

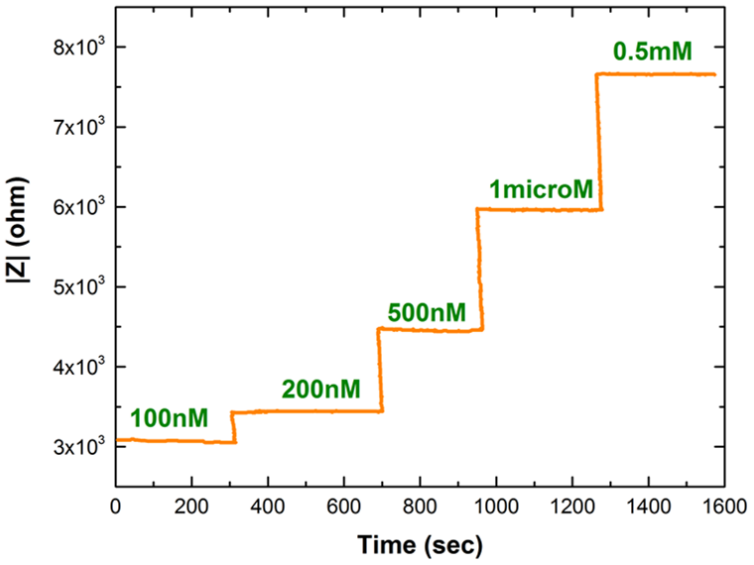

FIGURE 7.12: Impedance versus time for different concentration of FCCP added to mitochondrial suspension.

mitochondria in a dose-dependent manner[28, 51].

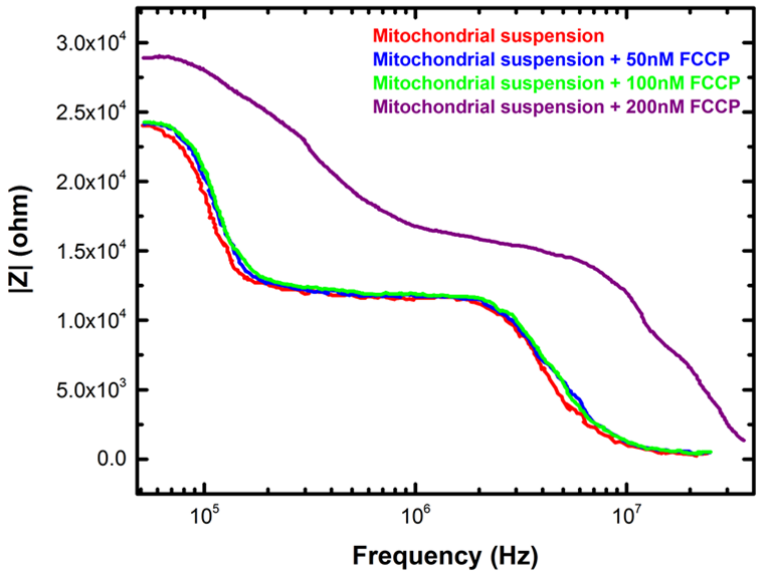

FIGURE 7.13: Change in impedance following FCCP treatment.

7.3 Effects of Dopamine on Mitochondria

As mentioned in Chapter 6, dopamine is a neurotransmitter, and has been related to mitochondrial dysfunction, which has been thought to contribute to the etiology of neurodegenerative diseases. In literature[76, 83, 134], a 35% decrease in State-3 oxygen uptake was found after 0.5mM-1mM dopamine incubation, thereby inducing significantly reduced mitochondrial respiratory control. High dopamine concentrations induce mitochondrial dysfunction through a loss of membrane potential mediated by free radical productions such as NO and H_2O_2[16, 40, 41]. Figure 7.14 shows that impedance rose quickly with an increase of dopamine concentration in mitochondrial suspension. This

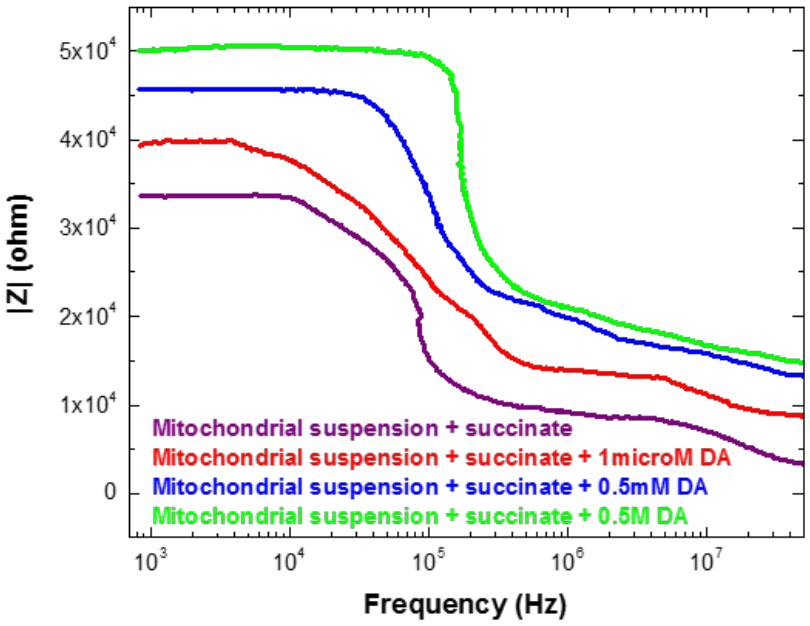

FIGURE 7.14: Impedance variation with frequency for 3 dopamine concentration.

observation provided a clear indication of a significant depolarization of the

mitochondrial membrane potential $\Delta\Psi_m$. More extensive depolarization was caused by FCCP, as was demonstrated in Figure 7.10. Similar characteristics to those in Figure 7.15 were also observed in the Bode plot for phase variation with frequency. As the phase angle decreased with a corresponding increase in the concentration of dopamine, we found there was a loss of electrochemical gradient and lowered bioenergetics in the mitochondrial membranes.

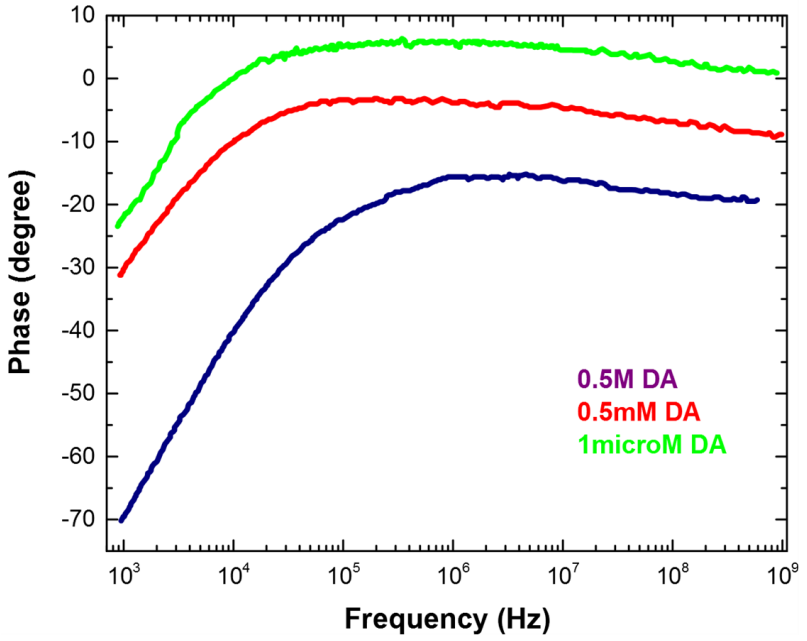

FIGURE 7.15: Bode diagram of the phase variation with frequency for mitochondrial suspension and dopamine added to it.

After incubation with 0.5 mM dopamine, it can be seen from Figure 7.16, that there was a huge leap in the impedance, suggesting that there was a loss of membrane potential. The level of polarization of the mitochondrial sample decreased when compared to the control group of untreated mitochondria. Thus, the results have shown that high dopamine concentrations have deleterious

effects on mitochondrial function, such as a decrease in mitochondrial respiration and a depolarization of mitochondrial membranes. Evaluation of mitochondrial membrane potential showed that low physiological dopamine concentrations do not affect mitochondrial membrane potential, while high dopamine concentration induced depolarization, which is evident from the changes in impedance shown in Figure 7.16.

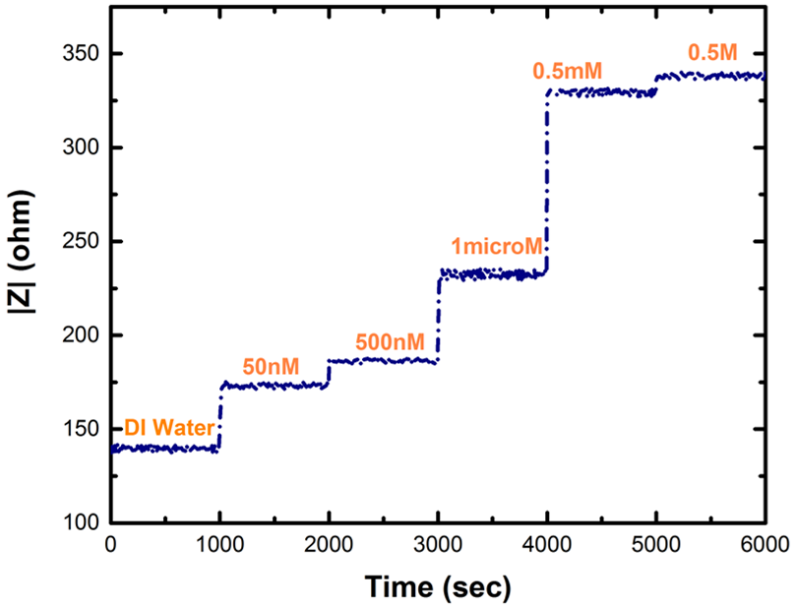

FIGURE 7.16: Impedance versus time for different concentration of DA in mitochondrial suspension.

Our data were consistent with those in an early study by Berman and Hastings[16], who found that dopamine induces mitochondrial permeability transition and produced membrane depolarization. According to our results, uncoupling of the respiratory chain and mitochondrial permeability transition could be the cause of dopamine-induced mitochondrial depolarization. For dopamine, similar to FCCP, we observe that the uncoupling of mitochondrial

electron transport from oxidative phosphorylation occurs in a dose-dependent manner. In neurodegenerative diseases, it is well known that cells with high dopamine concentrations, such as dopaminergic neurons, are highly vulnerable to degeneration[41, 85].

7.4 Correlating FCCP and Dopamine Results

In Figure 7.17 and Figure 7.18 a comparative study is shown, where mitochondrial suspension was incubated with 1mM of FCCP and dopamine (DA). Addition of the

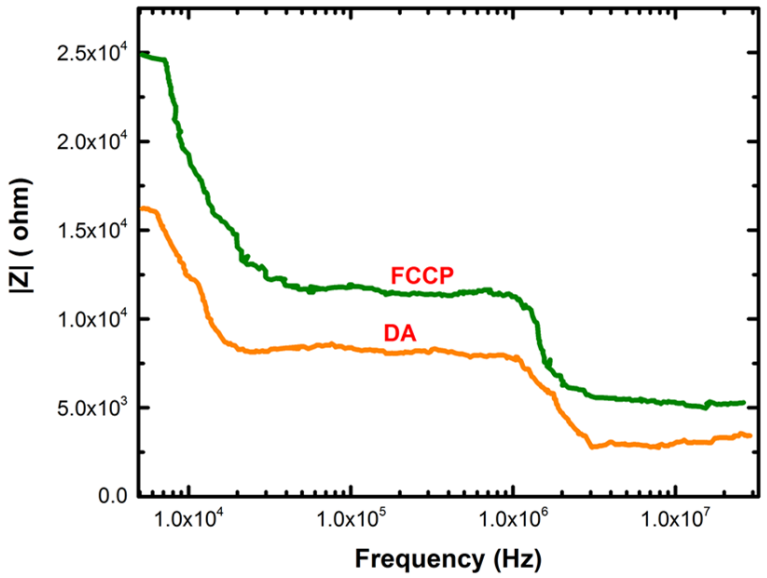

FIGURE 7.17: Comparison of impedance versus frequency for dopamine (DA) and FCCP in mitochondrial suspension.

identical concentration of the protonophore FCCP showed stronger mitochondrial depolarization when compared to the addition of dopamine[41]. Adding FCCP and dopamine increased the impedance of the mitochondrial membrane and thus,

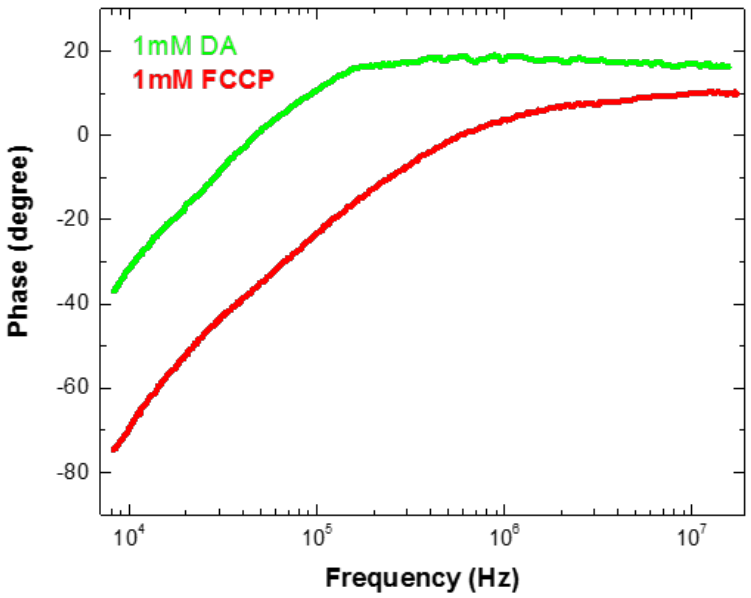

FIGURE 7.18: Comparison of phase versus frequency for dopamine (DA) and FCCP in mitochondrial suspension.

the stored charge was dissipated. This dissipation of membrane charge reduced the capacitance and the conductivity of the membrane, as shown in Figure 7.19.

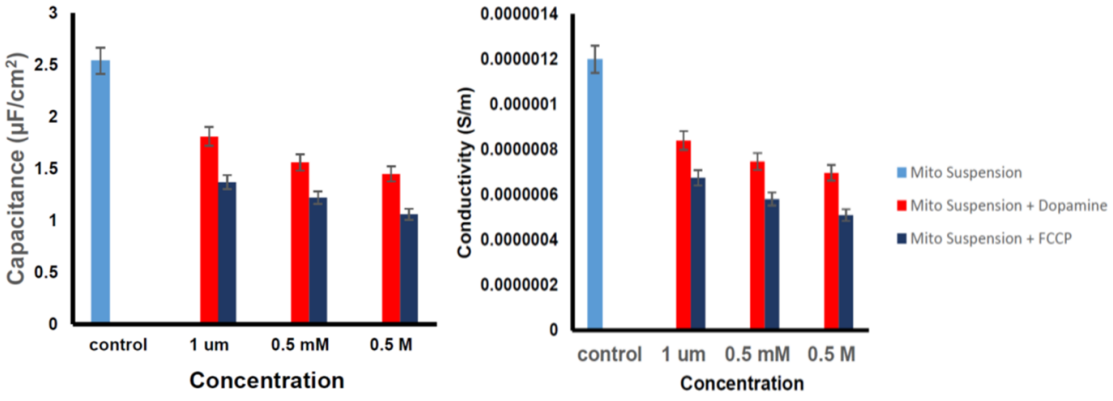

FIGURE 7.19: Comparison of capacitance and conductance of mitochondrial suspension after adding dopamine and FCCP.

The effects were more profound for FCCP than for dopamine. The physiological and psychological responses of changes in the human body due to

changes in the concentration of neurotransmitters has been proposed in a couple of studies[10, 67, 149]. Thus, computed variations in capacitance and conductivity with concentration may provide important clues in the treatment of various neurodegenerative diseases and will act as a stimulus for further research in various fields in biophysics, physiology, and psychology.

Chapter 8

Conclusion and Future Directions

8.1 Conclusion

The impedance technique as a method to monitor biological systems has become a fertile area for developing rapid and effective methods for the detection of the dysfunction of biological entities such as mitochondria. Our goal to explore impedance spectroscopy to identify mitochondrial functional integrity via its electrical characteristics was achieved with success. While the full implementation of this experimental method is not yet completely developed, the procedures show promise for future research.

One of the objectives of this study has been to investigate the electrical impedance properties of mitochondria in vivo using electrical impedance spectroscopy(EIS). The results so far suggest that impedance spectroscopy is a promising alternative technology to extract the electrical properties of the

mitochondrial membrane. It is a successful real-time, label–free, non-invasive, and cost-effective detection technique for the quantitative investigation of passive, non-biological parameters, and also for mitochondrial studies to enrich the clinical process.

The results suggest that this monitoring option is able to produce a signature to distinguish the abnormal mitochondria from normal ones. Apart from a couple of significant studies[117, 132], our impedance studies on mitochondria are a novel state-of-the-art approach. The impedance analysis method we devised is used extensively to describe the change in electrical properties as a function of frequency and time. Electrical impedance of mitochondrial suspensions is a complex quantity, combining resistance and capacitance, and it depends on the frequency of the AC voltage applied. This confirms that the membranes have components that have both conductive and charge storage properties.

Typical frequency spectra as were shown in Figure 7.4, showed that the real part is associated with the resistive pathways across the organelle and the imaginary part is associated with the capacitive pathways of the membrane. The real part is high at low frequency of $\sim$ 100 Hz or lower. As frequency increases, the imaginary part becomes more dominant. At very high frequencies of $\sim 10^8$ Hz, the imaginary part of impedance becomes very small, as the capacitive reactance $X_C = 1/2\pi fC$ tends to zero. The membrane appears as a short circuit. The electric field lines pass more uniformly through mitochondria.

Mitochondrial suspension also displays a significant β dispersion in the range

10^6 Hz. This is due to the Maxwell-Wagner effect at the interface between the mitochondrial membrane and the matrix or the cytoplasm. This illustrates a good correlation with that reported by Schawn[142] and is also analytically validated by studies from our group with a corresponding scaling[132]. The numerical application from Prodan's work[131, 132] showed that there is a very strong dependence of the dielectric dispersion curve on the membrane electrical potential. This has also been found in our experimental measurements.

To elucidate the correspondence further, we see that in Prodan *et al.*[131, 132] the average response of the cell under the influence of the electric field in the frequency range of around 1Hz- 100MHz evokes a development of the dipole moment through α relaxation process. We incorporated the models implemented in Prodan *et al.*[131, 132] via a shell model.

The system shown in Figure 8.1 consists of a composite dielectric structure which contains a dielectric shell representing the cell membrane parameterized by (ϵ_1, σ_1) and a homogeneous dielectric core which is labelled (ϵ_2, σ_2). The governing equations for the system are based on solving for the electric potential through the Laplace equation and the continuity equations for the bound charge. These are coupled with the boundary conditions at the membrane surfaces. The general formalism for determining the dipole moment μ and density ρ has been numerically implemented in Prodan *et al.*[131] using spectral projection operators of the Laplacian. A generic solution of the equations of motion is in principal quite tedious and needs to be solved numerically by choosing an appropriate basis, as

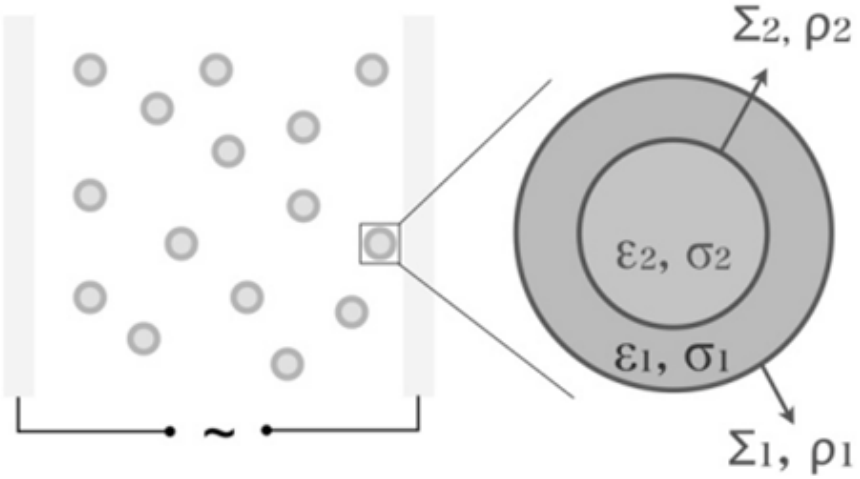

FIGURE 8.1: Model of suspension of live cells[132].

was shown by Prodan *et al.*[131]. However, in a subsequent work of Prodan *et al.* [132], a clever adoption of spherical coordinates with a choice of spherical harmonic basis functions leads to a solution in a closed form. The governing equations in such a case are given bythe following[132]:

$$\gamma_i \overrightarrow{\nabla}^2_{\sum_i} \Phi + D_i \overrightarrow{\nabla}^2_{\sum_i} \rho_i = \mathrm{i}\omega\rho_i \quad and \tag{8.1}$$

$$\epsilon^*_{i-1} \partial_{\overrightarrow{n}} \Phi^+_i - \epsilon^*_i \partial_{\overrightarrow{n}} \Phi^-_i = \rho_i, \tag{8.2}$$

where i runs from 1,2, n denotes the normal component, and ϵ_0 denotes the permittivity of vacuum. The model is characterized by a variety of parameters which include the radius and conductivities of the corresponding shells, along with the set of free parameters, conductivities γ_i and diffusion coefficient D_i on the respective membrane surfaces.

As we mentioned earlier, the system allows an analytical solution when

solved in a symmetrical spherical basis[132] to give the expression for the polarizability. This can eventually lead to determining quantities which can be experimentally verified. We have qualitatively denoted such a comparison in Figure 8.2. The typical parameters for the conductivity and diffusion for the

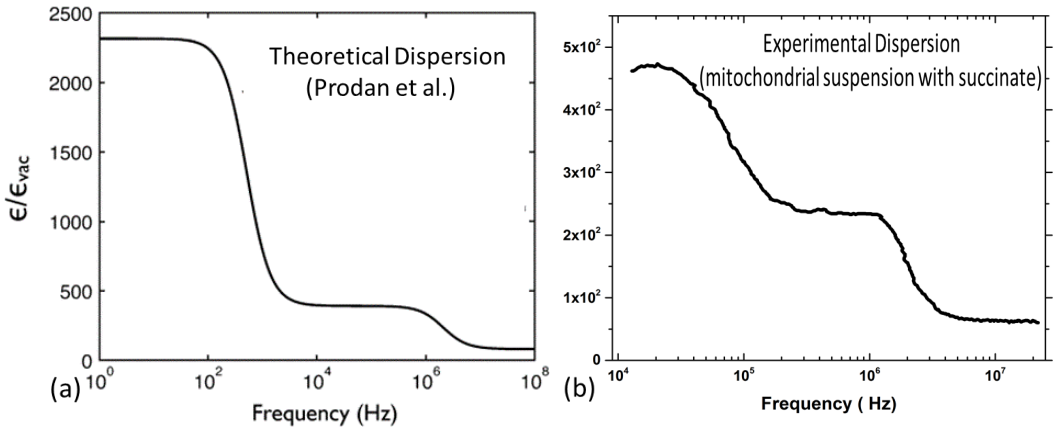

FIGURE 8.2: Frequency-dependent relative permittivity (a) theoretical model[132] and (b) experimental data.

model were kept as $D_1 = D_2 = 10^{-8}$ and $\gamma_1/D_1 = \gamma_1/D_1 = 0.1$. The mitochondrial suspensions depicted the behavior mainly at beta dispersion regimes, and thereby our comparison was limited to such cases. This is typical of biological systems where the model[132] has also been matched to experimental results of live yeast cells in a buffer solution[152] for the β dispersion domains. For our case, the results in the beta dispersion regions around 10^6 Hz clearly show a similarity between the experimental and theoretical permittivity. This can be seen in Figure 8.2, up to a scaling. However, it should be mentioned that since the parameters heavily influence the dispersion properties, the precise matching of the experimental results do involve tuning of the coefficients to

match a proper dielectric system for the mitochondrial suspension. The model has also been shown to match the α dispersion regime for erythrocytes and mammalian cells[21, 132, 133]. These observations, along with our experimental results, clearly indicate the validity and broad applicability of the shell model for the description of dielectric properties of mitochondria.

The theoretical study by Prodan *et al.*[132], employed perturbation analysis, to take into account the excitation of the biological cell, in the presence of an applied external electric field. As shown in the results presented in Figure 7.4, in the limit of low applied electrical fields, dielectric permittivity is directly proportional to membrane potential, and thus, only in this limit we can extract the membrane potential from the impedance response curves. It can also be seen that below 1kHz, the polarization effects increased substantially with decreasing frequency, but above 1kHz, the experimental results agree with the expected ones. Thus, our methodology can be successfully implemeted in the high frequency β dispersion domain.

Two energy carriers are known to donate energy to the electron transport chain, namely nicotine adenine dinucleotide (NAD) and flavin adenine dinucleotide (FAD). FAD is a bound part of the succinate dehydrogenase complex (Complex II). It is reduced when the substrate succinate binds the complex. So, it is expected that as we increase the concentration of succinate successively, the electron activity of Complex II is more extensively triggered. Eventually the membrane increasingly becomes more polarized, which is evident from the decrease in impedance shown

in Figure 7.8. There is an increase in the membrane potential till it reaches close to 150–180 mV, which is the mitochondrial membrane potential at rest. The magnitude of impedance thereby attains its saturation value.

Thus, it is a fascinating and interesting area of research to study the bioelectrical properties of mitochondria, the power house of the cell. Enhanced membrane potential is indicated through the increased values of dielectric constant ϵ capacitance C. Thus, $1/wC$ goes down, which is equivalent to decreasing Z, as explained theoretically in the analysis of Prodan's work[130, 132].

The uncoupler of mitochondrial oxidative phosphorylation FCCP is used in experimental research to investigate its role in the electrical properties of the mitochondria. It has already been established that FCCP lessen the proton motive force across the mitochondrial inner membrane and thereby increase the rate of mitochondrial respiration. This leads to a range of undesired effects, including mitochondrial membrane depolarization, thereby inhibiting mitochondrial membrane potential. To study the electric response of the mitochondrial membrane potential changes, we also added uncoupler FCCP and observed the impedance change. This was shown in Figure 7.10 and the results were validated by a recent study from our group[117]. The impedance increased because of the reduction in membrane potential and dielectric response. The membrane potential goes down with addition of FCCP, implying the decrease in both the dielectric constant ϵ and capacitance C. Thus, $1/wC$ goes up and Z

goes up[132]. This evoked increase in impedance, as expected, and also increased with the concentration of FCCP in a dose-dependent manner. This was shown in Figure 7.12. This is also validated by the oxygen treatment of FCCP shown in Figure 5.3. However, low concentrations of FCCP do not lead to complete membrane depolarization, as shown in Figure 7.13. Thus, we studied the effects of uncouplers on the impedance of a mitochondrial suspension and we found an understandable and promising correlation between impedance and membrane potential.

Previous studies have already shown that the severe mental illness schizophrenia involves excessive amounts of dopamine in the frontal lobes, whereas too little dopamine in the motor areas is responsible for Parkinson's disease, which involves uncontrollable muscle tremors[17, 112, 151]. Figure 5.7 showed that dopamine dissolved in DI water shows a decrease of impedance when concentration is increased. Figure 5.6 showed that capacitance and conductance also increased with concentration. Dopamine, being an oxidisable neurotransmitter, contributes to the conductivity variation[30]. Our study of this neurotransmitter may provide important clues in the treatment of various neurodegenerative diseases, and stimulus for further research in the various fields of biophysics, physiology and psychology and also in alternative medicine.

In Chapter 7, we also discussed that when dopamine is added to mitochondrial suspension, it shows an uncoupling effect, similar to that of FCCP, but comparatively less pronounced. This was shown in Figure 7.17 and 7.18.

Here, unlike the case of dopamine alone, as discussed in chapter 5, the conductivity and capacitance decreased with concentration, as seen in Figure 7.19. In Figure 7.16 we see that the impedance increased with concentration, thereby resulting in the dissipation of mitochondrial membrane potential.

Our results show a significant dose-dependent inhibition of mitochondrial ETC complexes, and thereby a loss of mitochondrial membrane potential, as observed in the case of FCCP[41]. Incubation of mitochondrial suspension with 0.5mM dopamine at 27 ^{o}C showed a significant, approximate 35% decrease in the respiratory control ratio. This is also reflected in Figure 7.16. High dopamine concentration has deleterious effects on mitochondrial function and we validated this for the first time using impedance studies. No previous research has been done relating the electrical response of mitochondrial membrane when adding dopamine.

Thus, our impedance spectroscopy technique also confirms the oxygen consumption method by which dopamine induces mitochondrial membrane depolarization. This plays an important role in the physiopathology of several psychiatric and neurological disorders such as Parkinson's disease and schizophrenia. Our study provides evidence by impedance measurements that high dopamine concentrations induce mitochondrial dysfunction through a decrease in mitochondrial respiratory control and loss of membrane potential, probably mediated by free radical production.

From our experience, when analyzing data in a real-time environment, two

things must be considered. First, proper time should be given for the sample to react to the changes in the applied frequency. Secondly, to determine the response time of the analyzer. However, there exists some ambiguity in understanding the response time of the instrument. A collection scheme too slow will miss critical data; however, a collection scheme too fast may not allow the system to stabilize before making a measurement. As this is quite subjective and completely depending on the experimentalist, slight variation in results can happen.

The Solartron frequency response analyzer used in our study is still an expensive and huge device. A practical device should be handy, easy to operate, and also cheap. Since the impedance spectroscopy method we present has the possibility for commercial use, development of a portable impedance analyzer would be of great importance. It could then be possible for the detection of mitochondrial dysfunction from bench to bedside.

Non-invasive diagnostics require a unique correlation between observed quantities and variation of geometrical and constitutional parameters of biological samples. In order to fulfil these criteria, knowledge is necessary about the relation between changes in sample features and their manifestation in the dielectric spectra, as well as a sensitive experimental set-up. In this direction, research efforts in our group towards the development of electrical impedance spectroscopy via the use of MEMS probes has been promising[117].

Our research presented here is the first step in understanding the

mitochondrial precursors and the main players in deciphering the role of mitochondria as biomarkers. Future research in extending our results to implement MEMS would definitely improve the technology. By using MEMS in future mitochondrial studies, researchers will be successful in maximizing the impedance signal, minimizing the volume of the testing sample, and increasing sensitivity. Such biosensor research is not only driving the ever-accelerating race to construct smaller, faster, cheaper, and more efficient devices, but may also ultimately result in the successful integration of electronic and biological systems. Any advancement in this field will have a positive effect on the future of diagnostics and health care.

Bibliography

[1] Aaberg, P. (2004). *Skin cancer as seen by electrical impedance*. Institutionen för laboratoriemedicin/Department of Laboratory Medicine (Thesis).

[2] Adekunle, A. S., Ayenimo, J. G., Fang, X.-Y., Doherty, W. O., Arotiba, O. A., and Mamba, B. B. (2011). Electrochemical response and impedimetric behaviour of Dopamine and Epinephrine at Platinum Electrode Modified with Carbon Nanotubes-Gold Nanocomposite. *Int. J. Electrochem. Sci*, 6:2826–2844.

[3] Alberts, B., Johnson, A., Lewis, J., Raff, M., Roberts, K., and Walter, P. (1997). Molecular Biology of the Cell (Garland Science, New York, 2002).

[4] Ammam, M. (2012). Electrophoretic deposition under modulated electric fields: a review. *RSC Advances*, 2(20):7633–7646.

[5] Andersson, S. G. and Kurland, C. G. (1999). Origins of mitochondria and hydrogenosomes. *Current opinion in microbiology*, 2(5):535–541.

[6] Aragonés, J., Schneider, M., Van Geyte, K., Fraisl, P., Dresselaers, T., Mazzone, M., Dirkx, R., Zacchigna, S., Lemieux, H., Jeoung, N. H., et al.

(2008). Deficiency or inhibition of oxygen sensor phd1 induces hypoxia tolerance by reprogramming basal metabolism. *Nature Genetics*, 40(2):170–180.

[7] Asami, K., Hanai, T., and Koizumi, N. (1977). Dielectric properties of yeast cells: effect of some ionic detergents on the plasma membranes. *The Journal of Membrane Biology*, 34(1):145–156.

[8] Asami, K. and Irimajiri, A. (1984). Dielectric analysis of mitochondria isolated from rat liver ii. intact mitochondria as simulated by a double-shell model. *Biochimica et Biophysica Acta (BBA) - Biomembranes*, 778(3):570–578.

[9] Atkinson, A. J., Colburn, W. A., DeGruttola, V. G., DeMets, D. L., Downing, G. J., Hoth, D. F., Oates, J. A., Peck, C. C., Schooley, R. T., Spilker, B. A., et al. (2001). Biomarkers and surrogate endpoints: Preferred definitions and conceptual framework. *Clinical Pharmacology & Therapeutics*, 69(3):89–95.

[10] Bains, J. S. and Shaw, C. A. (1997). Neurodegenerative disorders in humans: the role of glutathione in oxidative stress-mediated neuronal death. *Brain Research Reviews*, 25(3):335–358.

[11] Bandarenka, A. S. (2013). Exploring the interfaces between metal electrodes and aqueous electrolytes with electrochemical impedance spectroscopy. *Analyst*, 138(19):5540–5554.

[12] Bao, J. Z., Davis, C. C., and Schmukler, R. E. (1993). Impedance spectroscopy of human erythrocytes: system calibration, and nonlinear modeling. *Biomedical Engineering, IEEE Transactions on*, 40(4):364–378.

[13] Barsoukov, E. and Macdonald, J. R. (2005). *Impedance spectroscopy: theory, experiment, and applications*. John Wiley & Sons, New York.

[14] Bayne, K. (1996). Revised Guide for the Care and Use of Laboratory Animals available. American Physiological Society. *The Physiologist*, 39(4):199–208.

[15] Berg, J. M., Tymoczko, J. L., and Stryer, L. (2002). *Biochemistry, W. H.* Freeman and Company: New York.

[16] Berman, S. B. and Hastings, T. G. (1999). Dopamine oxidation alters mitochondrial respiration and induces permeability transition in brain mitochondria. *Journal of Neurochemistry*, 73(3):1127–1137.

[17] Bernheimer, H., Birkmayer, W., Hornykiewicz, O., Jellinger, K., and Seitelberger, F. . (1973). Brain dopamine and the syndromes of Parkinson and Huntington Clinical, morphological and neurochemical correlations. *Journal of the Neurological Sciences*, 20(4):415–455.

[18] Bhattacharya, S., Jang, J., Yang, L., Akin, D., and Bashir, R. (2007). BioMEMS and nanotechnology-based approaches for rapid detection of biological entities. *Journal of Rapid Methods & Automation in Microbiology*, 15(1):1–32.

[19] Blottcher, C. J. F., Van Belle, O. C., Bordewijk, P., Rip, A., and Yue, D. D. (1974). Theory of electric polarization. *Journal of The Electrochemical Society*, 121(6):211C–211C.

[20] Boore, J. L. (1999). Animal mitochondrial genomes. *Nucleic Acids Research*, 27(8):1767–1780.

[21] Bordi, F., Cametti, C., and Gili, T. (2001). Reduction of the contribution of electrode polarization effects in the radiowave dielectric measurements of highly conductive biological cell suspensions. *Bioelectrochemistry*, 54(1):53–61.

[22] Bot, C. and Prodan, C. (2009). Probing the membrane potential of living cells by dielectric spectroscopy. *European Biophysics Journal*, 38(8):1049–1059.

[23] Bot, C. T. and Prodan, C. (2010). Quantifying the membrane potential during e. coli growth stages. *Biophys Chem*, 146(2-3):133–7.

[24] Bozdemir, S. (1989). A critical examination Of The dielectric relaxation theories about non-debye response. *Communications de la Faculte des sciences de l'Universite d'Ankara: Physics, Engineering Physics and Astronomy*, 38(1-2):47.

[25] Brand, M. D., Chien, L.-F., Ainscow, E. K., Rolfe, D. F., and Porter, R. K. (1994). The causes and functions of mitochondrial proton leak. *Biochimica et Biophysica Acta (BBA)-Bioenergetics*, 1187(2):132–139.

[26] Brand, M. D. and Nicholls, D. G. (2011). Assessing mitochondrial dysfunction in cells. *Biochemical Journal*, 435(2):297–312.

[27] Brehm-Stecher, B. F. and Johnson, E. A. (2004). Single-cell microbiology: tools, technologies, and applications. *Microbiology and molecular biology reviews*, 68(3):538–559.

[28] Brennan, J. P., Berry, R. G., Baghai, M., Duchen, M. R., and Shattock, M. J. (2006a). Fccp is cardioprotective at concentrations that cause mitochondrial oxidation without detectable depolarisation. *Cardiovasc Res*, 72(2):322–30. Brennan, Jonathan P Berry, Roger G Baghai, Max Duchen, Michael R Shattock, Michael J Netherlands Cardiovasc Res. 2006 Nov 1;72(2):322-30. Epub 2006 Aug 16.

[29] Brennan, J. P., Southworth, R., Medina, R. A., Davidson, S. M., Duchen, M. R., and Shattock, M. J. (2006b). Mitochondrial uncoupling, with low concentration fccp, induces ros-dependent cardioprotection independent of katp channel activation. *Cardiovasc Res*, 72(2):313–21.

[30] Bruns, D. (2004). Detection of transmitter release with carbon fiber electrodes. *Methods*, 33(4):312–321.

[31] Buchanan, T. J., Haggis, G. H., Hasted, J. B., and Robinson, B. G. (1952). The dielectric estimation of protein hydration. *Proceedings of the Royal Society of London. Series A. Mathematical and Physical Sciences*, 213(1114):379–391.

[32] Callister, W. D. and Rethwisch, D. G. (2007). *Materials science and engineering: an introduction*, volume 7. Wiley New York.

[33] Capuano, F., Guerrieri, F., and Papa, S. (1997). Oxidative phosphorylation enzymes in normal and neoplastic cell growth. *Journal of Bioenergetics and Biomembranes*, 29(4):379–384.

[34] Carmichael, J., DeGraff, W. G., Gazdar, A. F., Minna, J. D., and Mitchell, J. B. (1987). Evaluation of a tetrazolium-based semiautomated colorimetric assay: assessment of chemosensitivity testing. *Cancer Research*, 47(4):936–942.

[35] Chandel, N. S. and Schumacker, P. T. (2000). Cellular oxygen sensing by mitochondria: old questions, new insight. *Journal of Applied Physiology*, 88(5):1880–1889.

[36] Chao, P.-J., Huang, E.-Y., Cheng, K.-S., and Huang, Y.-J. (2013). Electrical impedance spectroscopy as electrical biopsy for monitoring radiation sequelae of intestine in rats. *BioMed Research International*, 2013.

[37] Cole, K. S. and Cole, R. H. (1941). Dispersion and absorption in dielectrics I. Alternating current characteristics. *The Journal of Chemical Physics*, 9(4):341–351.

[38] Cortassa, S. and Aon, M. A. (2014). *Dynamics of Mitochondrial Redox and Energy Networks: Insights from an Experimental–Computational Synergy*, pages 115–144. Springer.

[39] Cotney, J. L. (2008). *Divergent evolution of the paralogous human mitochondrial transcription factors, h-mtTFB1 and h-mtTFB2, to fulfill unique functions in mitochondrial gene expression, biogenesis, and retrograde signaling.* PhD thesis, Emory University.

[40] Czerniczyniec, A., Bustamante, J., and Lores-Arnaiz, S. (2007). Dopamine enhances mtNOS activity: implications in mitochondrial function. *Biochimica et Biophysica Acta (BBA)-Bioenergetics*, 1767(9):1118–1125.

[41] Czerniczyniec, A., Bustamante, J., and Lores-Arnaiz, S. (2010). Dopamine modifies oxygen consumption and mitochondrial membrane potential in striatal mitochondria. *Molecular and Cellular Biochemistry*, 341(1-2):251–257.

[42] Davidson, D. W. and Cole, R. H. (1951). Dielectric relaxation in glycerol, propylene glycol, and n-propanol. *The Journal of Chemical Physics*, 19(12):1484–1490.

[43] Debye, P. P. and Conwell, E. M. (1954). Electrical properties of N-type germanium. *Physical Review*, 93(4):693.

[44] DeLacey, E. H. and White, L. R. (1981). Dielectric response and conductivity of dilute suspensions of colloidal particles. *Journal of the Chemical Society, Faraday Transactions 2: Molecular and Chemical Physics*, 77(11):2007–2039.

[45] Di Biasio, A., Ambrosone, L., and Cametti, C. (2010). The dielectric behavior of nonspherical biological cell suspensions: an analytic approach. *Biophys J*,

99(1):163–74. Di Biasio, A Ambrosone, L Cametti, C Biophys J. 2010 Jul 7;99(1):163-74. doi: 10.1016/j.bpj.2010.04.006.

[46] Duchen, M. R. (2004). Mitochondria in health and disease: perspectives on a new mitochondrial biology. *Mol Aspects Med*, 25(4):365–451.

[47] Dukhin, S. S. and Shilov, V. N. (1974). Dielectric phenomena and the double layer in disperse systems and polyelectrolytes, John Wiley & Sons, New York.

[48] Ellappan, P. and Sundararajan, R. (2005). A simulation study of the electrical model of biological cells. *J Electrostat*, 63:297–307.

[49] Emmert, S., Wolf, M., Gulich, R., Krohns, S., Kastner, S., Lunkenheimer, P., and Loidl, A. (2011). Electrode polarization effects in broadband dielectric spectroscopy. *The European Physical Journal B*, 83(2):157–165.

[50] Evgenij, B. and Macdonald, J. R. (2005). Impedance spectroscopy theory, experiment, and applications, wiley, new jersey.

[51] Feeney, C. J., Pennefather, P. S., and Gyulkhandanyan, A. V. (2003). A cuvette-based fluorometric analysis of mitochondrial membrane potential measured in cultured astrocyte monolayers. *Journal of Neuroscience Methods*, 125(1):13–25.

[52] Feldman, Y., Puzenko, A., and Ryabov, Y. (2002). Non-Debye dielectric relaxation in complex materials. *Chemical Physics*, 284(1):139–168.

[53] Fixman, M. (1980). Charged macromolecules in external fields. I. The sphere. *The Journal of Chemical Physics*, 72(9):5177–5186.

[54] Foster, K. R. and Schwan, H. P. (1988). Dielectric properties of tissues and biological materials: a critical review. *Critical Reviews in Biomedical Engineering*, 17(1):25–104.

[55] Frey, T. G. and Mannella, C. A. (2000). The internal structure of mitochondria. *Trends in Biochemical Sciences*, 25(7):319–324.

[56] Frezza, C., Cipolat, S., and Scorrano, L. (2007). Organelle isolation: functional mitochondria from mouse liver, muscle and cultured filroblasts. *Nature protocols*, 2(2):287–295.

[57] Fricke, H. (1933). The electric impedance of suspensions of biological cells. *Cold Spring Harbor Symposia on Quantitative Biology*, 1(0):117–124.

[58] Fröhlich, H. (1958). *Theory of dielectrics: dielectric constant and dielectric loss*. Clarendon Press, Oxford.

[59] Gabriel, C. (2006). Dielectric properties of biological materials. *Bioengineering and Biophysical Aspects of Electromagnetic Fields*, 1:87–136.

[60] Gabriel, C., Gabriel, S., and Corthout, E. (1996). The dielectric properties of biological tissues: I. Literature survey. *Physics in Medicine and Biology*, 41(11):2231.

[61] Gangwal, S., Cayre, O. J., Bazant, M. Z., and Velev, O. D. (2008). Induced-charge electrophoresis of metallodielectric particles. *Physical Review Letters*, 100(5):058302.

[62] Garcia-Ruiz, C., Colell, A., Morales, A., Kaplowitz, N., and Fernández-Checa, J. C. (1995). Role of oxidative stress generated from the mitochondrial electron transport chain and mitochondrial glutathione status in loss of mitochondrial function and activation of transcription factor nuclear factor-kappa B: studies with isolated mitochondria and rat hepatocytes. *Molecular Pharmacology*, 48(5):825–834.

[63] Gasch, A. P., Spellman, P. T., Kao, C. M., Carmel-Harel, O., Eisen, M. B., Storz, G., Botstein, D., and Brown, P. O. (2000). Genomic expression programs in the response of yeast cells to environmental changes. *Molecular Biology of the Cell*, 11(12):4241–4257.

[64] Gersing, E., Kelleher, D. K., and Vaupel, P. (2003). Tumour tissue monitoring during photodynamic and hyperthermic treatment using bioimpedance spectroscopy. *Physiological Measurement*, 24(2):625.

[65] Giaever, I. and Keese, C. R. (1984). Monitoring fibroblast behavior in tissue culture with an applied electric field. *Proceedings of the National Academy of Sciences*, 81(12):3761–3764.

[66] Gonzalez, J. E. and Tsien, R. Y. (1997). Improved indicators of cell membrane potential that use fluorescence resonance energy transfer. *Chemistry & Biology*, 4(4):269–277.

[67] Gramigni, E., Cozzi, A., Pancani, T., De Gaudio, R. A., Pellegrini-Giampietro, D. E., Adembri, C., Venturi, L., Tani, A., and Chiarugi, A. (2006). Neuroprotective effects of propofol in models of cerebral ischemia: inhibition of mitochondrial swelling as a possible mechanism. *Anesthesiology*, 104(1):80–89.

[68] Grant, E. H., Sheppard, R. J., and South, G. P. (1978). Dielectric behaviour of biological molecules in solution, clarendon press, oxford.

[69] Grimnes, S., Rikshospitalet, O., and Schwan, N. H. P. (2002). Interface phenomena and dielectric properties of biological tissue. *Encyclopedia of Surface and Colloid science*, 20:2643–2653.

[70] Gusmano, G., Bianco, A., Montesperelli, G., and Traversa, E. (1996). An EIS study of the humidity-sensitive electrical conduction of alkali-doped TiO_2 films. *Electrochimica Acta*, 41(7):1359–1368.

[71] Gustafsson, Å. B. and Gottlieb, R. A. (2007). Heart mitochondria: gates of life and death. *Cardiovascular Research*.

[72] Harris, C. M. and Kell, D. B. (1985). On the dielectrically observable consequences of the diffusional motions of lipids and proteins in membranes. *European Biophysics Journal*, 13(1):11–24.

[73] Havriliak, S. and Negami, S. (1966). A complex plane analysis of α dispersions in some polymer systems, Journal of Polymer Science Part C: Polymer Symposia. volume 14, pages 99–117. Wiley Online Library.

[74] Hilger, I., Geyer, C., Thiel, F., di Clemente, F. S., Seifert, F., Rimkus, G., Sachs, J., Dahlke, K., Helbig, M., Hein, M., and others (2013). *UltraMEDIS-ultra-wideband sensing in medicine*. INTECH Open Access Publisher.

[75] Hollenbeck, P. J., Bray, D., and Adams, R. J. (1985). Effects of the uncoupling agents FCCP and CCCP on the saltatory movements of cytoplasmic organelles. *Cell Biology International Reports*, 9(2):193–199.

[76] Holloszy, J. O. (1967). Biochemical adaptations in muscle effects of exercise on mitochondrial oxygen uptake and respiratory enzyme activity in skeletal muscle. *Journal of Biological Chemistry*, 242(9):2278–2282.

[77] Huttemann, M., Lee, I., Pecinova, A., Pecina, P., Przyklenk, K., and Doan, J. W. (2008). Regulation of oxidative phosphorylation, the mitochondrial membrane potential, and their role in human disease. *Journal of Bioenergetics and Biomembranes*, 40(5):445–456.

[78] Irvine, J. T., Sinclair, D. C., and West, A. R. (1990). Electroceramics: characterization by impedance spectroscopy. *Advanced Materials*, 2(3):132–138.

[79] Itzhaki, R. F. and Gill, D. M. (1964). A micro-biuret method for estimating proteins. *Analytical Biochemistry*, 9(4):401–410.

[80] Jayalakshmi, M. and Balasubramanian, K. (2008). Simple capacitors to supercapacitors-an overview. *Int. J. Electrochem. Sci*, 3(11):1196–1217.

[81] Jones, T. B. and Jones, T. B. (2005). *Electromechanics of particles*. Cambridge University Press, Cambridge.

[82] Kadenbach, B., Ramzan, R., Moosdorf, R., and Vogt, S. (2011). The role of mitochondrial membrane potential in ischemic heart failure. *Mitochondrion*, 11(5):700–706.

[83] Kamo, N., Muratsugu, M., Hongoh, R., and Kobatake, Y. (1979). Membrane potential of mitochondria measured with an electrode sensitive to tetraphenyl phosphonium and relationship between proton electrochemical potential and phosphorylation potential in steady state. *The Journal of Membrane Biology*, 49(2):105–121.

[84] Kao, K. C. (2004). *Dielectric phenomena in solids*. Academic Press, New York.

[85] Khan, F. H., Sen, T., Maiti, A. K., Jana, S., Chatterjee, U., and Chakrabarti, S. (2005). Inhibition of rat brain mitochondrial electron transport chain activity by dopamine oxidation products during extended in vitro incubation: implications for Parkinson's disease. *Biochimica et Biophysica Acta (BBA)-Molecular Basis of Disease*, 1741(1):65–74.

[86] Klingenberg, M. (2008). The ADP and ATP transport in mitochondria and its carrier. *Biochimica et Biophysica Acta (BBA)-Biomembranes*, 1778(10):1978–2021.

[87] Klösgen, B., Rümenapp, C., and Gleich, B. (2011). Bioimpedance spectroscopy. In *BetaSys*, pages 241–271. Springer, Copenhagen.

[88] Kötz, R. and Carlen, M. (2000). Principles and applications of electrochemical capacitors. *Electrochimica Acta*, 45(15):2483–2498.

[89] Kuang, W. and Nelson, S. O. (1997). Low-frequency dielectric dispersion from ion permeability of membranes. *Journal of Colloid and Interface Science*, 193(2):242–249.

[90] Kyle, U. G., Bosaeus, I., De Lorenzo, A. D., Deurenberg, P., Elia, M., Gómez, J. M., Heitmann, B. L., Kent-Smith, L., Melchior, J.-C., Pirlich, M., et al. (2004). Bioelectrical impedance analysis-part 1: review of principles and methods. *Clinical Nutrition*, 23(5):1226–1243.

[91] Labajova, A., Vojtiskova, A., Krivakova, P., Kofranek, J., Drahota, Z., and Houstek, J. (2006). Evaluation of mitochondrial membrane potential using a computerized device with a tetraphenylphosphonium-selective electrode. *Anal Biochem*, 353(1):37–42.

[92] Lei, K. F. (2014). Review on impedance detection of cellular responses in micro/nano environment. *Micromachines*, 5(1):1–12.

[93] Lin, M. T. and Beal, M. F. (2006). Mitochondrial dysfunction and oxidative stress in neurodegenerative diseases. *Nature*, 443(7113):787–795.

[94] Ling, G. and Gerard, R. W. (1949). The normal membrane potential of frog sartorius fibers. *Journal of Cellular and Comparative Physiology*, 34(3):383–396.

[95] Ly, J. D., Grubb, D., and Lawen, A. (2003). The mitochondrial membrane potential ($\delta\psi$m) in apoptosis; an update. *Apoptosis*, 8(2):115–128.

[96] Macdonald, J. R. and Johnson, W. B. (2005). Fundamentals of impedance spectroscopy. *Impedance Spectroscopy: Theory, Experiment, and Applications, Second Edition*, pages 1–26.

[97] Maechler, P. and Wollheim, C. B. (2001). Mitochondrial function in normal and diabetic β–cells. *Nature*, 414(6865):807–812.

[98] Malleo, D. (2009). *Impedance spectroscopy for cellular and biomolecular analysis*. PhD thesis, University of Southampton.

[99] Mangelsdorf, C. and White, L. (1997). Dielectric response of a dilute suspension of spherical colloidal particles to an oscillating electric field. *Journal of the Chemical Society, Faraday Transactions*, 93(17):3145–3154.

[100] Manickam, A., Chevalier, A., McDermott, M., Ellington, A. D., and Hassibi, A. (2010). A cmos electrochemical impedance spectroscopy (eis) biosensor array. *Biomedical Circuits and Systems, IEEE Transactions on*, 4(6):379–390.

[101] Margulis, L. and others (1981). *Symbiosis in cell evolution*. WH freeman, Boston.

[102] Markovsky, B., Levi, M. D., and Aurbach, D. (1998). The basic electroanalytical behavior of practical graphite–lithium intercalation electrodes. *Electrochimica Acta*, 43(16):2287–2304.

[103] Mascini, M. and Tombelli, S. (2008). Biosensors for biomarkers in medical diagnostics. *Biomarkers*, 13(7-8):637–657.

[104] Michael, A. C., Borland, L. M., John, C. E., and Jones, S. R. (2007). Fast Scan Cyclic Voltammetry of Dopamine and Serotonin in Mouse Brain Slices, crc press, boca raton.

[105] Mohsin, M. A., Banica, F.-G., Oshima, T., and Hianik, T. (2011). Electrochemical impedance spectroscopy for assessing the recognition of cytochrome c by immobilized calixarenes. *Electroanalysis*, 23(5):1229–1235.

[106] Molleman, A. (2003). *Patch clamping: an introductory guide to patch clamp electrophysiology*. John Wiley & Sons, New York.

[107] Mourier, A., Matic, S., Ruzzenente, B., Larsson, N.-G., and Milenkovic, D. (2014). The respiratory chain supercomplex organization is independent of cox7a2l isoforms. *Cell Metabolism*, 20(6):1069–1075.

[108] Muobarak, J. T. (2012). Bioelectrical impedance as a diagnostic factor in the clinical practice and prognostic factor for survival in cancer patients: prediction, accuracy and reliability. *Journal of Biosensors & Bioelectronics*.

[109] Nicholls, D. G. (2004). Mitochondrial membrane potential and aging. *Aging Cell*, 3(1):35–40.

[110] Nichols, D. G. and Ferguson, S. J. (2002). *Bioenergetics*, Academic Press, Amsterdam.

[111] O'Brien, R. W. (1982). The response of a colloidal suspension to an alternating electric field. *Advances in Colloid and Interface Science*, 16(1):281–320.

[112] Ohara, K., Ulpian, C., Seeman, P., Sunahara, R. K., Van Tol, H. H., and Niznik, H. B. (1993). Schizophrenia: dopamine D1 receptor sequence is normal, but has DNA polymorphisms. *Neuropsychopharmacology*, 8(2):131–135.

[113] O'Rourke, B., Cortassa, S., and Aon, M. A. (2005). Mitochondrial ion channels: gatekeepers of life and death. *Physiology (Bethesda)*, 20:303–15.

[114] Osterman, K. S., Hoopes, P. J., DeLorenzo, C., Gladstone, D. J., and Paulsen, K. D. (2004). Non-invasive assessment of radiation injury with electrical impedance spectroscopy. *Physics in Medicine and Biology*, 49(5):665.

[115] Paatsch, W. (1991). Electrochemical impedance spectroscopy (EIS) A powerful in-situ technioque for electrode processes. *Transactions of the Institute of Metal Finishing*, 69:90–91.

[116] Padmaraj, D., Miller Jr, J. H., Wosik, J., and Zagozdzon-Wosik, W. (2011). Reduction of electrode polarization capacitance in low-frequency impedance spectroscopy by using mesh electrodes. *Biosensors and Bioelectronics*, 29(1):13–17.

[117] Padmaraj, D., Pande, R., Miller Jr, J. H., Wosik, J., and Zagozdzon-Wosik, W. (2014). Mitochondrial membrane studies using impedance spectroscopy with parallel pH monitoring. *PloS One*, 9(7):1–8.

[118] Palade, G. E. (1953). An electron microscope study of the mitochondrial structure. *J Histochem Cytochem*, 1(4):188–211.

[119] Palmer, J. W., Tandler, B., and Hoppel, C. L. (1977). Biochemical properties of subsarcolemmal and interfibrillar mitochondria isolated from rat cardiac muscle. *Journal of Biological Chemistry*, 252(23):8731–8739.

[120] Park, K. S., Jo, I., Pak, K., Bae, S. W., Rhim, H., Suh, S. H., Park, J., Zhu, H., So, I., and Kim, K. W. (2002). Fccp depolarizes plasma membrane potential by activating proton and na+ currents in bovine aortic endothelial cells. *Pflugers Arch*, 443(3):344–52.

[121] Parsons, R. (1964). The kinetics of electrode reactions and the electrode material. *Surface Science*, 2:418–435.

[122] Pauly, H., Packer, l., and Schwan, H. (1960). Electrical properties of mitochondrial membranes. *J Biophys Biochem Cytol.*, 7(4):589–601.

[123] Pedersen, P. L. and Morris, H. P. (1974). Uncoupler-stimulated adenosine triphosphatase activity. Deficiency in intact mitochondria from morris hepatomas and ascites tumor cells. *J Biol Chem*, 249(11):3327–34. Pedersen, P L Morris, H P J Biol Chem. 1974 Jun 10;249(11):3327-34.

[124] Pennock, B. E. and Schwan, H. P. (1969). Further observations on the electrical properties of hemoglobin-bound water. *The Journal of Physical Chemistry*, 73(8):2600–2610.

[125] Pethig, R. (1984). Dielectric properties of biological materials: Biophysical and medical applications. *Electrical Insulation, IEEE Transactions on*, (5):453–474.

[126] Pethig, R. (1987). Dielectric properties of body tissues. *Clinical Physics and Physiological Measurement*, 8(4A):5.

[127] Pethig, R. (2010). Review article-dielectrophoresis: status of the theory, technology, and applications. *Biomicrofluidics*, 4(2):022811.

[128] Plášek, J. and Sigler, K. (1996). Slow fluorescent indicators of membrane potential: a survey of different approaches to probe response analysis. *Journal of Photochemistry and Photobiology B: Biology*, 33(2):101–124.

[129] Pooreydy, B., Jafari, M., Tajik, F., Karimi, M., Rezaei-Tavirani, M., Ghassempour, A., Rezadoost, H., and Khodabandeh, M. (2013). Organelle isolation for proteomics: mitochondria from peripheral blood mononuclear cells. *Journal of Paramedical Sciences*, 4:78–87.

[130] Prodan, C., Mayo, F., Claycomb, J. R., Miller Jr, J. H., and Benedik, M. J. (2004). Low-frequency, low-field dielectric spectroscopy of living cell suspensions. *Journal of Applied Physics*, 95(7):3754–3756.

[131] Prodan, C. and Prodan, E. (1999). The dielectric behaviour of living cell suspensions. *Journal of Physics D: Applied Physics*, 32(3):335.

[132] Prodan, E., Prodan, C., and Miller Jr, J. H. (2008). The dielectric response of spherical live cells in suspension: an analytic solution. *Biophysical Journal*, 95(9):4174–4182.

[133] Raicu, V., Saibara, T., and Irimajiri, A. (1998). Dielectric properties of rat liver in vivo: a noninvasive approach using an open-ended coaxial probe at audio/radio frequencies. *Bioelectrochemistry and Bioenergetics*, 47(2):325–332.

[134] Rossi, C. S. and Lehninger, A. L. (1964). Stoichiometry of respiratory stimulation, accumulation of Ca++ and phosphate, and oxidative

phosphorylation in rat liver mitochondria. *Journal of Biological Chemistry*, 239(11):3971–3980.

[135] Rottenberg, H. and Wu, S. (1998). Quantitative assay by flow cytometry of the mitochondrial membrane potential in intact cells. *Biochimica et Biophysica Acta (BBA) - Molecular Cell Research*, 1404(3):393–404.

[136] Rustin, P., Munnich, A., and Roetig, A. (2002). Succinate dehydrogenase and human diseases: new insights into a well-known enzyme. *European Journal of of Human Genetics:*, 10(5):289–291.

[137] Sanchez, B., Aroul, P., Lourdes, A., Bartolome, E., Soundarapandian, K., and Bragos, R. (2014). Propagation of measurement errors through body composition equations for body impedance analysis. *Instrumentation and Measurement, IEEE Transactions on*, 63(6):1535–1544.

[138] Scheffler, I. E. (2001). A century of mitochondrial research: achievements and perspectives. *Mitochondrion*, 1(1):3–31.

[139] Schiefelbein, S. L., Fried, N. A., Rhoads, K. G., and Sadoway, D. R. (1998). A high-accuracy, calibration-free technique for measuring the electrical conductivity of liquids. *Review of Scientific Instruments*, 69(9):3308–3313.

[140] Schwan, H. P. (1965). Electrical properties of bound water. *Annals of the New York Academy of Sciences*, 125(2):344–354.

[141] Schwan, H. P. (1981). Electrical properties of cells: principles, some recent results, and some unresolved problems, the Biophysical appproach to excitable systems. pages 3–24. Springer, New York, 2 edition.

[142] Schwan, H. P. (1992). Linear and nonlinear electrode polarization and biological materials. *Annals of Biomedical Engineering*, 20(3):269–288.

[143] Schwan, H. P. (2013). Determination of biological impedances. *Physical techniques in biological research*, 6(Part B):323–407.

[144] Schwan, H. P. and Foster, K. R. (1980). RF-field interactions with biological systems: electrical properties and biophysical mechanisms. *Proceedings of the IEEE*, 68(1):104–113.

[145] Schwarz, G. (1962). A theory of the low-frequency dielectric dispersion of colloidal particles in electrolyte solution1, 2. *The Journal of Physical Chemistry*, 66(12):2636–2642.

[146] Scott, M., Kaler, K. V., and Paul, R. (2001). Theoretical model of electrode polarization and AC electroosmotic fluid flow in planar electrode arrays. *Journal of Colloid and Interface Science*, 238(2):449–451.

[147] Seifter, J. L. and Aronson, P. S. (1986). Properties and physiologic roles of the plasma membrane sodium-hydrogen exchanger. *Journal of Clinical Investigation*, 78(4):859–864.

[148] Shamah, S. M. and Cunningham, B. T. (2011). Label-free cell-based assays using photonic crystal optical biosensors. *Analyst*, 136(6):1090–1102.

[149] Soane, L., Kahraman, S., Kristian, T., and Fiskum, G. (2007). Mechanisms of impaired mitochondrial energy metabolism in acute and chronic neurodegenerative disorders. *Journal of Neuroscience Research*, 85(15):3407–3415.

[150] Srinivasan, B., Tung, S., Li, Y., and Varshney, M. (2006). Simulation of an electrical impedance based microfluidic biosensor for detection of E. coli cells, Proceedings of the COMSOL Users Conference. pages 22–24.

[151] Sternberg, D. E., VanKammen, D. P., Lerner, P., and Bunney, W. E. (1982). Schizophrenia: dopamine beta-hydroxylase activity and treatment response. *Science*, 216(4553):1423–1425.

[152] Stoneman, M., Chaturvedi, A., Jansma, D. B., Kosempa, M., Zeng, C., and Raicu, V. (2007). Protein influence on the plasma membrane dielectric properties: In vivo study utilizing dielectric spectroscopy and fluorescence microscopy. *Bioelectrochemistry*, 70(2):542–550.

[153] Stuart, G. J. and Palmer, L. M. (2006). Imaging membrane potential in dendrites and axons of single neurons. *Pflügers Archiv*, 453(3):403–410.

[154] Sun, T. and Morgan, H. (2010). Single-cell microfluidic impedance cytometry: a review. *Microfluidics and Nanofluidics*, 8(4):423–443.

[155] Tait, S. W. and Green, D. R. (2012). Mitochondria and cell signalling. *J Cell Sci*, 125(Pt 4):807–15.

[156] Thomasset, M. A. (1962). Bioelectric properties of tissue. impedance measurement in clinical medicine. significance of curves obtained. *Lyon Medical*, 94:107–118.

[157] To, M.-S., Aromataris, E. C., Castro, J., Roberts, M. L., Barritt, G. J., and Rychkov, G. Y. (2010). Mitochondrial uncoupler fccp activates proton conductance but does not block store-operated ca 2+ current in liver cells. *Archives of Biochemistry and Biophysics*, 495(2):152–158.

[158] Wallace, D. C. (2005). A mitochondrial paradigm of metabolic and degenerative diseases, aging, and cancer: a dawn for evolutionary medicine. *Annu Rev Genet*, 39:359–407.

[159] West, A. R. (1991). Solid electrolytes and mixed ionic–electronic conductors: an applications overview. *J. Mater. Chem.*, 1(2):157–162.

[160] Williams, G. and Thomas, D. K. (1998). Phenomenological and molecular theories of dielectric and electrical relaxation of materials. *Novocontrol Application Note Dielectrics*, 3:1–29.

[161] Wyatt, O. H. and Dew-Hughes, D. (1974). *Metals, ceramics and polymers*, Cambridge University Press, London.

[162] Xing, P., Miled, M. A., and Sawan, M. (2013). Glutamate, GABA and dopamine hydrochloride concentration effects on the conductivity and impedance of cerebrospinal fluid, Neural Engineering (NER), 2013 6th International IEEE/EMBS Conference. pages 1037–1040.

[163] Zhang, Y., Marcillat, O., Giulivi, C., Ernster, L., and Davies, K. J. (1990). The oxidative inactivation of mitochondrial electron transport chain components and ATPase. *Journal of Biological Chemistry*, 265(27):16330–16336.

[164] Zoratti, M. and Szabò, I. (1995). The mitochondrial permeability transition. *Biochimica et Biophysica Acta (BBA)-Reviews on Biomembranes*, 1241(2):139–176.